A THEORETICAL AND EXPERIMENTAL INVESTIGATION OF TURBULENT JET INTERACTION

by

Steven Brian Weeks

United States
Naval Postgraduate School

THESIS

A THEORETICAL AND EXPERIMENTAL INVESTIGATION OF

TURBULENT JET INTERACTION

by

Steven Brian Weeks

October 1969

A Theoretical and Experimental Investigation of Turbulent Jet Interaction

by

Steven Brian Weeks
Lieutenant (junior grade), United States Navy
B.S.M.E., University of California, Berkeley, 1968

Submitted in partial fulfillment of the
requirements for the degree of

MASTER OF SCIENCE IN MECHANICAL ENGINEERING

from the

NAVAL POSTGRADUATE SCHOOL
October 1969

ABSTRACT

The interaction of two impinging plane turbulent jets has been investigated for the purpose of understanding the performance of proportional fluid amplifiers and momentum-exchange devices. Velocity and turbulence profiles were measured across and at various distances along the combined jet axis through the use of a constant temperature hot-wire anemometer. Experimentally determined jet deflection angles were found to agree quite well with those predicted in a previous work by the free-streamline theory. The results, which are presented in terms of normalized parameters, show that the jet interaction may be divided into three regions: mixing; transition; and fully developed. A vena-contracta effect was found to exist in the mixing region. A discussion of each of the three regions is presented in detail along with generalizations for similar geometries.

TABLE OF CONTENTS

LIST OF ILLUSTRATIONS

LIST OF SYMBOLS

a_m	polynomial coefficients
CF(P)	pressure correction factor
D	distance to any station on the jet axis from the intersection of the inner walls of the jet channels
E	instantaneous anemometer voltage output
$\overline{E}$	anemometer voltage output with flow
$\overline{E}_o$	anemometer voltage output with no flow
$\Delta\overline{E}$	$\overline{E}-\overline{E}_o$
$\sqrt{\overline{e^2}}$	Root Mean Square (R.M.S.) value of anemometer voltage output
K	a constant
n	a constant
P	manometer pressure (psig)
Q	flow rate (scfm)
U	instantaneous velocity
$\overline{U}$	local mean velocity
U_c	average velocity in the control jet
U_{cent}	centerline velocity
U_m	average velocity in the main jet
U_{max}	maximum velocity in a jet profile
U_{max1}	largest maximum velocity in mixing region
U_{max2}	second largest maximum velocity in mixing region
U_{maxm}	maximum velocity in the main jet
U_o	velocity through calibration orifice
$\sqrt{\overline{u^2}}$	R.M.S. value of the fluctuating component of velocity

V	natural log of U
W	width of the main and control jet channels
X	distance from jet center measured along lines perpendicular to the jet axis
Y	natural log of E
α	jet deflection angle
ρ	air density (lbm/ft^3)

SUBSCRIPTS

c	control flow
m	main flow

ACKNOWLEDGEMENT

The work described herein was made possible through the sponsorship of the U. S. Army Research Office, Durham, North Carolina. The author wishes to express his appreciation to Professor T. Sarpkaya for his patience, guidance, and encouragement during the course of the investigation. A special note of thanks is also given to Messrs. K. Mothersell, J. Beck, and J. McKay, of the Mechanical Engineering Machine Shop, for their efforts and advice in the construction of the experimental apparatus.

ACKNOWLEDGEMENT

The work described herein was made possible through the sponsorship of the U. S. Army Research Office, Durham, North Carolina. The author wishes to express his appreciation to Professor T. Sarpkaya for his patience, guidance, and encouragement during the course of the investigation. A special note of thanks is also given to Messrs. K. Mothersell, J. Beck, and J. McKay, of the Mechanical Engineering Machine Shop, for their efforts and advice in the construction of the experimental apparatus.

I. INTRODUCTION

In recent years, the need for a thorough understanding of the interaction of two or three jets has become quite evident because of the increased application of jet interaction in fluid power technology. There are several important applications which may be cited herein. In the field of fuel mixing, such as in jet or spacecraft engines, the intricate blending of two or more fuel jets is a crucial factor in determining the engine performance. Another example is found in the area of fluidics. The fluidic devices operate on a principle that one or more low energy control jets can impart sufficient deflection to a power jet and, thus, cause a significant change between the power levels of the receivers.

The proportional fluid amplifier makes use of the most direct application of the interaction of three jets. Another fluidic element or logic device called "AND" gate operates through the interaction of two normally impinging jets. A simplified diagram of a proportional amplifier is shown in Fig. 1. The deflection of the main jet is achieved by an imbalance in the velocities or power levels of the two symmetrical control jets. Whenever a differential pressure exists between the control ports, the power jet is deflected by the momentum imparted by the control jets. This leads to a large or amplified pressure signal between the receiver or load ports. The interaction region of the amplifier is vented in order to avoid wall attachment due to the Coanda effect. Thus, the only external influence on the main jet is due to control flows.

Although discovered in 1959, very little is actually known about the fluid dynamics of proportional amplifiers. A number of studies have been conducted on the overall performance of such amplifiers, but the general approach in these investigations has been restricted to a "black box"

treatment rather than to a detailed understanding of the internal mechanism of the jet interaction. The realization for the need for a better understanding of the fluid dynamics of proportional or momentum-exchange devices has resulted, in the last few years, in the publication of several works (Refs. 1-4).

Some basic research on jet interaction has been undertaken by Professor T. Sarpkaya in the Department of Mechanical Engineering of the Naval Postgraduate School. The present research is part of the investigation sponsored by the U. S. Army Research Office, Durham, North Carolina.

The present thesis is a continuation of a project undertaken by N. Gungor (Ref. 5) to examine the interaction of two impinging jets. The evolution of the mixing region and the jet deflection angles were studied through the use of a constant temperature hot-wire anemometer. The velocity and turbulence intensity profiles in the combined jet were obtained for various control and power jet velocity combinations.

II. EXPERIMENTAL EQUIPMENT

The experimental apparatus together with the instrumentation used is shown in Fig. 2. The basic components of the equipment were: (a) jet assembly; (b) supply system; (c) hot-wire anemometer system; and (d) the hot-wire calibrator.

A. JET ASSEMBLY

The plexiglass jet assembly is shown in Fig. 3. In order to model part of a proportional amplifier, the axes of the two jets were made to intersect at 90 degrees. The jet-assembly design was essentially similar to that used by Gungor (5) with the exception of some additional modifications to increase the accuracy and ease of measurements.

The basic construction consisted of two 10 inch long, 1 inch deep, and 1/4 inch wide channels sandwiched between two 1/2 inch plexiglass plates. The control flow channel had a 1/4 inch setback as shown in Fig. 6. The outer wall of each channel was cut to a sharp point (1/32 inch) to prevent attachment of the jet due to the Coanda effect. All sections were firmly assembled with dowels, and critical dimensions set with gage blocks to an accuracy of 0.001 inch. The channel surfaces were carefully hand-polished with rouge.

The supply lines for each channel were 3/4 inch diameter Tygon tubing connected to special inlet devices to provide for the transition from circular to rectangular flow channels. Wire screens were attached between the tubing and the inlet device by a flange connection. These screens served a dual purpose: (1) Eliminate any swirl that may have been imparted to the flow in the supply tubing; and (2) Filter any foreign matter out of the flow.

The top and bottom plates had two slots cut out to enable the hot-wire anemometer mechanism to traverse along lines parallel to the combined jet axis. A telescope and slide mechanism were attached to the bottom plate. Degree marks were scribed (away from the interaction region) into the bottom plate, and a pointer was attached to the telescope slide.

B. SUPPLY SYSTEM

Air was supplied to the system from a 50 Hp. compressor at approximately 200 psig. The air was first passed through a microfilter to remove oil, dust, and other impurities from the flow and then through the primary pressure regulator (maximum input 400 psig and maximum output of 125 psig.). Both the main and control jets were supplied air independently from this primary pressure regulator.

Each jet supply line had a series of pressure regulators (10 to 130 psig.) providing an accurately regulated flow into a Fisher-Porter rotameter. Both the main and control rotameters were identical having a maximum capacity of 14.6 scfm at 14.7 psia and 70°F with an FP-3/4-27-G-10 tube and a 3/4-GNSVGT-54 float. Since actual flow rates were not measured at 14.7 psia, each rotameter was equipped with a pressure gage, and the flow rates were obtained by:

$$Q = (\text{rotameter reading (\% of full flow)}) \times (14.6) \times CF(P)$$

where $CF(P)$ = pressure correction factor obtained from a chart provided by the Fisher-Porter company for the rotameter.

C. HOT-WIRE ANEMOMETER SYSTEM

The Model 1050 constant temperature hot-wire anemometer manufactured by the Thermo-Systems, Inc. was used in the measurement of velocities and turbulence. The hot-wire probe used in the experiments was also manufactured

by the Thermo-Systems, Inc. (wire # 1272-T1.5). The wire had a cold resistance of 7.07 ohms and an operating resistance of 10.61 ohms.

A special probe holder was constructed and is shown in Fig. 4. This holder fit into slots in the jet assembly which enabled the probe to move along lines parallel to the combined jet axis. A micrometer mechanism on the holder provided transverse movement of the hot-wire across the jet with an accuracy of 0.001 inch.

D. HOT-WIRE CALIBRATOR

The hot-wire probe was calibrated with the Thermo-Systems, Inc. Model 1125 Calibrator shown in Fig. 5. The calibrations were made with the high range calibration orifice having a diameter of 0.150 inch. The pressure in the calibration chamber was measured with water manometers with various ranges of pressure to increase the accuracy of the calibration. The use of the calibrator will be discussed in the next section.

A schematic drawing of the entire experimental system is shown in Fig. 7.

III. EXPERIMENTAL PROCEDURE

The experimental procedure consisted of the following six main steps: (a) Calibration of the hot-wire probe; (b) Determination of the approximate jet deflection angles; (c) Adjusting of the hot-wire anemometer instrumentation; (d) Setting of the selected flow rates for each jet; (e) Measurement of local mean velocities and turbulence intensities; and (f) Data reduction.

A. CALIBRATION

The calibration consisted of the establishment of the exact relationship between the anemometer voltage outputs and the corresponding velocities. The Model 1125 Calibrator was used for this purpose.

First, the hot-wire probe was placed about 1/16 inch above the orifice of the calibrator as recommended by the manufacturer (Ref. 6). Air was then let through the orifice, and the pressure in the orifice chamber was measured by a manometer. From these pressure readings, the velocity through the orifice was calculated by:

$$U_o = \sqrt{\frac{2P}{\rho}}$$

where P is the chamber pressure in psig., and ρ is the air density. For each velocity the corresponding voltage output of the hot-wire anemometer was recorded. Finally, a calibration curve of velocity versus volts was plotted as shown in Fig. 8.

The calibration curve in this form is not very useful since it cannot be used easily for a large number of measurements. In addition the derivatives of the calibration curve, which are needed for the turbulence intensity calculations, cannot be obtained from a calibration curve of

this type. A polynomial approximation is obviously necessary, especially for computerized data reduction.

The hot-wire anemometer characteristics follow King's Law (Ref. 7) which is essentially a power law relation between voltage and velocity. A plot of log (velocity) versus log (voltage) data is shown in Fig. 9 and is seen to be very near to a straight line. A second degree polynomial approximation of this curve was found to fit almost exactly to the logarithmic form of the data points. The derivation of this equation is given in Appendix A. The polynomial approximation to the calibration-curve is shown in Fig. 10 together with the actual data points for comparison.

The calibration curve described above was checked frequently during the course of the experimentation. It was found that the wire performance remained essentially the same.

B. APPROXIMATE JET DEFLECTION ANGLE

In order to properly place the hot-wire probe near the center of the jet, the approximate jet deflection angle, α , had to be determined. Two approximate methods were used by Gungor (5), but they were found to be rather time consuming and tedious. Since the accuracy required was only $\pm$ 2 degrees, a simple needle and thread method was used to determine α .

The apparatus consisted of a plastic holder with a long needle attached. At the end of the needle an eight inch piece of yarn was carefully glued so as to have no preferred directional effects due to the method of attachment. The needle end was then placed at the center of the nozzle (Point M in Fig. 11). For each main and control flow combination, the approximate jet angle could easily be read from the angle the thread made with the axis of the main jet.

C. ADJUSTING OF ANEMOMETER INSTRUMENTS

Prior to each experiment, the anemometer was turned on and allowed to warm up for about one-half hour. The cold resistance of the wire was recorded and checked to make sure that it had not deviated from previous values. Next the operating resistance was set into the device in accordance with the operating instructions (Ref. 6). The system was then switched to the "RUN" operation mode.

The fluctuating signal was monitored by an oscilloscope throughout the experiment. The internal feedback stability was adjusted by the "TRIM" dial on the anemometer to render the system stable within the range of velocities used.

D. SETTING OF FLOW RATES

The channel flow rates were measured by the main and control rotameters and adjusted by two pressure regulators. The main jet was maintained at an average velocity of 87.5 ft/sec which corresponded to a rotameter setting of 60% of full flow and a Reynolds number of 11,140. The control jet flow rate was varied in the experiment to obtain different deflection angles. The control flow rates used and the corresponding velocities and Reynolds numbers are tabulated below.

Control Flow Rate (% full flow)	Q_c scfm	U_c ft/sec	Reynolds Number	U_c/U_m
60	9.11	87.5	11,140	1.00
50	7.59	72.9	9,287	0.834
40	6.01	57.7	7,340	0.66
30	4.47	42.9	5,465	0.491
20	2.95	28.3	3,600	0.323
10	1.46	14.02	1,786	0.1605
NOTE: Reynolds numbers are based on the width of the main channel.				

E. MEASUREMENT OF VELOCITY AND TURBULENCE INTENSITIES

Velocity and turbulence-intensity measurements were made along lines perpendicular to the jet axis at nine different distances from the intersection of the inner walls of the jet channels. These nine stations were chosen to give both an accurate picture of the mixing region and the fully developed region. The following station distances were used: 0.15 inch; 0.30 inch; 0.45 inch; 0.60 inch; 0.80 inch; 1.00 inch; 1.50 inchs; 2.50 inches; and 4.00 inches.

The probe was positioned using the telescope assembly discussed previously. The telescope was first set to the approximate jet deflection angle. The probe was then centered at a particular station with the use of the telescope crosshairs.

Once the probe was positioned, the traversing limits were determined to give an accurate picture of the jet profile. The hot-wire probe was then moved at suitable increments along the traversing line, and both the wire voltages and the R.M.S. voltages were recorded.

A schematic drawing of the traversing line together with the appropriate nomenclature is shown in Fig. 11.

F. DATA REDUCTION

All data was reduced and plotted using the IBM-360 computer. The main data reduction program is presented in Computer Program B. Velocities and turbulence intensities were calculated using the polynomial calibration-curve approximation previously described.

The turbulence intensity was calculated by:

$$\frac{\sqrt{u^2}}{\bar{U}} = \frac{\sqrt{e^2}}{\bar{U}} \cdot \frac{d\bar{U}}{d\bar{E}}$$

where $\sqrt{e^2}$ is the R.M.S. voltage reading and $\frac{d\bar{U}}{d\bar{E}}$ is the derivative of the calibration curve evaluated at the value of the local mean velocity $\bar{U}$. The derivation of the above equation is given in Appendix B.

IV. DISCUSSION OF RESULTS

The main purpose of this investigation was to gain a better understanding of the mixing of two turbulent jets. This interaction was found to be dominated by three regions: (1) the mixing region; (2) the transition region; and (3) the fully developed region. The important characteristics of each of these regions will be discussed in terms of the velocity and turbulence intensity measurements. General similarity in jet interaction for similar geometries will then be discussed through a comparison of the data presented herein with those obtained by Gungor (5).

The most important characteristic in any jet interaction study is obviously the jet deflection angle. Figure 12 shows the comparison of experimental jet deflection angles with those predicted by the free-streamline theory (5). Also plotted on this graph are the jet deflection angles based on a simple momentum equation:

$$\alpha = \tan^{-1} \left(\frac{U_c}{U_m} \right)^2$$

It is apparent that the predictions of the free-streamline analysis and the experimental values agree quite satisfactorily. Deflection angles based on the momentum equation do not agree well at all. This is to be expected since the equation does not take into account the control channel setback.

Gungor (5) also measured the deflection angles through the use of a model half the size of that used in the present investigation, i.e., W = 1/8 inch, aspect ration = 8. The table below gives a comparison of the two sets of deflection angles. Both sets of data have similar geometries and comparable Reynolds numbers with the exception of the aspect ratios.

Flow Ratio Q_c/Q_m	6/6	5/6	4/6	3/6	2/6	1/6
W = 1/4 in.	35	30	25	18.5	11	2
W = 1/8 in. (Gungor)	35	30	25	18	10	2.5

It is obvious that the deflection angles are almost identical although the actual magnitudes of the velocities were quite different in each case. Apparently, the deflection angle depends only on the velocity ratio rather than the actual magnitudes of the velocities.

The three regions of the jet interaction can be seen clearly in Figs. 13-21. In these graphs the velocity and turbulence intensity profiles for equal main and control jet velocities are plotted for various distances along the jet axis. The mixing region is near the nozzle exit, and the two flows remain essentially separate with two velocity peaks. At larger distances from the exit, the two jets mix together until a single symmetrical jet emerges at a distance of about 6W as shown in Fig. 19. This is the fully-developed region. The area between the mixing and the fully-developed regions is the transition region.

Also shown in this set of graphs are the turbulence intensity profiles. This combination of velocity and turbulence profiles shows graphically the two turbulent mixing regions at the outer edges of the jet. These mixing regions are caused by the free shear layers. A third turbulent mixing region exists in the central core between the two jets and will be discussed later.

A complete set of data, for nine stations along the jet axis, is presented for $U_c/U_m = 1.00$. Only two representative velocity and turbulence intensity profile combinations are presented for each of the remaining velocity ratios (Figs. 22-31). This is because all of the control flows exhibited similar characteristics. Turbulence intensities for $U_c/U_m = 0.1605$ have not been presented because of the inaccuracies in the derivatives of the calibration curve for low velocities.

The mixing-region normalized-velocity profiles, for each flow ratio, are presented in Figs. 32-37. From these graphs the actual mixing process of the jets can be seen quite clearly. Close to the channel exit, the two velocity maximums are far apart with a large velocity minimum or "trough" between them. This preservation, for a short distance, of the identity of the main and control jets has been attributed by Douglas and Neeve (2) to a "brick wall effect". Further down the jet axis, the peaks move closer together as the momentum transfer across the turbulent shear layer decreases. Attemps were made to find some kind of similarity variable for the mixing-region velocity profiles but to no avail. Similarity will probably be obtained by analyzing each velocity mixing region separately as mentioned in Pai (Ref. 8).

In the mixing region the turbulence intensities are higher on the control jet side than on the main jet side. This higher turbulence intensity is caused by the low local mean velocities and not by the R.M.S. value of turbulence. With decreasing control flow, the difference between the control and main jet turbulence intensity peaks rise which supports the above reasoning. This same trend is also verified by Gungor (5).

As previously mentioned, there are three turbulent mixing regions. The graphs cited above presented only the turbulence intensities in the exterior regions of the velocity profiles. Figures 38-40 show, on an extended scale, the internal turbulence profiles for three velocity ratios. The intensity of internal turbulence decreases with increasing distance from the channels, as would be expected. By comparing Figs. 38 and 40, it is seen that the greater the velocity difference between the two jets, the greater the internal turbulence intensity. This internal turbulence is a result of the mixing of the two jets due to vortex motion. The turbulence decreases because of the vortex decay in the shear layer.

It is apparent from the definition of turbulence intensity (see Appendix B) that it also represents the relative noise in the jet. Moynihan (Ref. 3) took the total pressure ratio as a qualitative measure of noise in a jet interaction. In graphs similar to those presented here, he showed three distinct noise levels in the jet of about equal magnitude. The results presented herein show that they are, in fact, not equal. The amount of turbulence ($\sqrt{\overline{u^2}}$) is much less in the internal shear layer than in the external mixing regions. In proportional amplifier design, this fact is very important to keep in mind.

The transition region has been defined as an area where the velocity profiles do not exhibit dual velocity maximums nor are they symmetrical as in a fully-developed jet profile. A good example of this type of velocity profile is shown by Curve A in Fig. 43. Using crude terminology to explain the transition process, the jet "pops" from the mixing region, through the transition region, and into the fully developed region. The length of this transition region, for all control flows, was less than

one channel width. This region is short because of the characteristics of the vortex decay in the inner shear layer. As time increases, the turbulent vortices decay very quickly, causing a very short transition before a fully developed jet appears.

In Figs. 41-46, similarity profiles are presented for the fully-developed velocity region. These graphs confirm the findings of Gungor (5) that fully developed profiles are similar when plotted against x/D. For convenience the transition region profiles have also been included in these plots. Since transition profiles are not symmetric, they cannot be expected to follow such a similarity trend.

The effective pivot point of the jet, for each flow ratio, was examined by plotting jet maximum points along the jet axis similar to that shown in Fig. 11. Within the accuracy of this experiment, the pivot point was found to be approximately at the intersection of the centerlines of the main and control channels (Point M in Fig. 11) for all velocity ratios. For this reason, all of the deflection angles were measured relative to this point. This stationary pivot verifies the findings of Moynihan and Reilly (4).

One of the most interesting plots of the mixing-region velocity data is shown in Fig. 47. This graph shows that the ratio of the two velocity maximums for a given flow ratio remains nearly a constant in the mixing region. This fact could be very important in attempts to modify the free-streamline theory to better describe the mixing region. It is also seen from these curves, that the length of the mixing region increases with increasing control flow. The maximum length is 6W for $U_c/U_m = 1.00$. The dashed lines to the right of each curve represent the transition region and show how small this region actually is (about 0.5W).

Figure 48 shows the acceleration of flow and the presence of a vena-contracta in the mixing region. Here the ratio of the largest maximum velocity in a particular profile to the maximum velocity in the main jet channel has been plotted against D/W. A maximum occurs at a distance of 2.5W for almost all flow ratios. This may be interpreted as a "pinching" or vena-contracta of the combined jet.

This vena-contracta effect is caused by two phenomena. First, the control jet "pinches" the main jet because of the direction of the initial control jet momentum. Secondly, as the jet moves further from the nozzle, surrounding air is entrained by the turbulent mixing. Eventually, this entrainment and mixing causes the jet to expand and decrease in velocity. The net result is a vena-contracta type of velocity profile. The amount of pinching of the main jet is certainly related to the relative momentum of the control flow. The vena-contracta is almost non-existant for low control flows.

One of the primary purposes of this investigation was to determine if any general similarity in jet interaction existed for similar geometries. In order to accomplish this, the results for W = 1/4 inch were compared, wherever possible, with the results of Gungor (5) for W = 1/8 inch.

A comparison of centerline velocities, for various distances along the combined jet, is presented in Figs. 49-54. The U_{cent}/U_m ratio is seen to have the same general functional relationship with D/W even though velocities and channel widths are quite different. Figure 55 is a graph of D/W (corresponding to the maximum centerline velocity) versus the flow ratio. It appears that the centerline velocity is a function of D/W and U_c/U_m for similar geometries and comparable Reynolds numbers.

V. CONCLUSIONS

The following conclusions can be drawn from the data presented herein:

(1) Experimental jet deflection angles agree with the predictions of the free-streamline theory.

(2) The jet deflection angle is independent of the magnitudes of the main and control jet velocities for similar geometries and depends only on velocity ratio.

(3) For two impinging jets, there are three turbulent mixing regions with the turbulence intensity directly dependent on velocity differences.

(4) Fully-developed jet profiles for each flow ratio are similar when plotted against x/D.

(5) The effective pivot point of the deflected jet is the same for all flow ratios, i.e., at the intersection of the channel axes.

(6) In the mixing region, the ratio of the two velocity maximums is nearly constant for each flow ratio.

(7) The length of the mixing region increases with increasing control flow.

(8) A vena-contracta effect is present in the combined jet at distances of about 2.5W from the channel exits.

(9) The centerline velocity in the combined jet is a function of only D/W and velocity ratio for similar geometries and comparable Reynolds numbers.

VI. RECOMMENDATIONS FOR FURTHER WORK

The investigation described herein should be extended to the study of the following areas:

(1) The effect of different setbacks and aspect ratios on the jet deflection, velocity, and turbulence distributions.

(2) Effect of low Reynolds number or laminar flow on the jet interaction.

(3) A more thorough investigation of the turbulence in the jets using two-wire correlation to check for dominant noise frequencies and self-preserving turbulence.

(4) Verification of theoretical predictions for similarity in the three velocity mixing regions.

(5) An extension of the free-streamline theory approximation for the mixing region of two impinging jets to include two unequal free stream velocities of constant ratio.

APPENDIX A

LOGARITHMIC CALIBRATION CURVE APPROXIMATION

The basic relationship between the voltage and velocity for a hot-wire anemometer is given by King's Law:

$$(1) \quad \Delta\bar{E} = K\,\bar{U}^n$$

where

$\Delta\bar{E}$ = differential voltage
$\bar{U}$ = local mean velocity
K,n constants

taking the logarithm of (1)

$$(2) \quad \ln(\Delta\bar{E}) = \ln(K) + n\ln(\bar{U})$$

letting

$$y = \ln(\Delta\bar{E})$$

$$V = \ln(\bar{U})$$

and approximating (2) with a polynomial one has

$$(3) \quad V = a_1 + a_2 y + a_3 y^2 + \ldots + a_{m+1} y^m$$

Various values of m were tried using a Chebyschev Curve-Fit as shown in Computer Program A. A second degree (m = 2) polynomial approximation was found to give the best fit to the actual data (see Fig. 10).

The coefficients a_m for the polynomial were found to be:

a_m	
a_1	3.494994
a_2	3.008039
a_3	-0.003591135

APPENDIX B

DERIVATION OF TURBULENCE-INTENSITY EQUATION

For a turbulent flow, the instantaneous value of the anemometer output is given by:

$$(1) \quad E = \bar{E} + \sqrt{\overline{e^2}}$$

where

$\bar{E}$ = voltage output corresponding to the mean velocity at a given point ($\bar{U}$).

$\sqrt{\overline{e^2}}$ = R.M.S. value of the voltage output corresponding to the R.M.S. value of the fluctuating component of velocity ($\sqrt{\overline{u^2}}$).

Thus from equation (1) we can write the equation for the instantaneous velocity

$$(2) \quad U = \bar{U} + \sqrt{\overline{u^2}}$$

and

$$(3) \quad E = f(U) = f(\bar{U} + \sqrt{\overline{u^2}})$$

also

$$(4) \quad dE = f'(U)dU$$

since the fluctuating component of velocity, $\sqrt{\overline{u^2}}$, is relatively small, we can expand equation (3) in a Taylor Series neglecting higher order terms,

$$(5) \quad f(\bar{U} + \sqrt{\overline{u^2}}) = f(\bar{U}) + \sqrt{\overline{u^2}} f'(\bar{U}) + \ldots.$$

therefore

$$(6) \quad E = \bar{E} + \sqrt{\overline{e^2}} = f(\bar{U}) + \sqrt{\overline{u^2}} f'(\bar{U})$$

by definition $\bar{E} = f(\bar{U})$ so that

$$(7) \quad \sqrt{\overline{e^2}} = \sqrt{\overline{u^2}} f'(\bar{U})$$

and

$$(8)\quad \sqrt{\overline{u^2}} = \frac{\sqrt{\overline{e^2}}}{f'(\bar{U})}$$

the turbulence intensity is defined as

$$(9)\quad \frac{\sqrt{\overline{u^2}}}{\bar{U}} = \frac{\sqrt{\overline{e^2}}}{\bar{U}\, f'(\bar{U})}$$

since $f'(\bar{U}) = \frac{d\bar{E}}{d\bar{U}}$

the final expression for turbulence becomes

$$(10)\quad \frac{\sqrt{\overline{u^2}}}{\bar{U}} = \frac{\sqrt{\overline{e^2}}}{\bar{U}} \cdot \frac{d\bar{U}}{d\bar{E}}$$

Equation (10) is easily adaptable for computerized data reduction as shown in Computer Program B. The values of $\bar{U}$, and $d\bar{U}/d\bar{E}$ are obtained from the polynomial calibration curve.

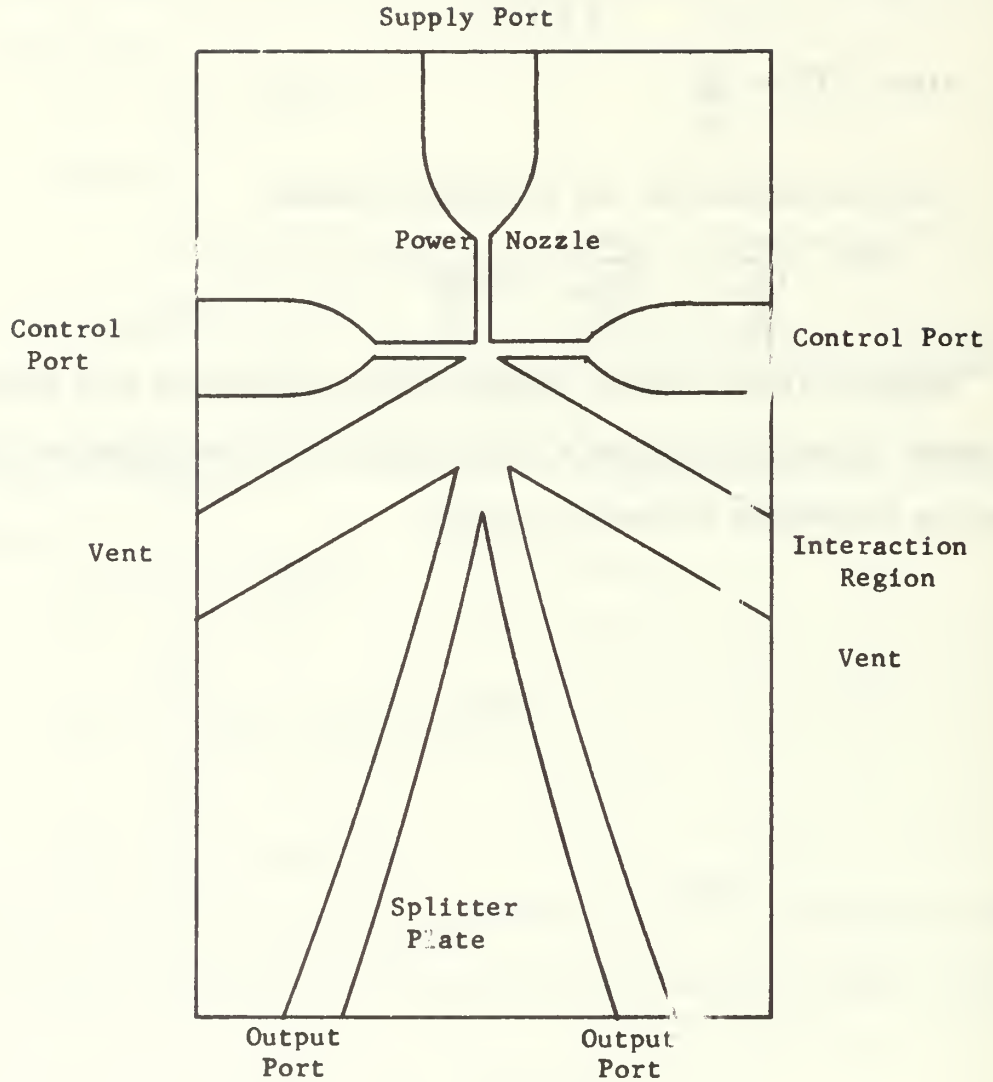

FIGURE 1. PROPORTIONAL AMPLIFIER

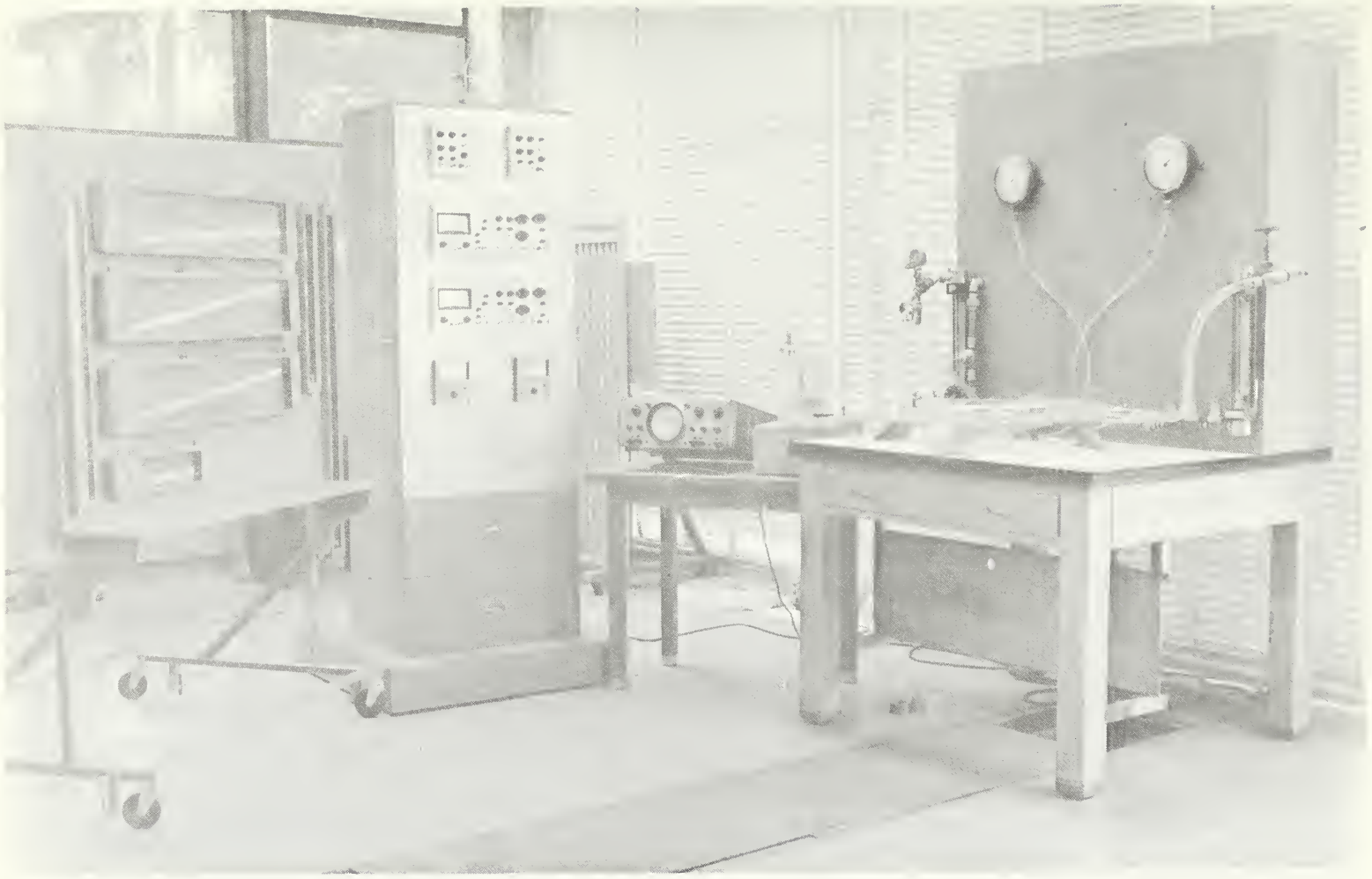

FIGURE 2. EXPERIMENTAL SYSTEM

FIGURE 5. JET ASSEMBLY

FIGURE 4. HOT-WIRE PROBE HOLDER

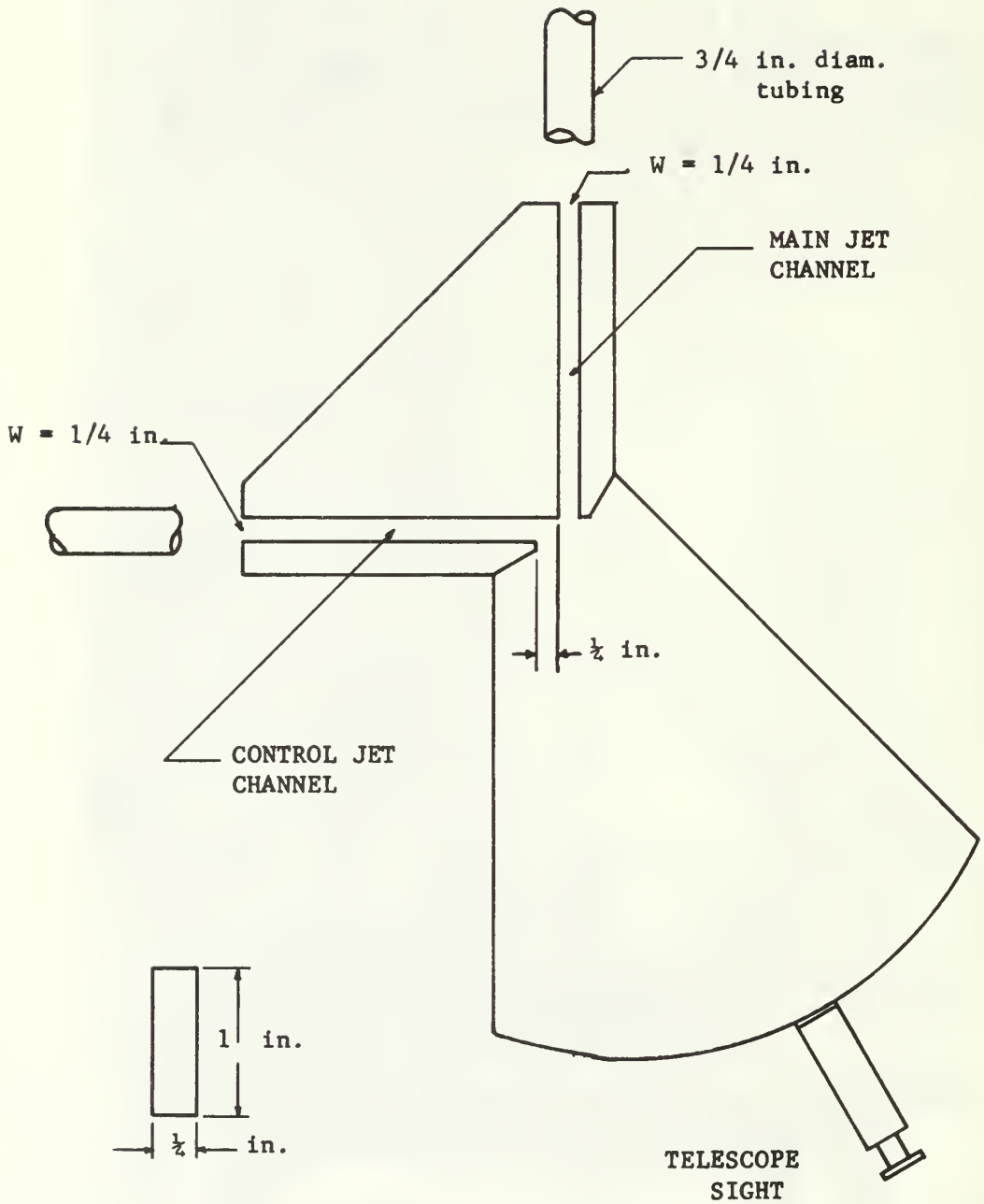

FIGURE 6. SCHEMATIC OF JET ASSEMBLY

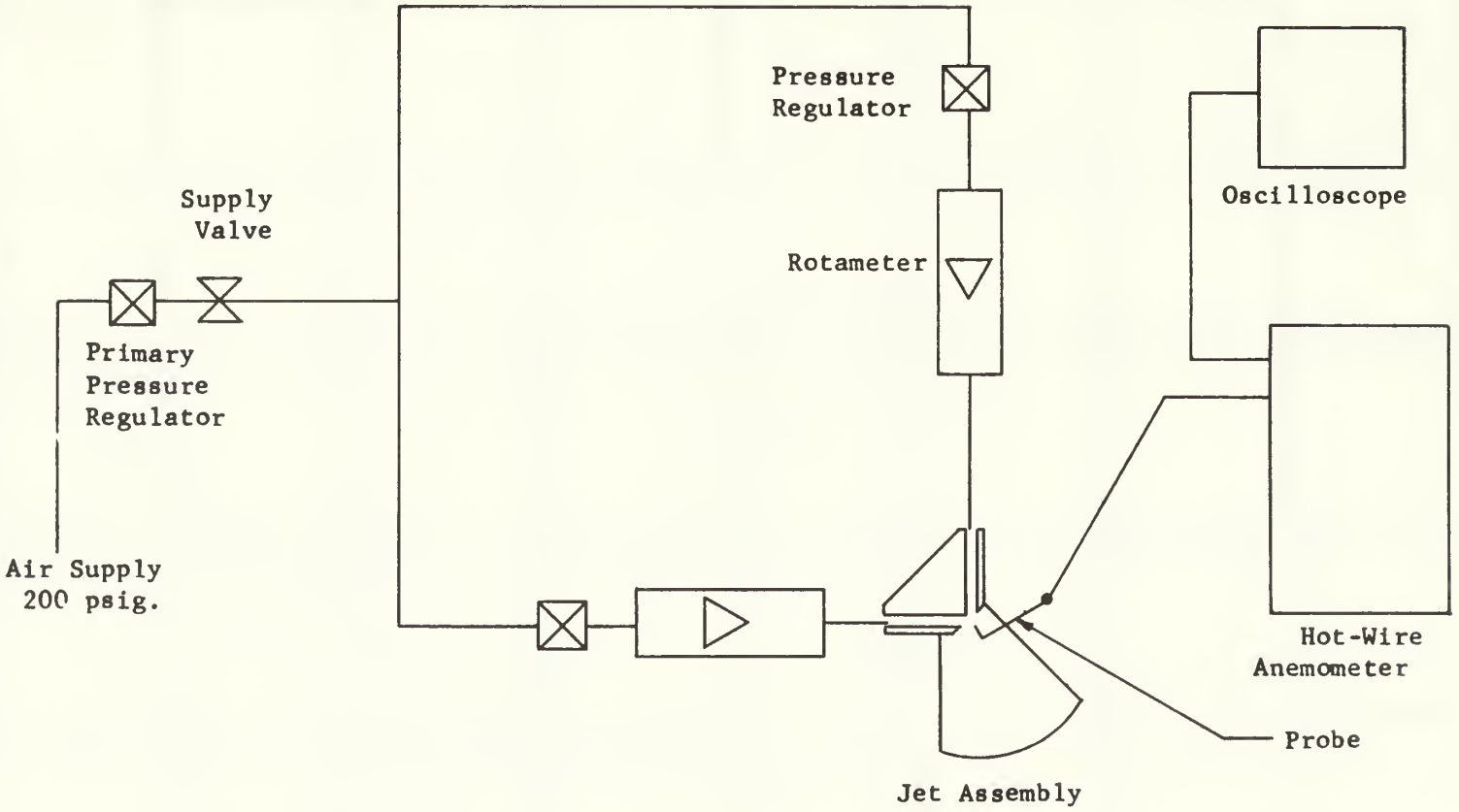

FIGURE 7. SCHEMATIC OF EXPERIMENTAL SYSTEM

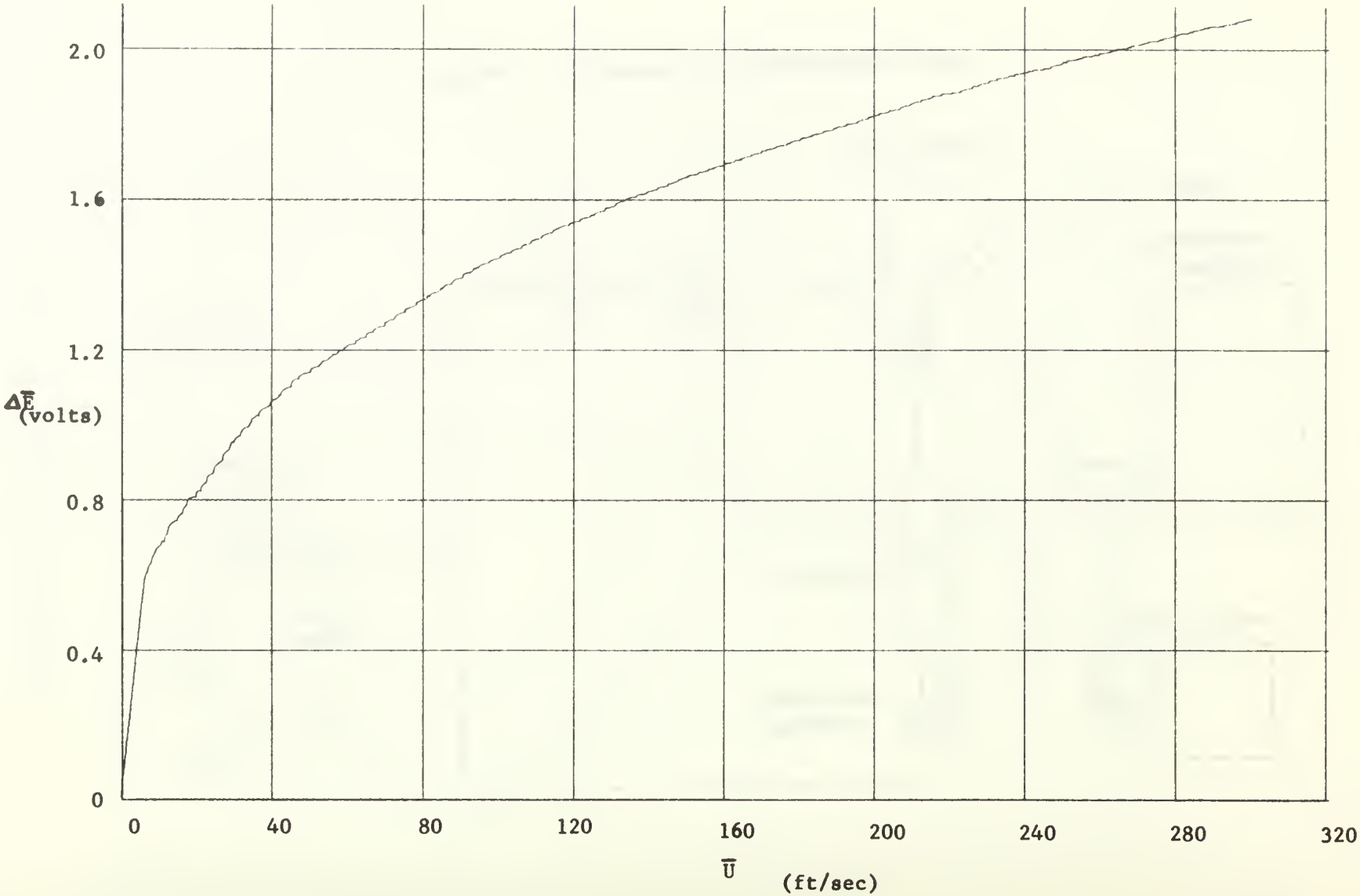

FIGURE 8. CALIBRATION CURVE

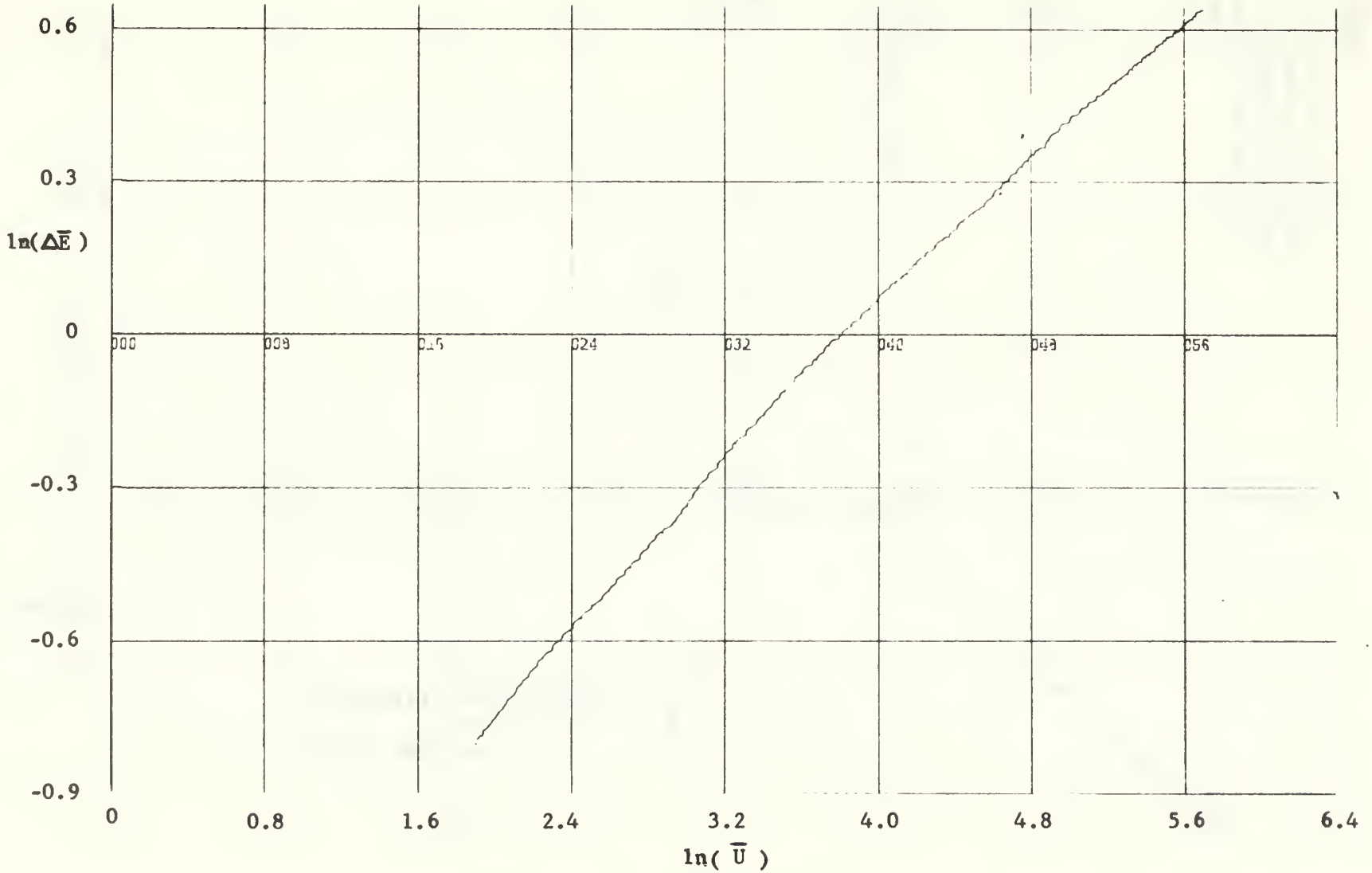

FIGURE 9. LOGARITHMIC CALIBRATION CURVE

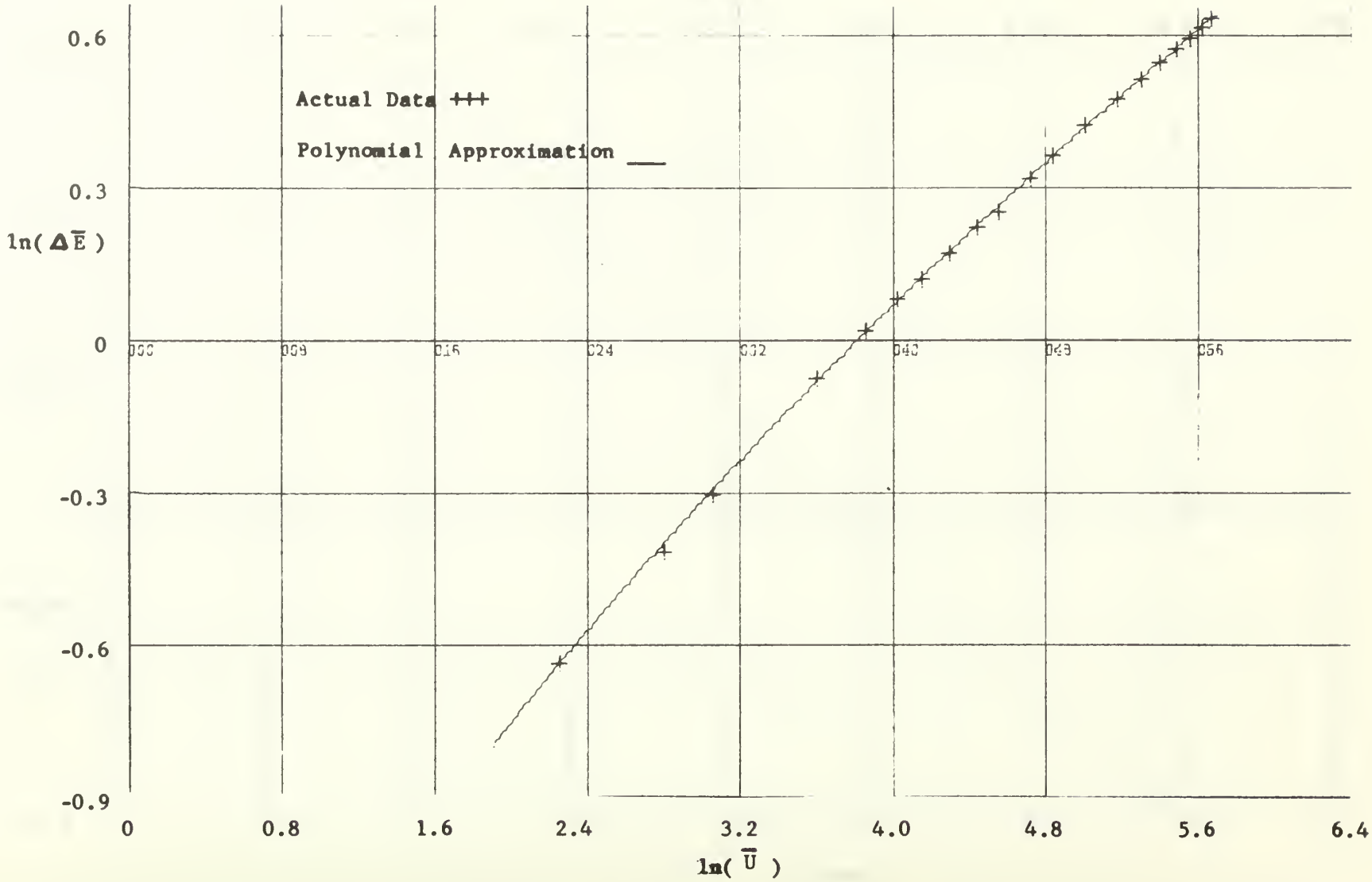

FIGURE 10. CALIBRATION CURVE APPROXIMATION

M = Jet Pivot Point
x = Traversing Distance
D = Station Distance
α = Deflection Angle

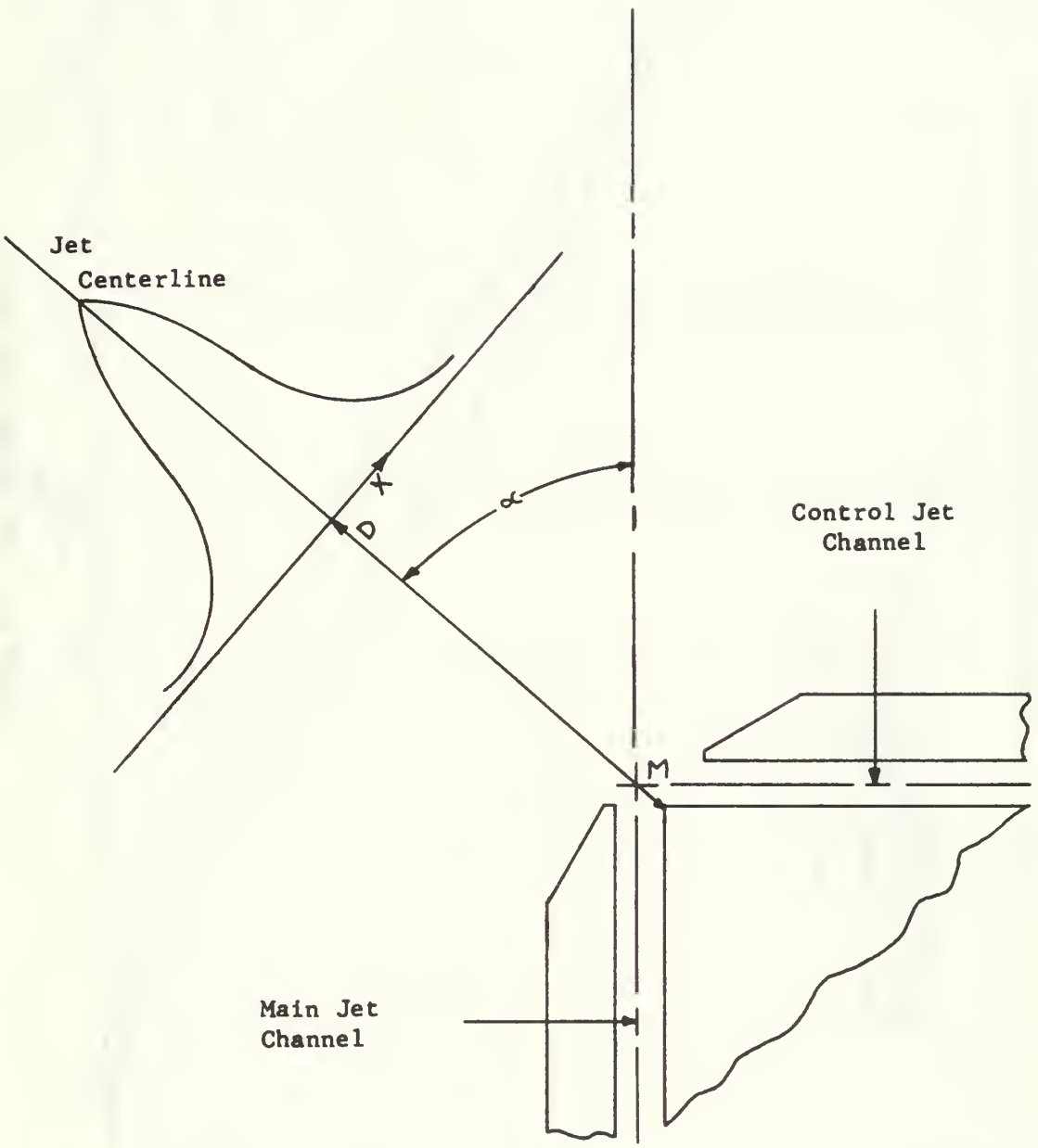

FIGURE 11. DIAGRAM OF TRAVERSING LINE

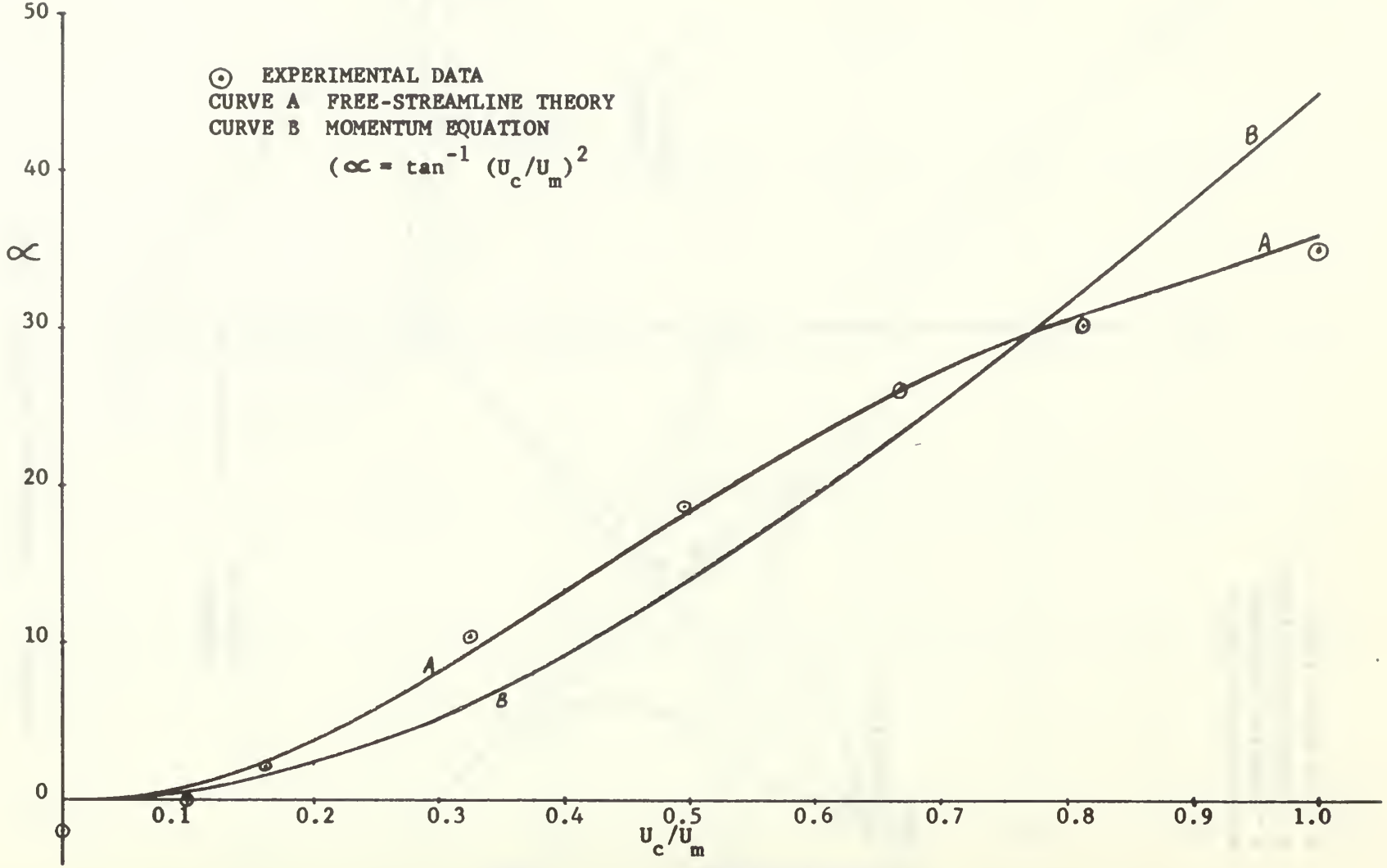

FIGURE 12. JET DEFLECTION ANGLE

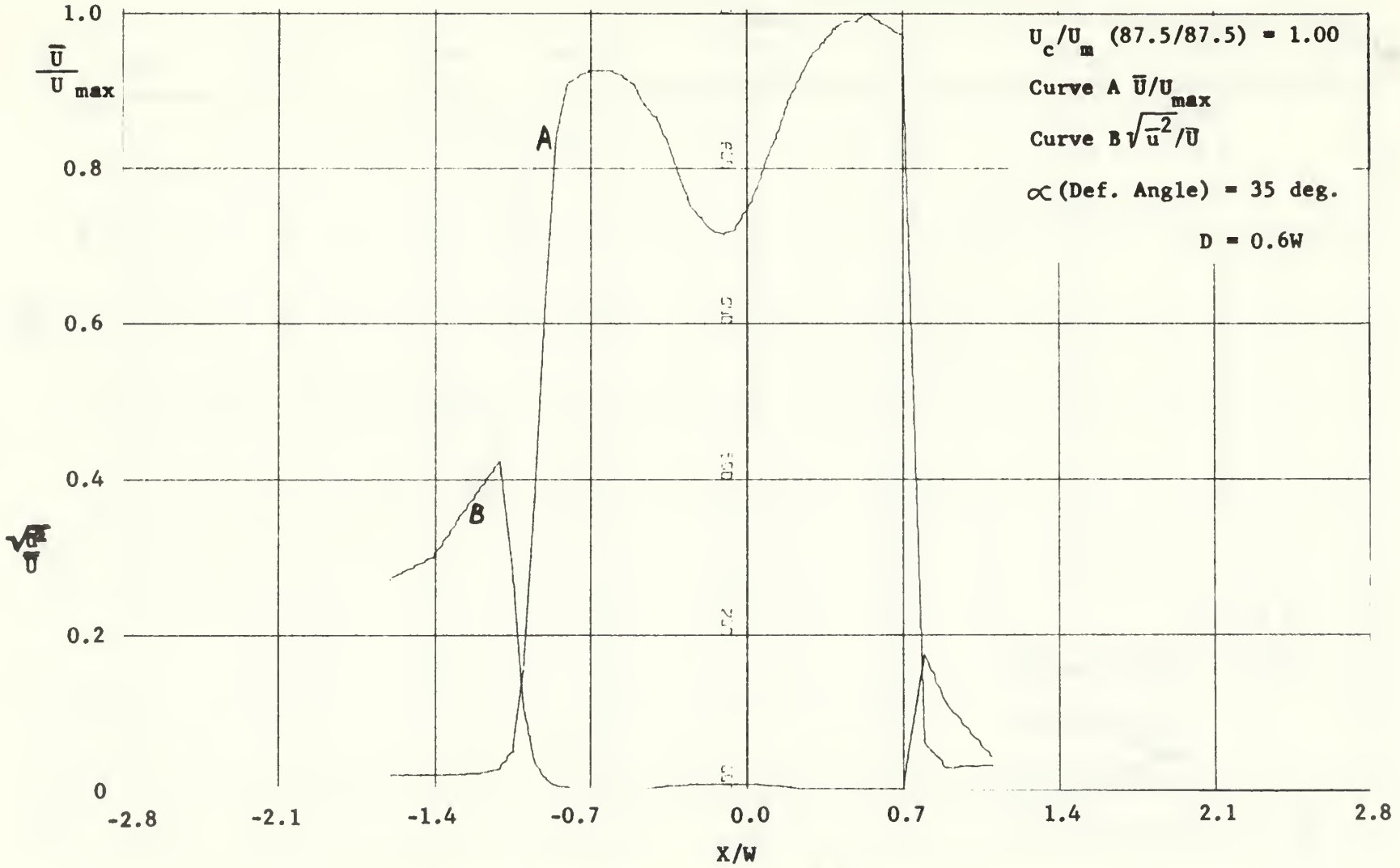

FIGURE 13. VELOCITY AND TURBULENCE INTENSITY PROFILES

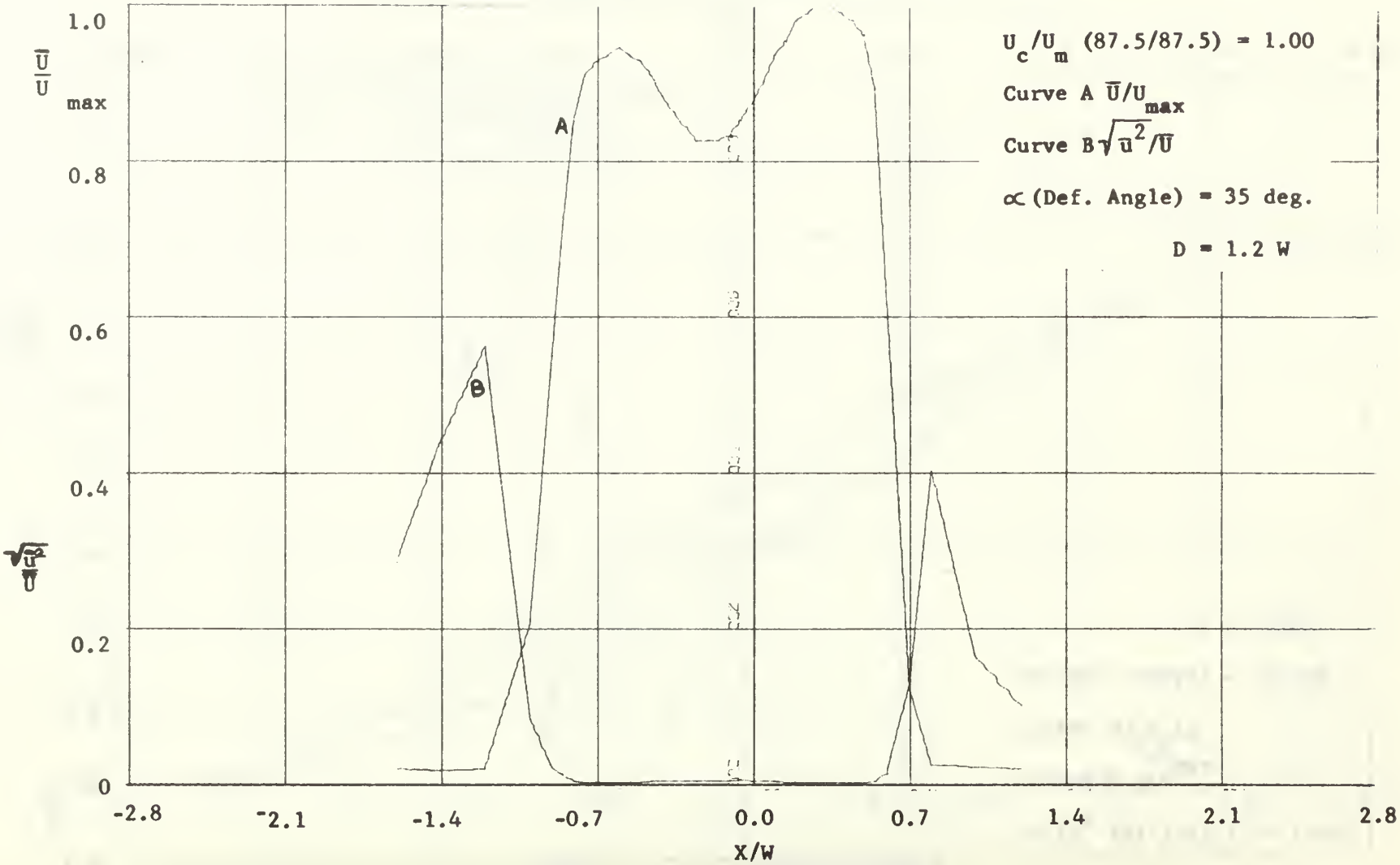

FIGURE 14. VELOCITY AND TURBULENCE INTENSITY PROFILES

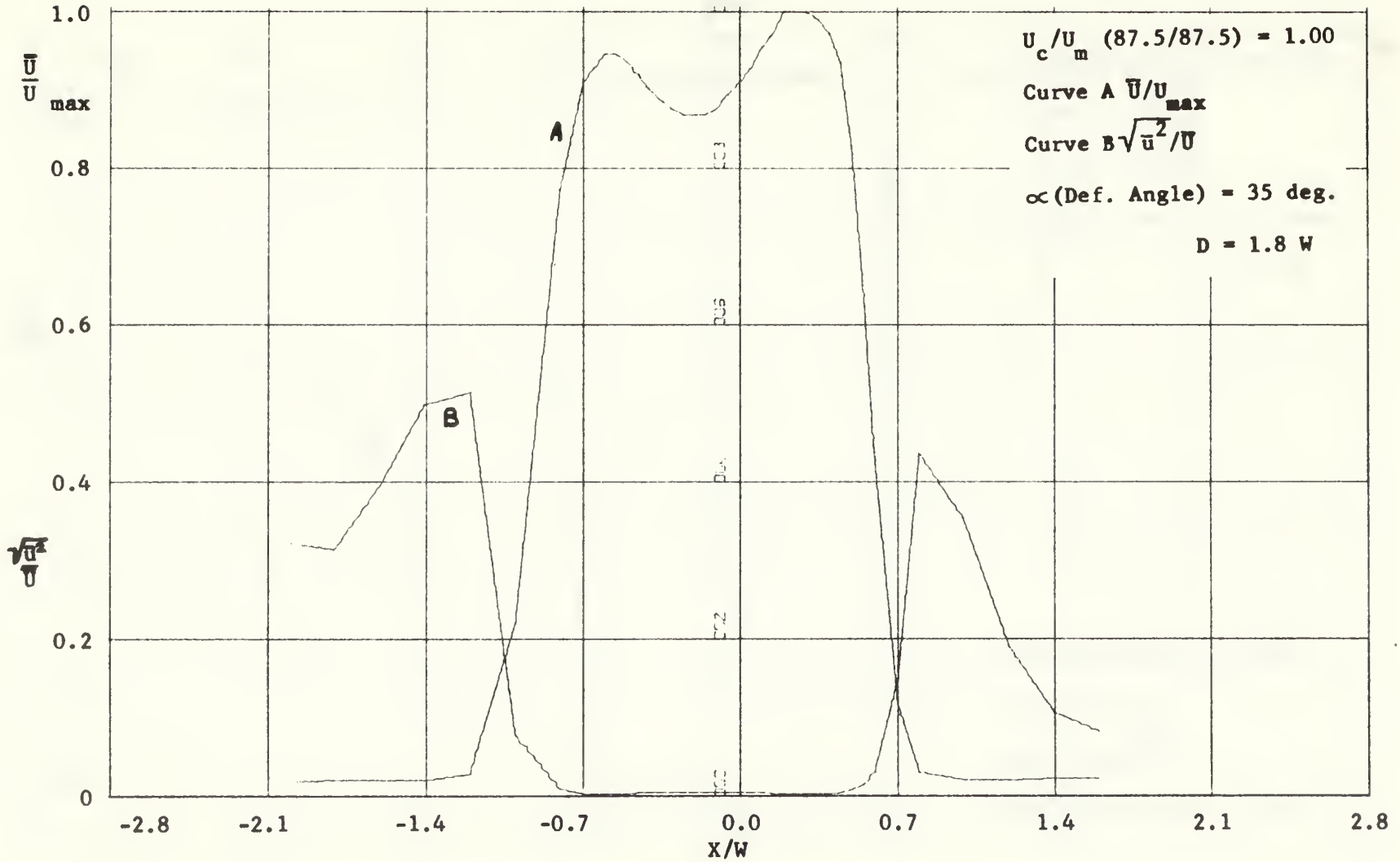

FIGURE 15. VELOCITY AND TURBULENCE INTENSITY PROFILES

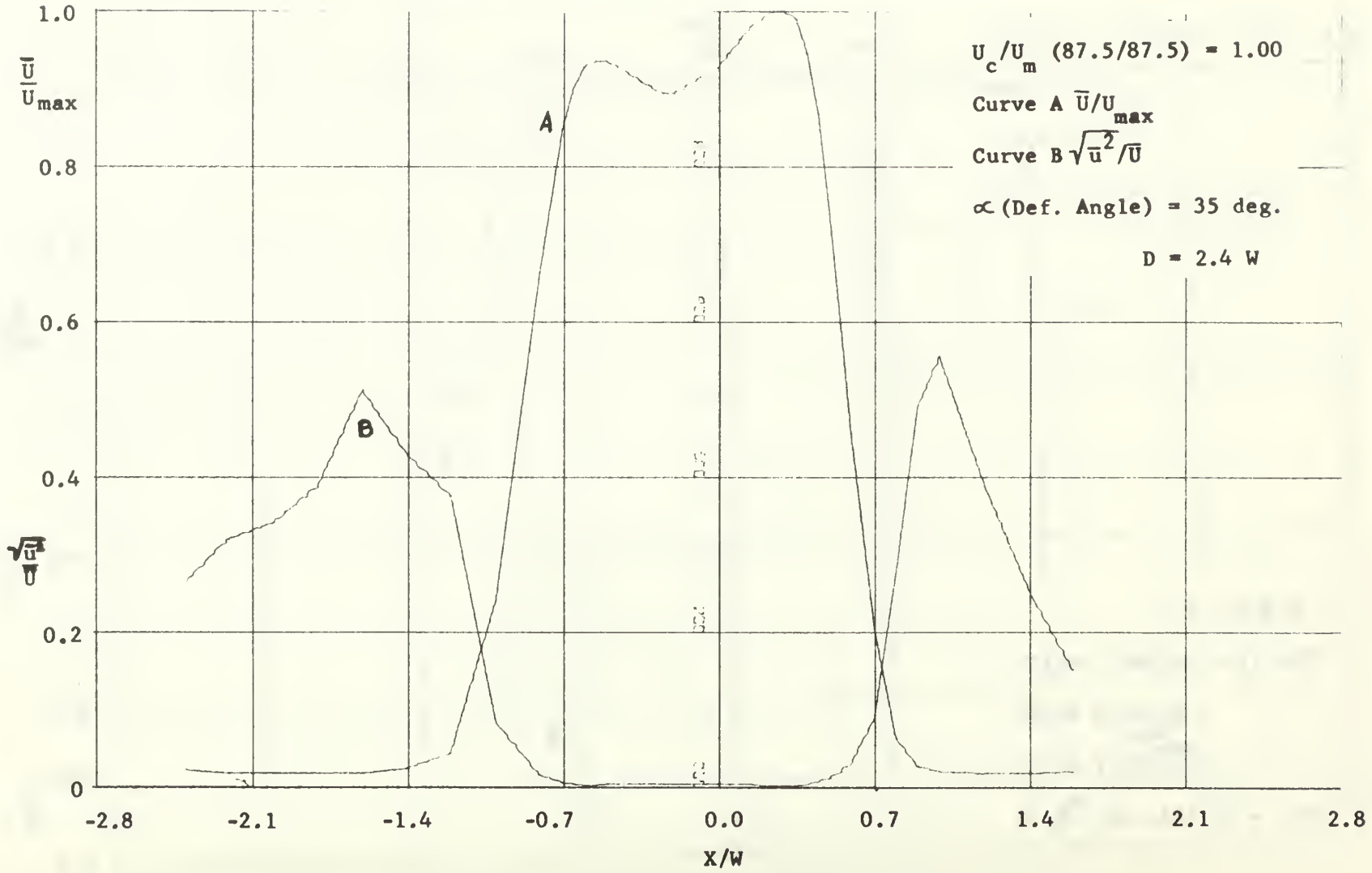

FIGURE 16. VELOCITY AND TURBULENCE INTENSITY PROFILES

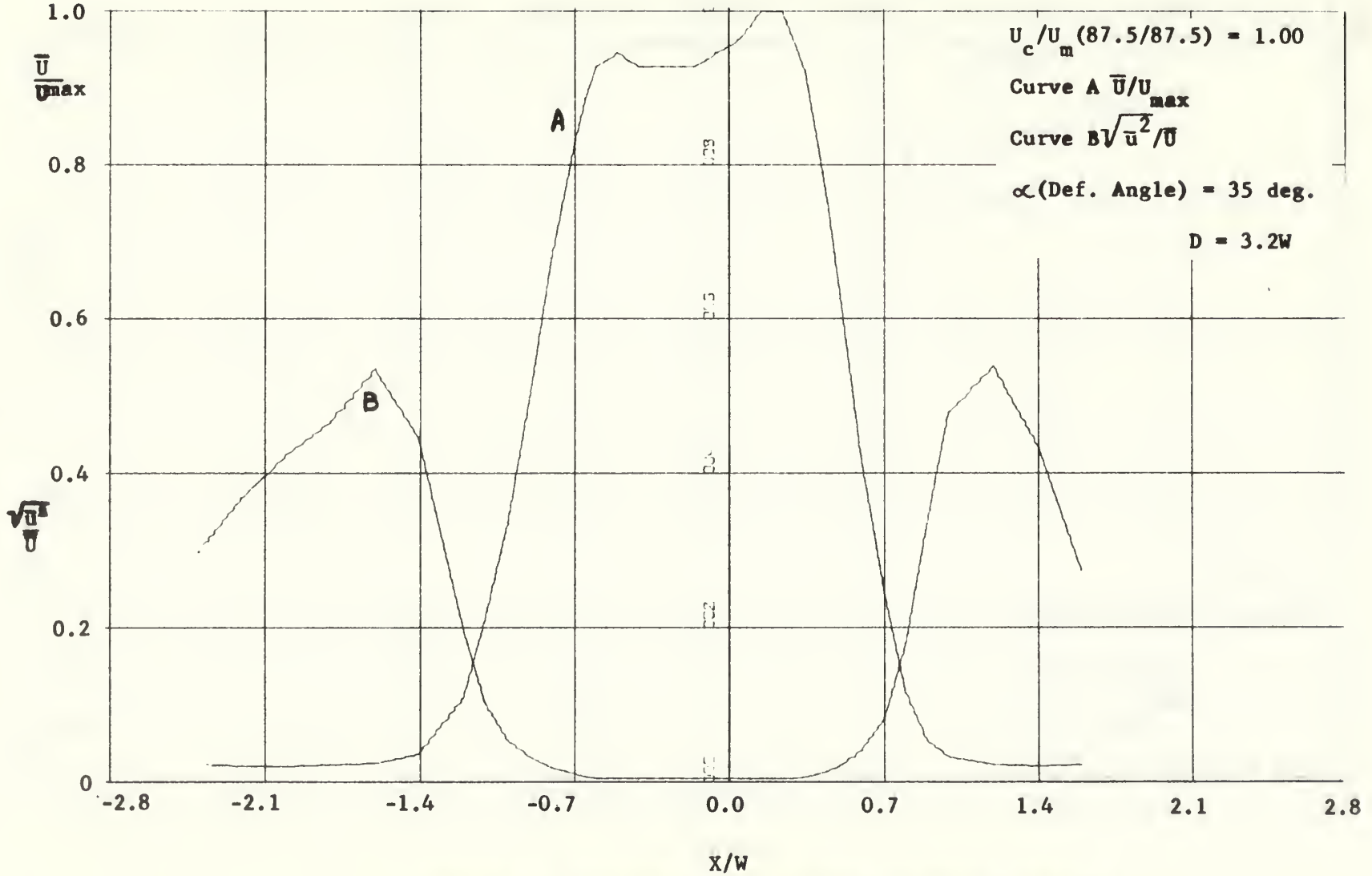

FIGURE 17. VELOCITY AND TURBULENCE INTENSITY PROFILES

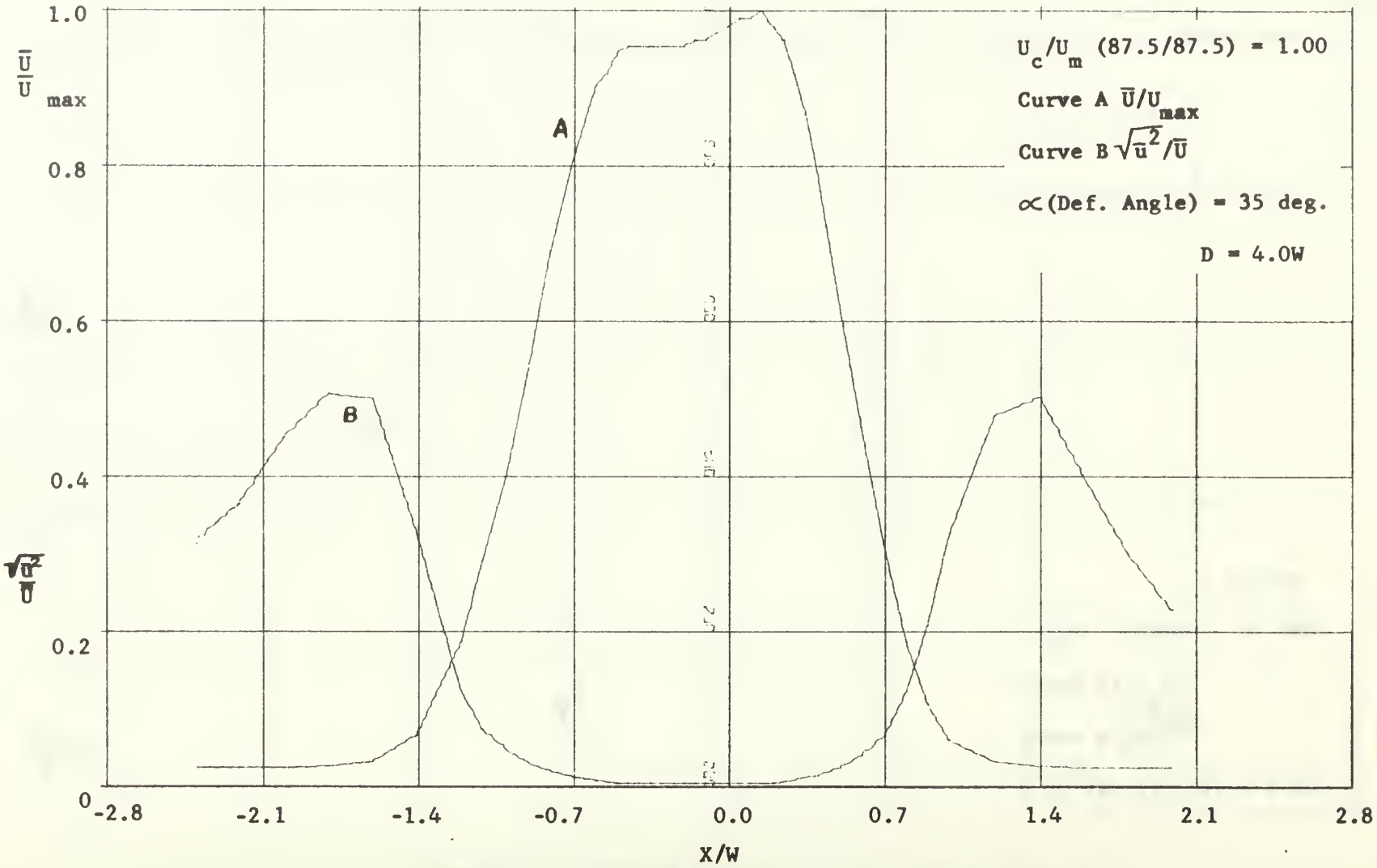

FIGURE 18. VELOCITY AND TURBULENCE INTENSITY PROFILES

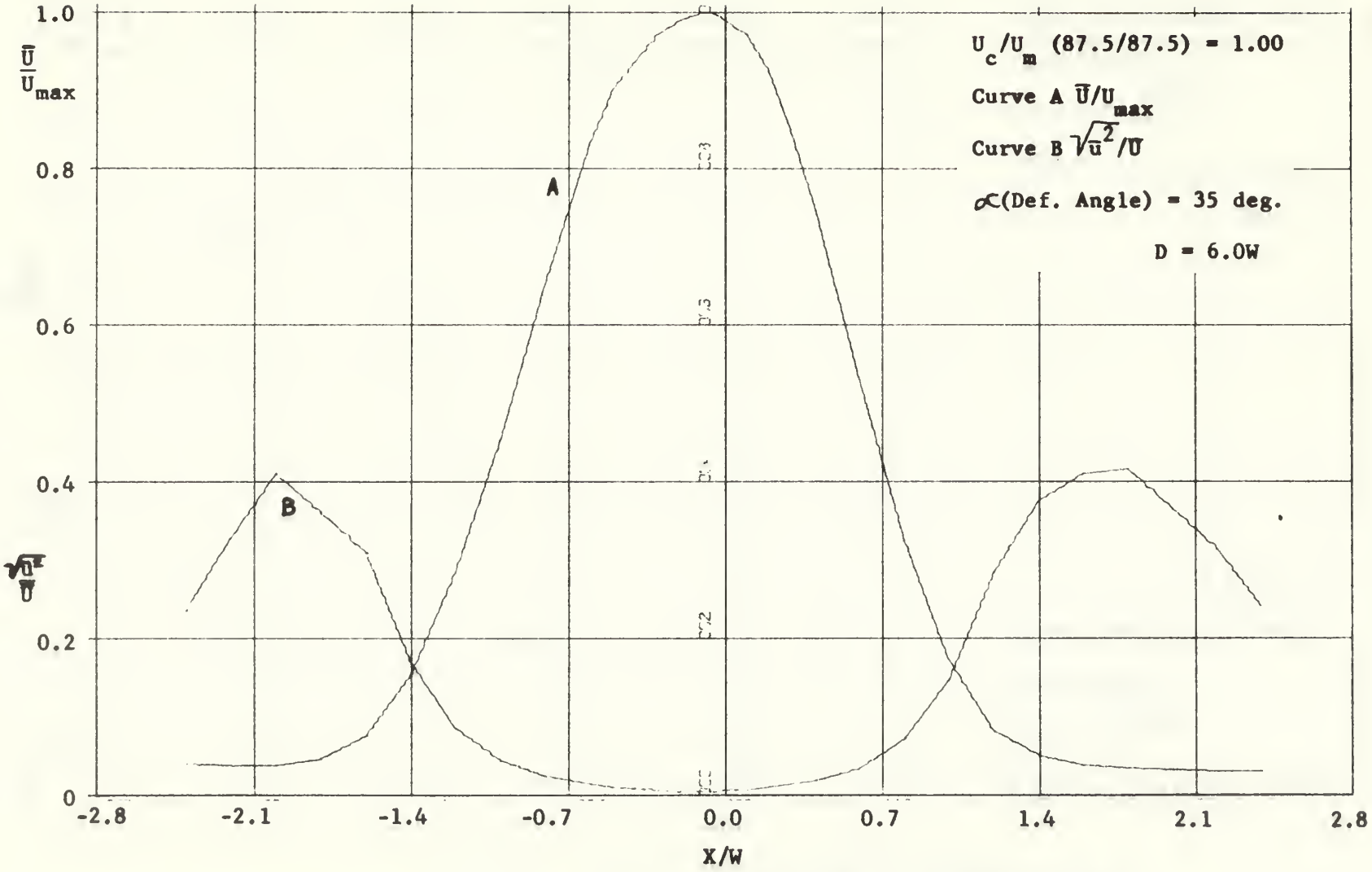

FIGURE 19. VELOCITY AND TURBULENCE INTENSITY PROFILES

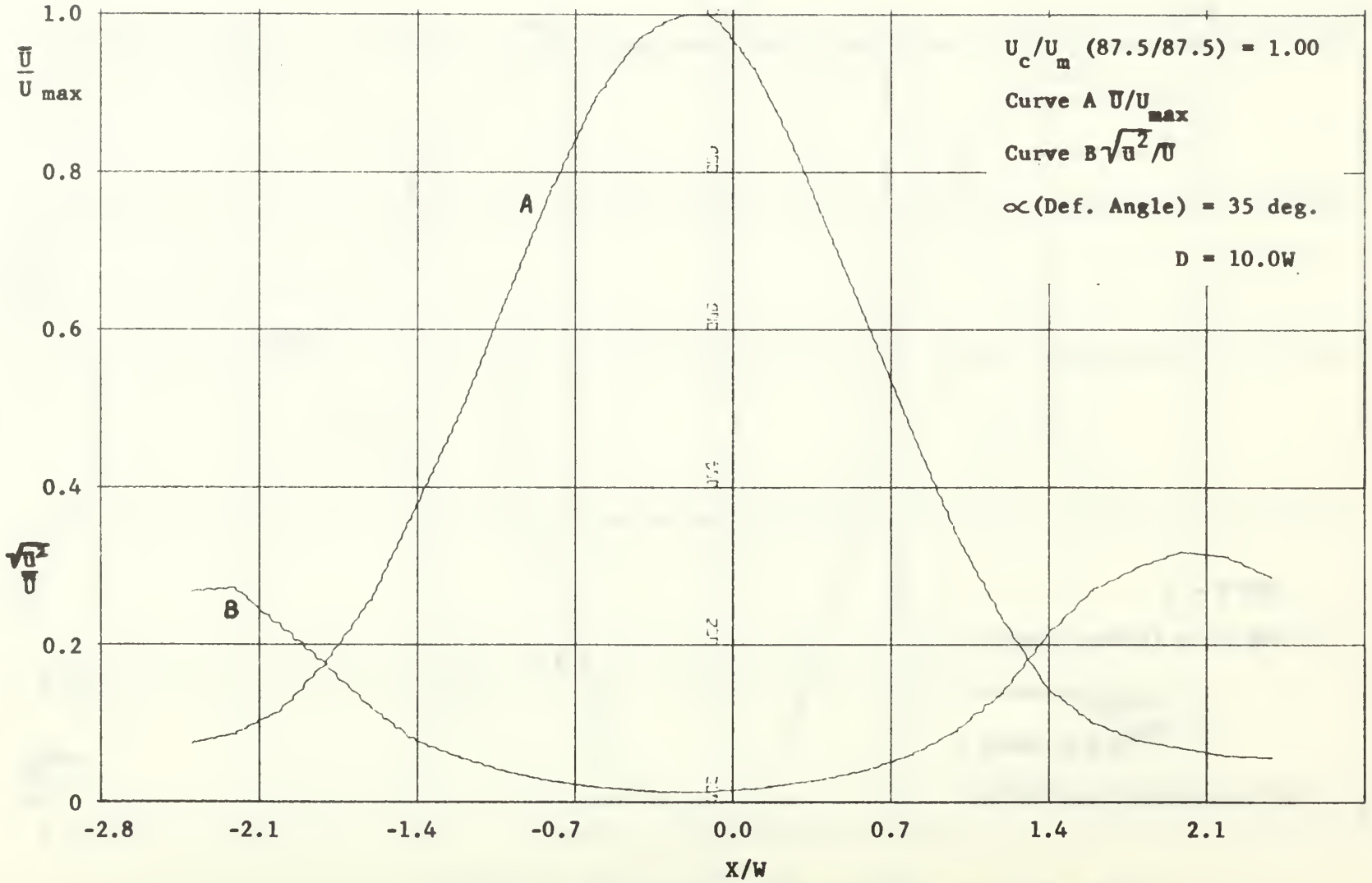

FIGURE 20. VELOCITY AND TURBULENCE INTENSITY PROFILES

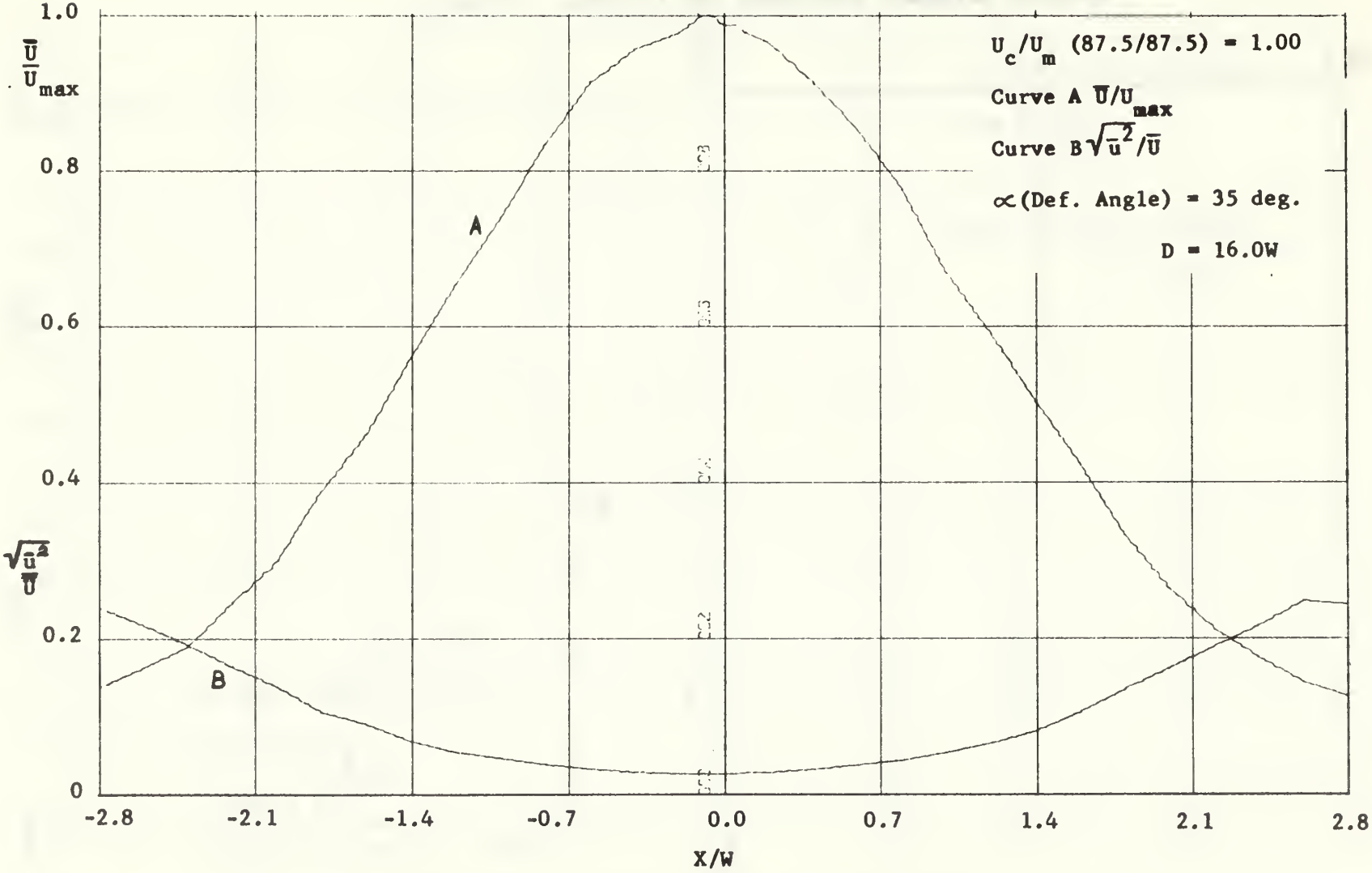

FIGURE 21. VELOCITY AND TURBULENCE INTENSITY PROFILES

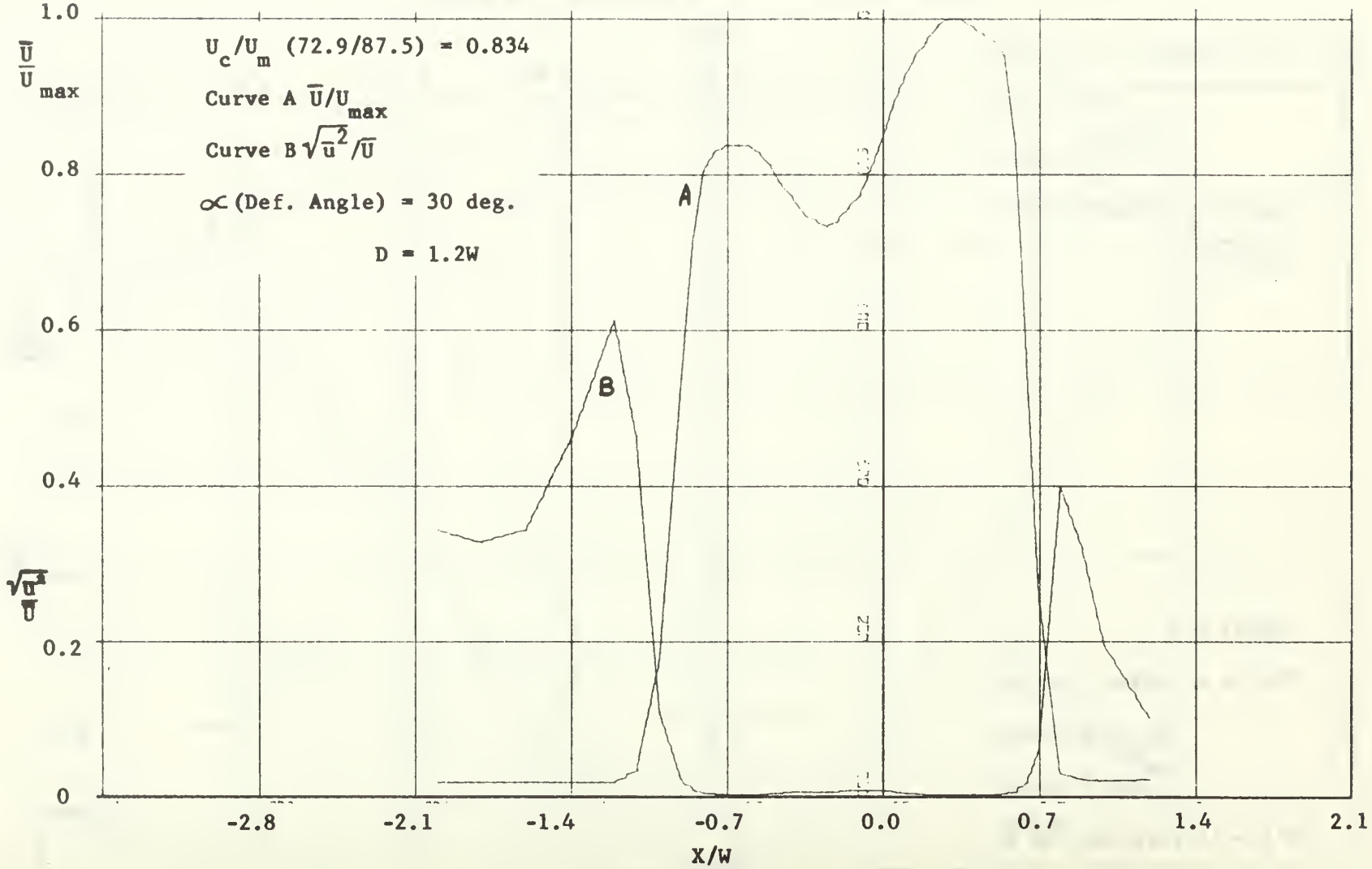

FIGURE 22. VELOCITY AND TURBULENCE INTENSITY PROFILES

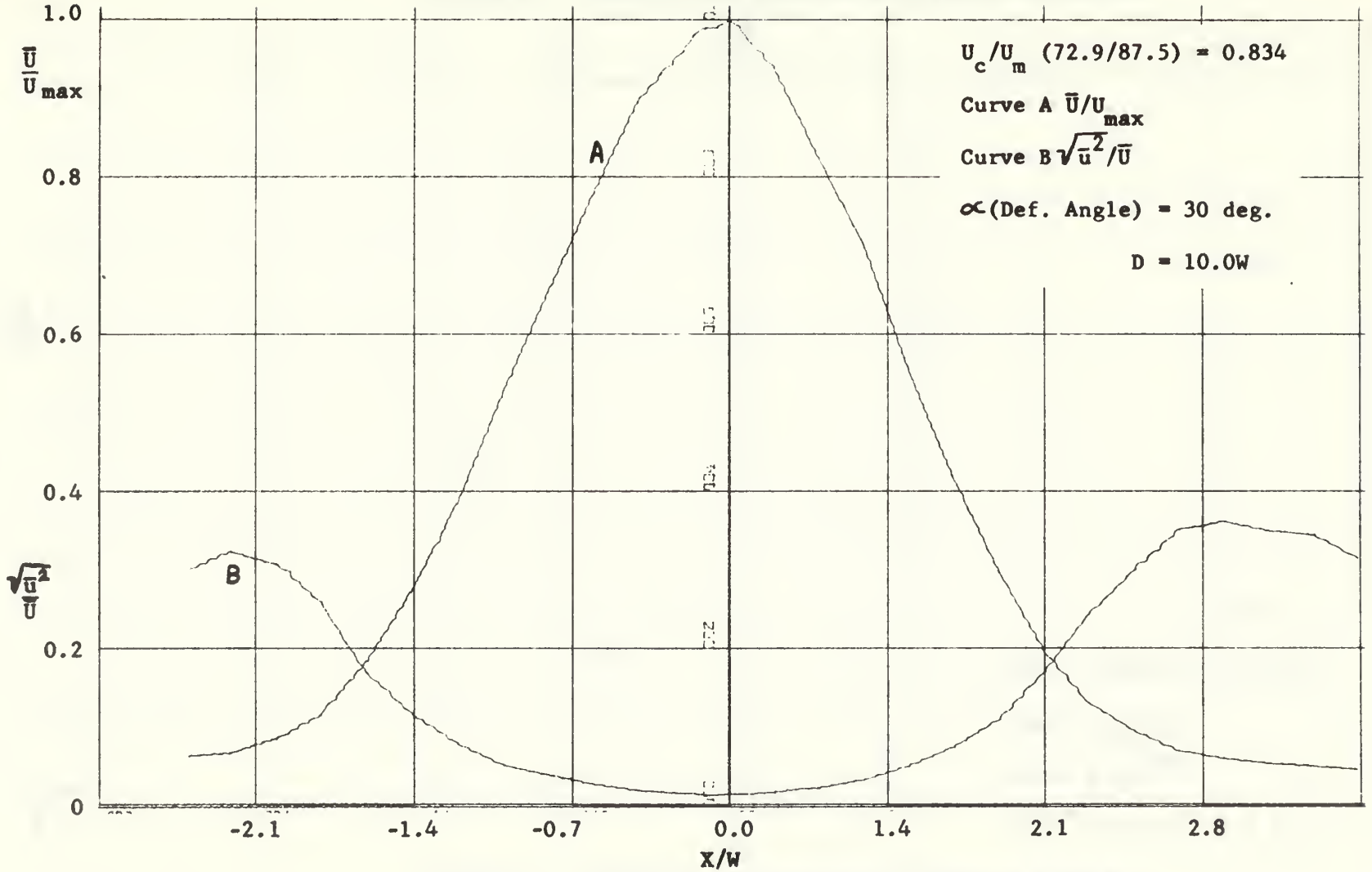

FIGURE 23. VELOCITY AND TURBULENCE INTENSITY PROFILE

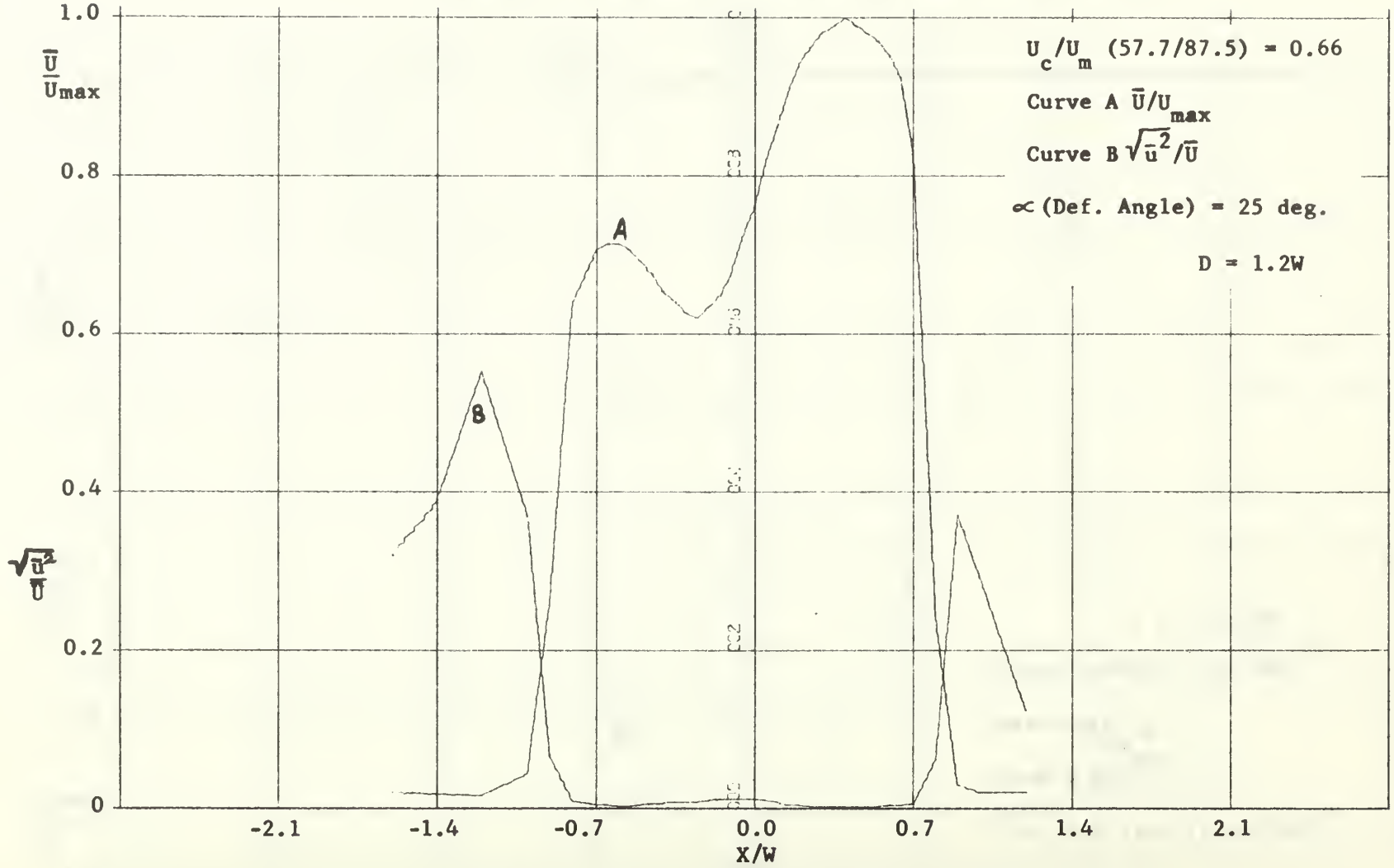

FIGURE 24. VELOCITY AND TURBULENCE INTENSITY PROFILES

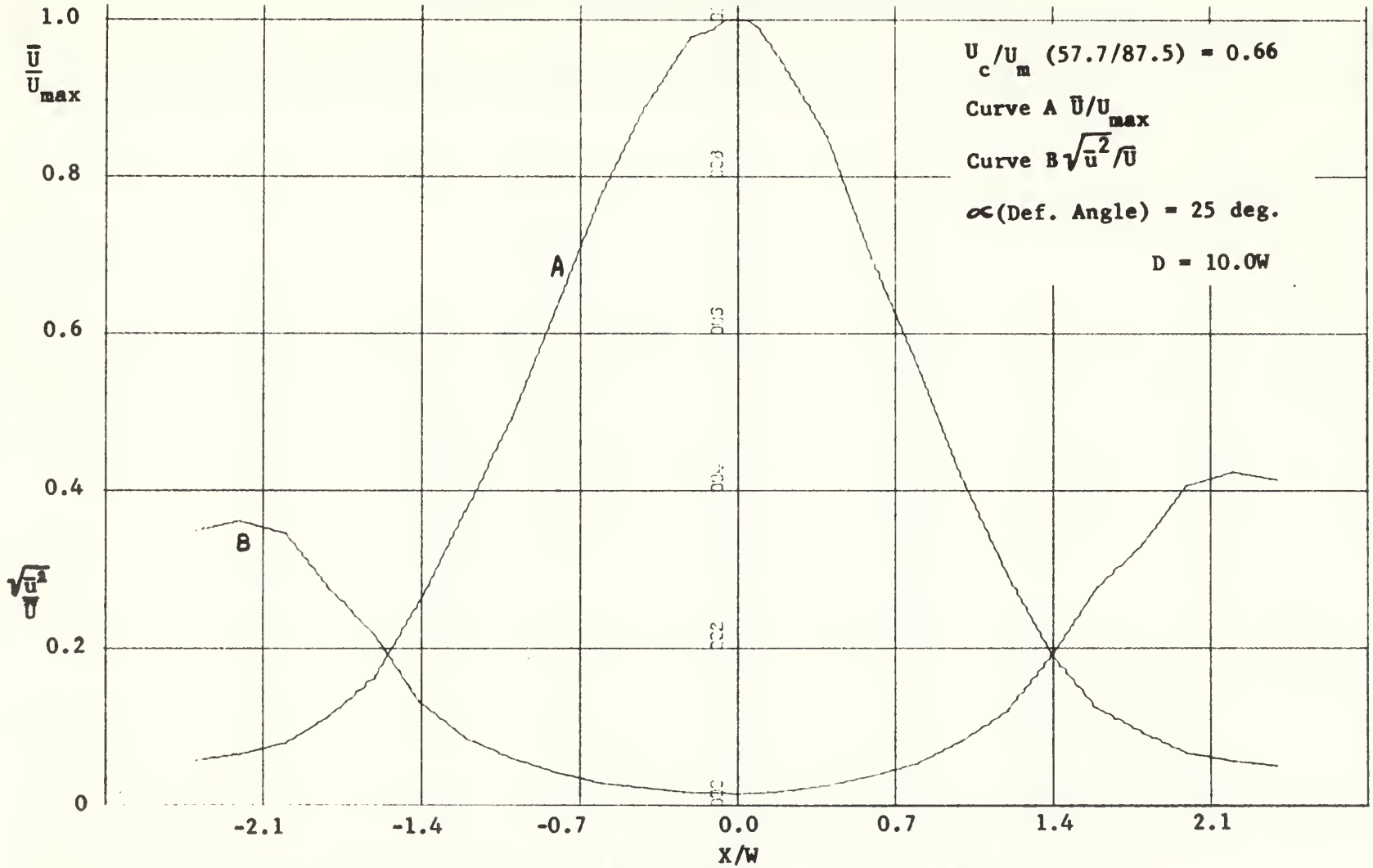

FIGURE 25. VELOCITY AND TURBULENCE INTENSITY PROFILES

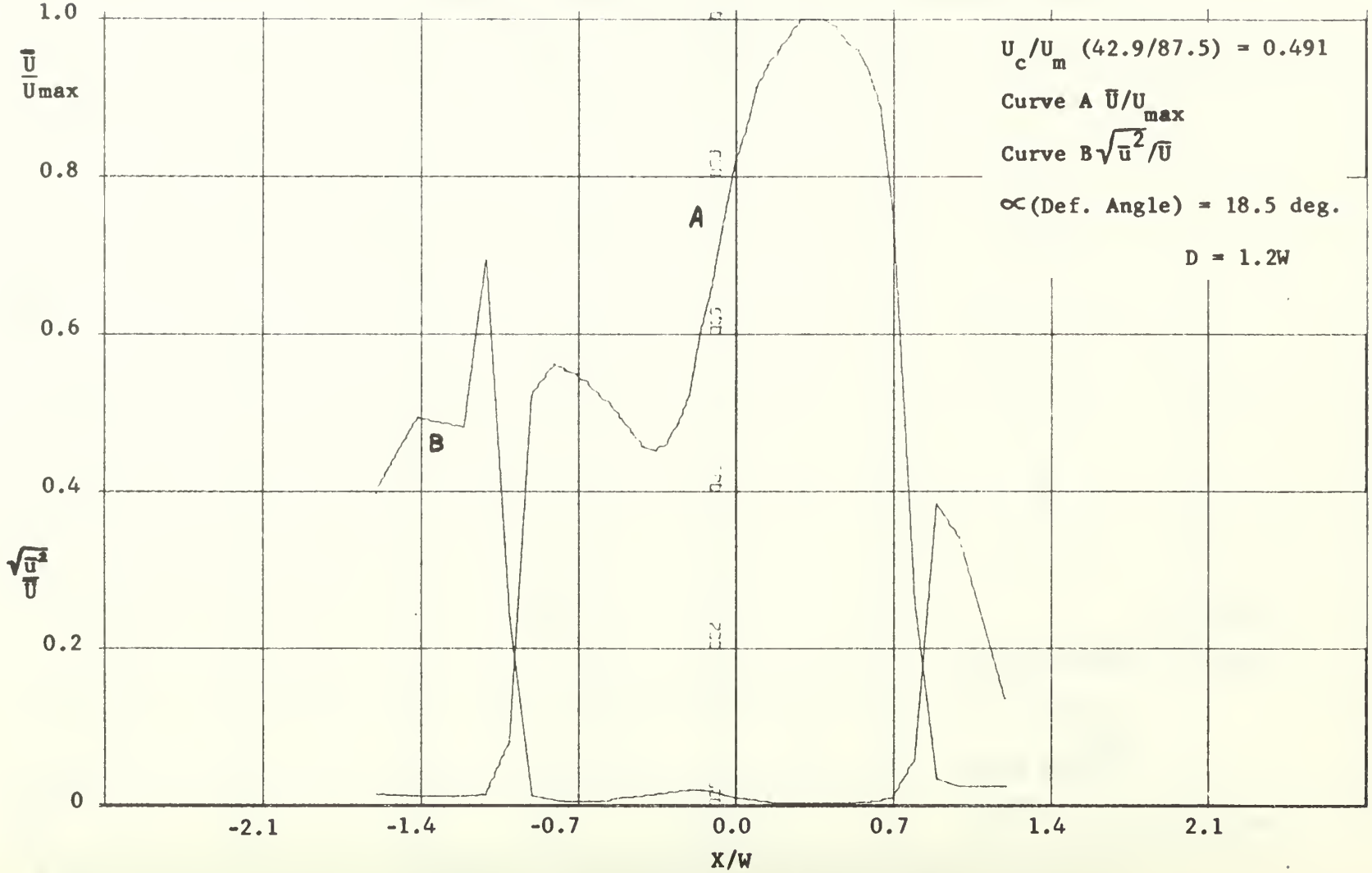

FIGURE 26. VELOCITY AND TURBULENCE INTENSITY PROFILES

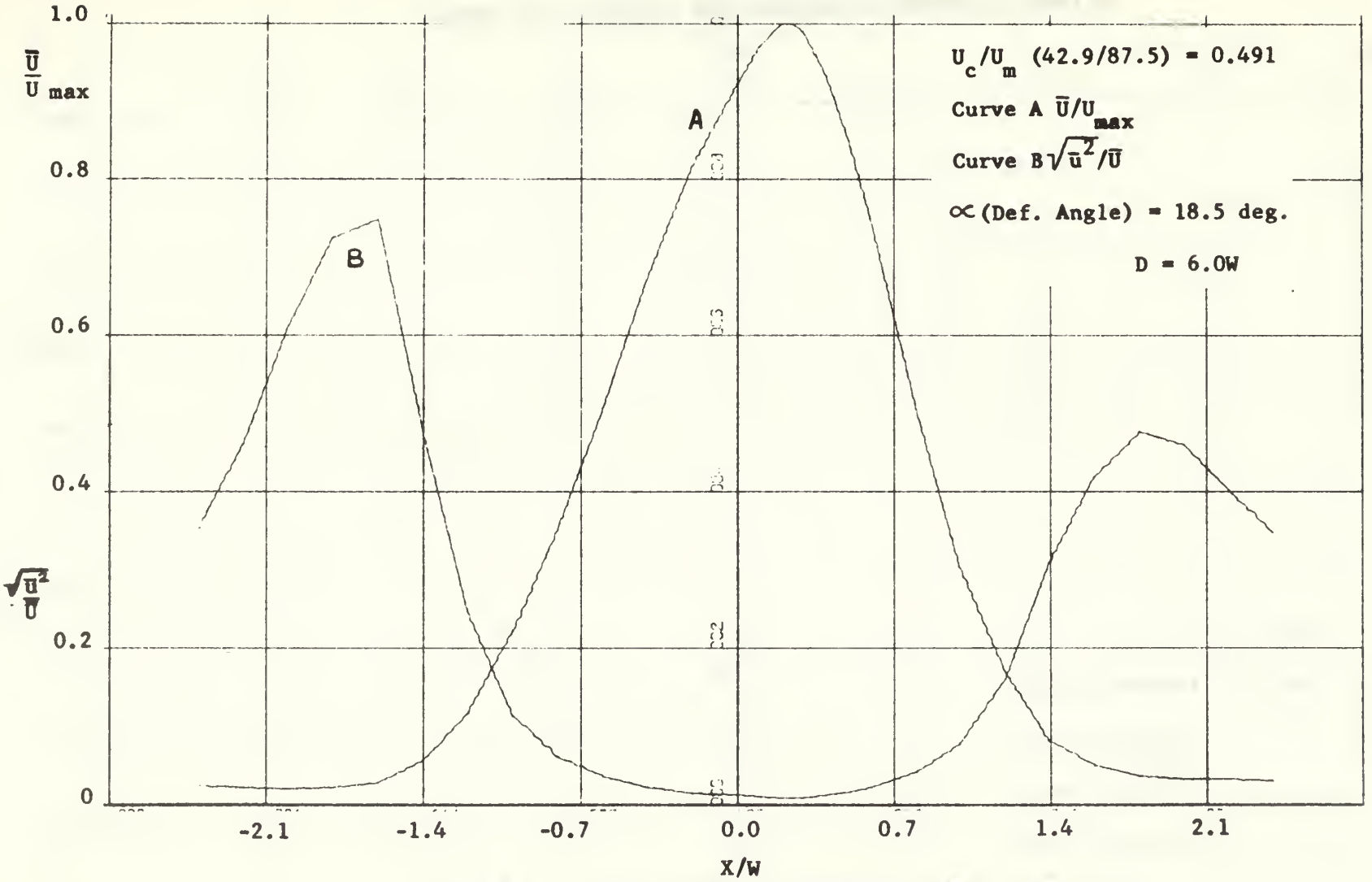

FIGURE 27. VELOCITY AND TURBULENCE INTENSITY PROFILES

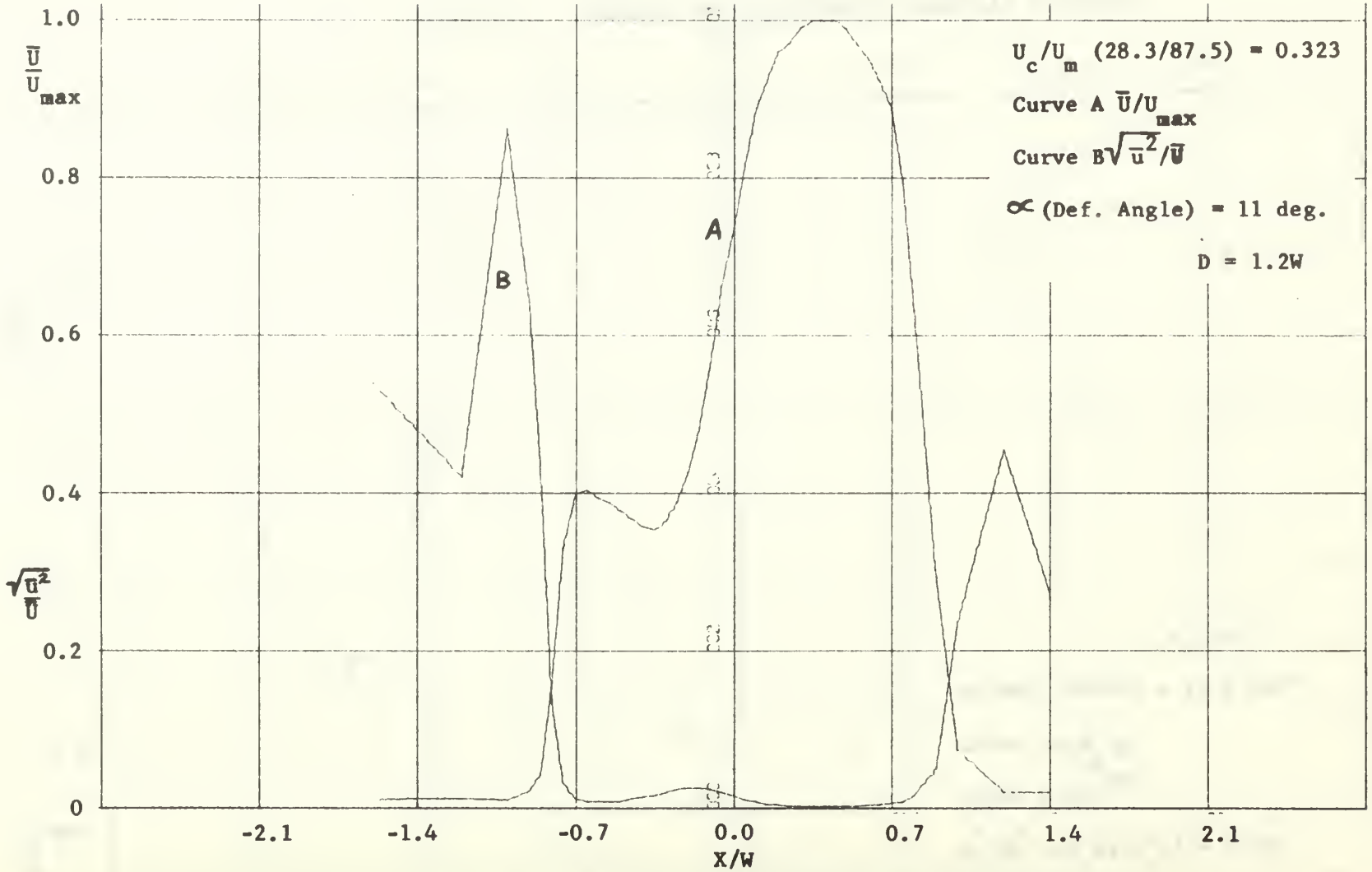

FIGURE 28. VELOCITY AND TURBULENCE INTENSITY PROFILES

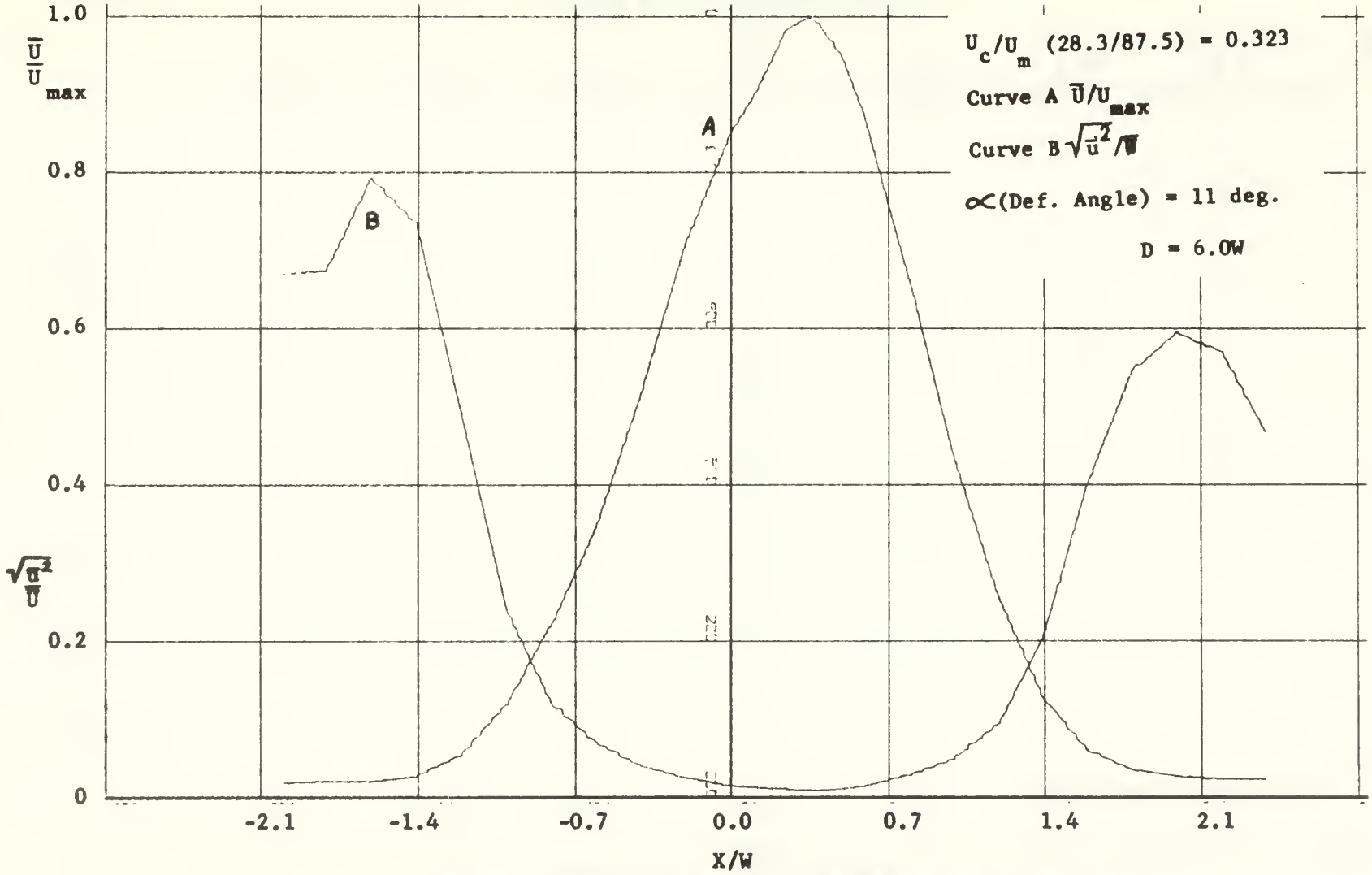

FIGURE 29. VELOCITY AND TURBULENCE INTENSITY PROFILES

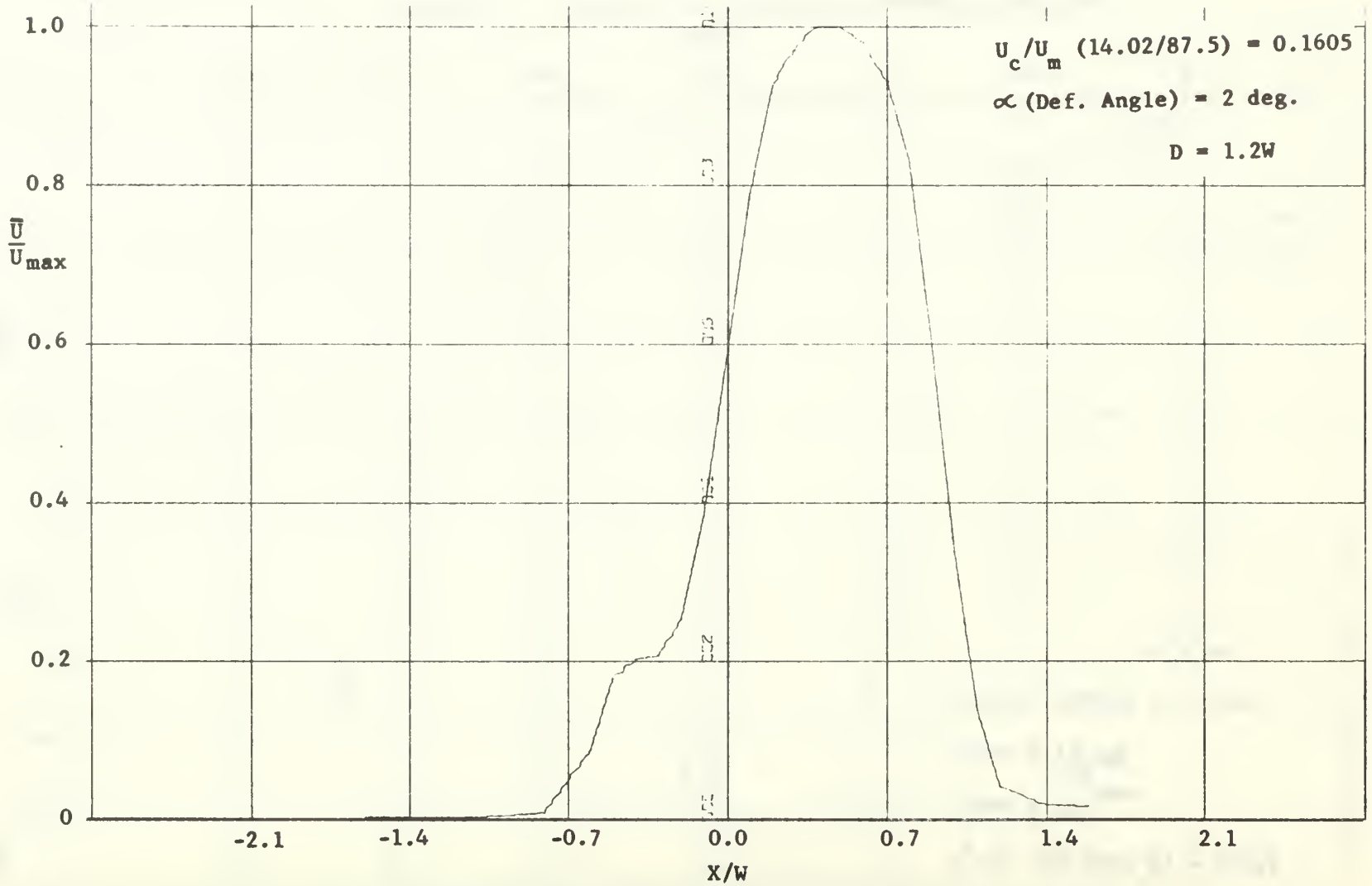

FIGURE 30. VELOCITY PROFILE

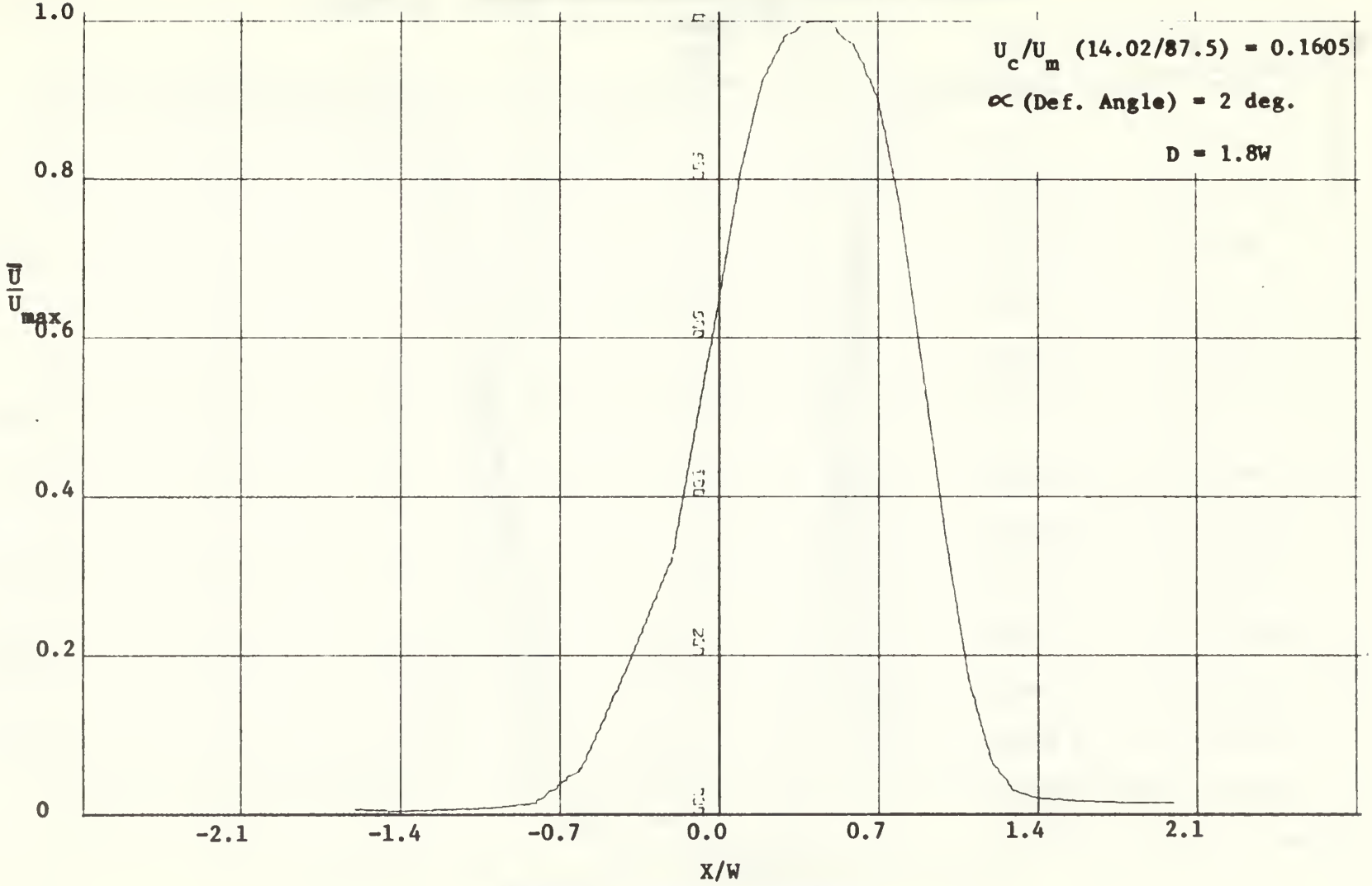

FIGURE 31. VELOCITY PROFILE

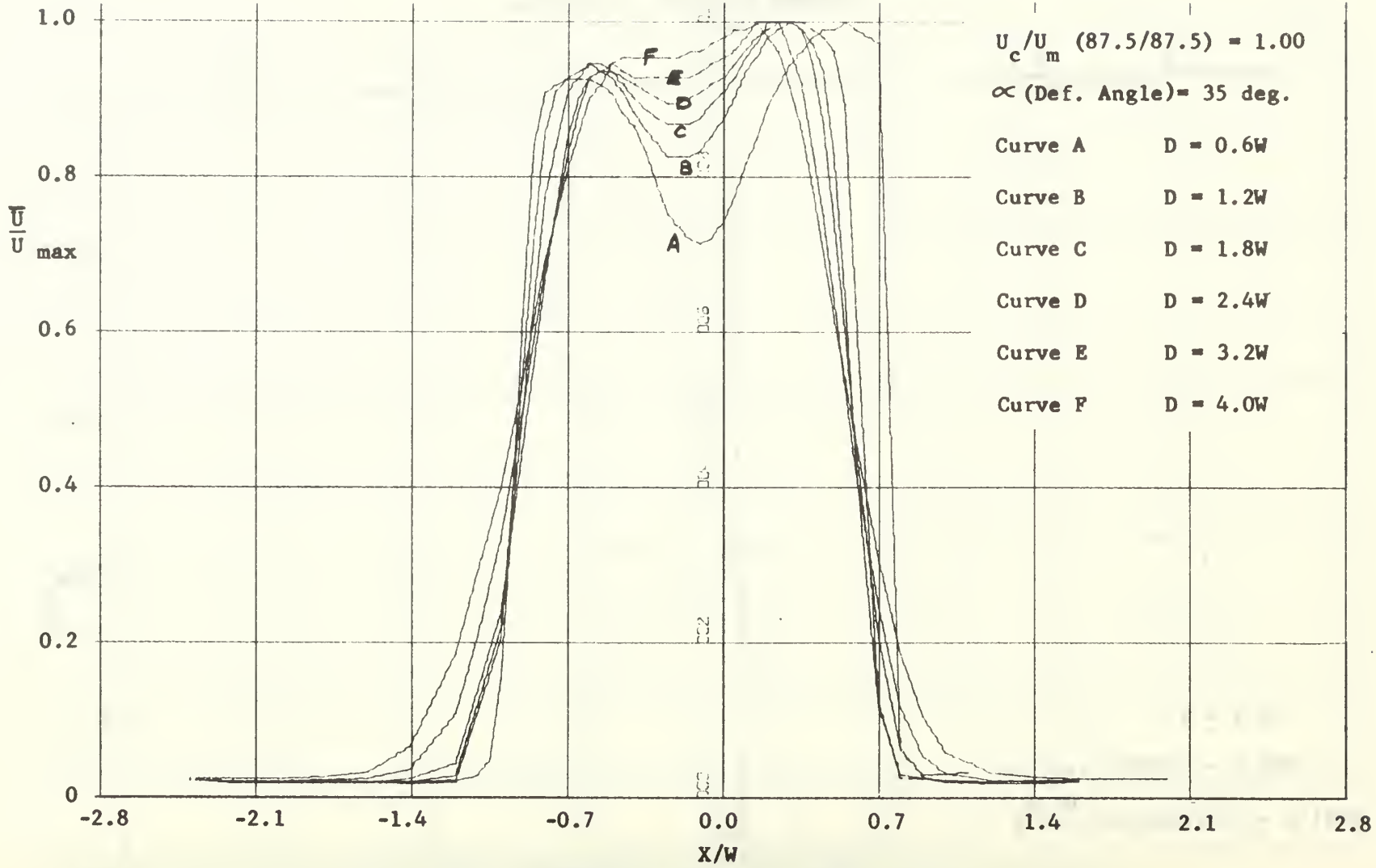

FIGURE 32. MIXING-REGION NORMALIZED VELOCITY PROFILES

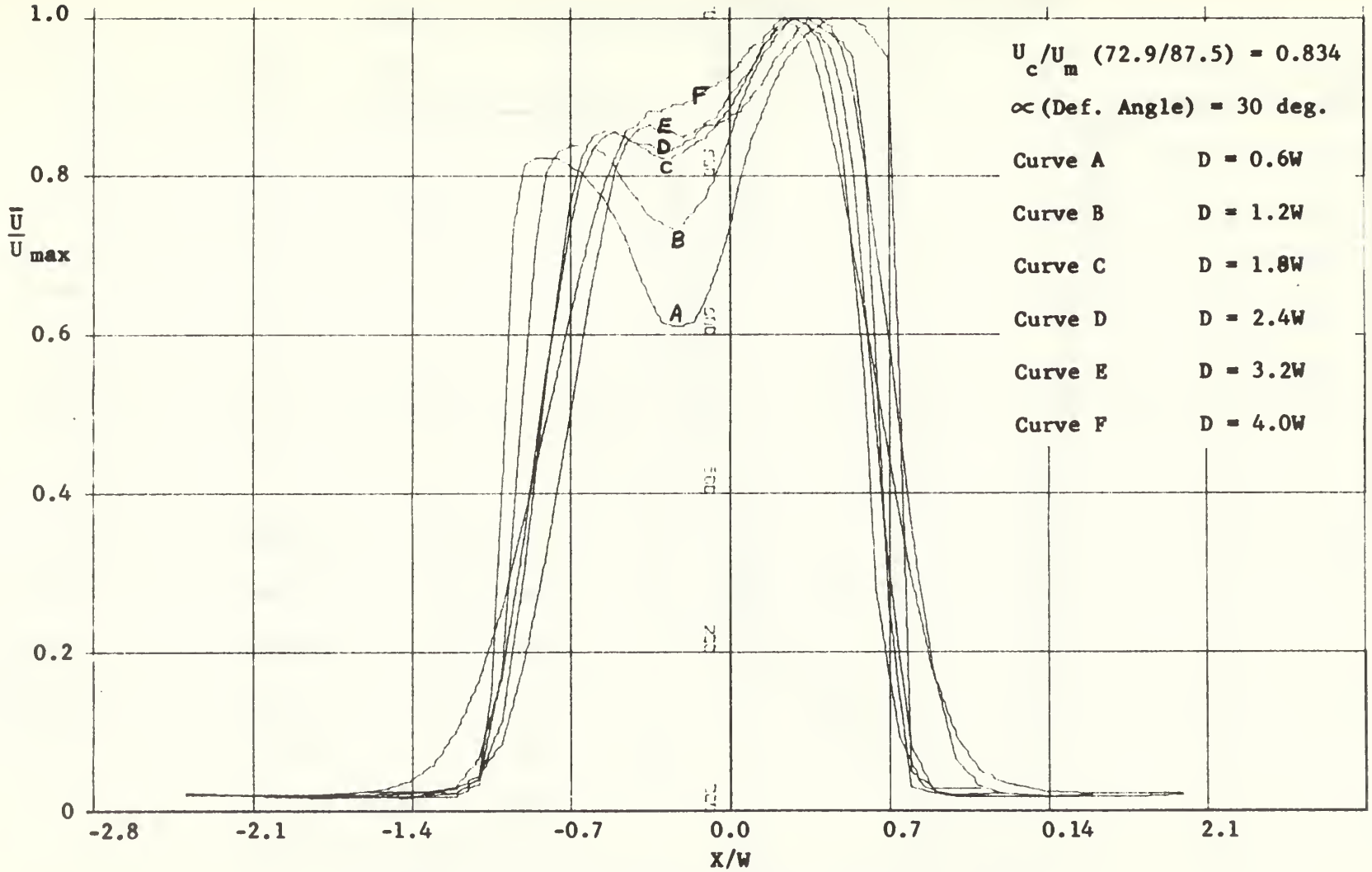

FIGURE 33. MIXING-REGION NORMALIZED VELOCITY PROFILES

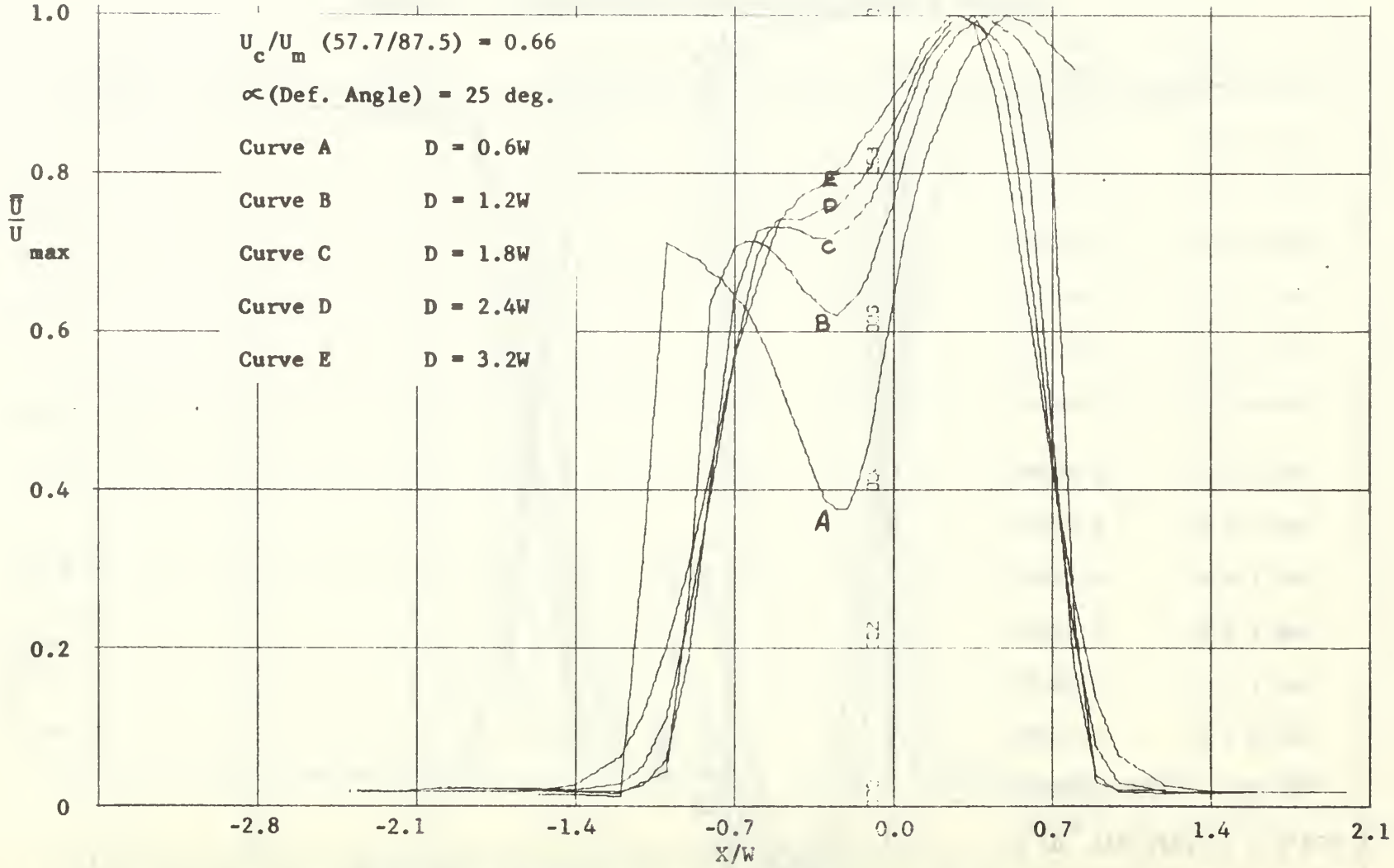

FIGURE 34. [illegible]XING-REGION NORMALIZED [illegible]ES

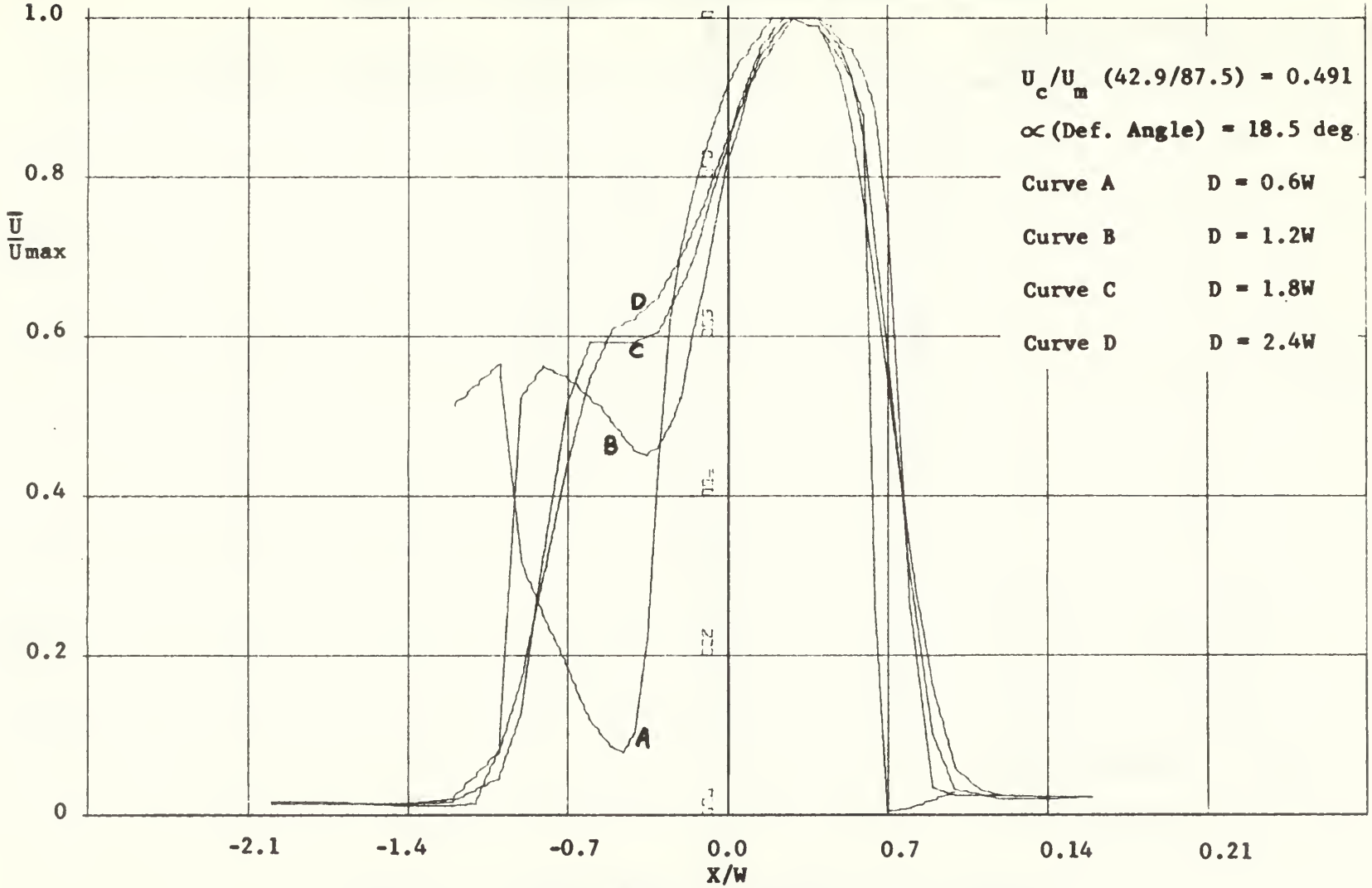

FIGURE 35. MIXING-REGION NORMALIZED VELOCITY PROFILES

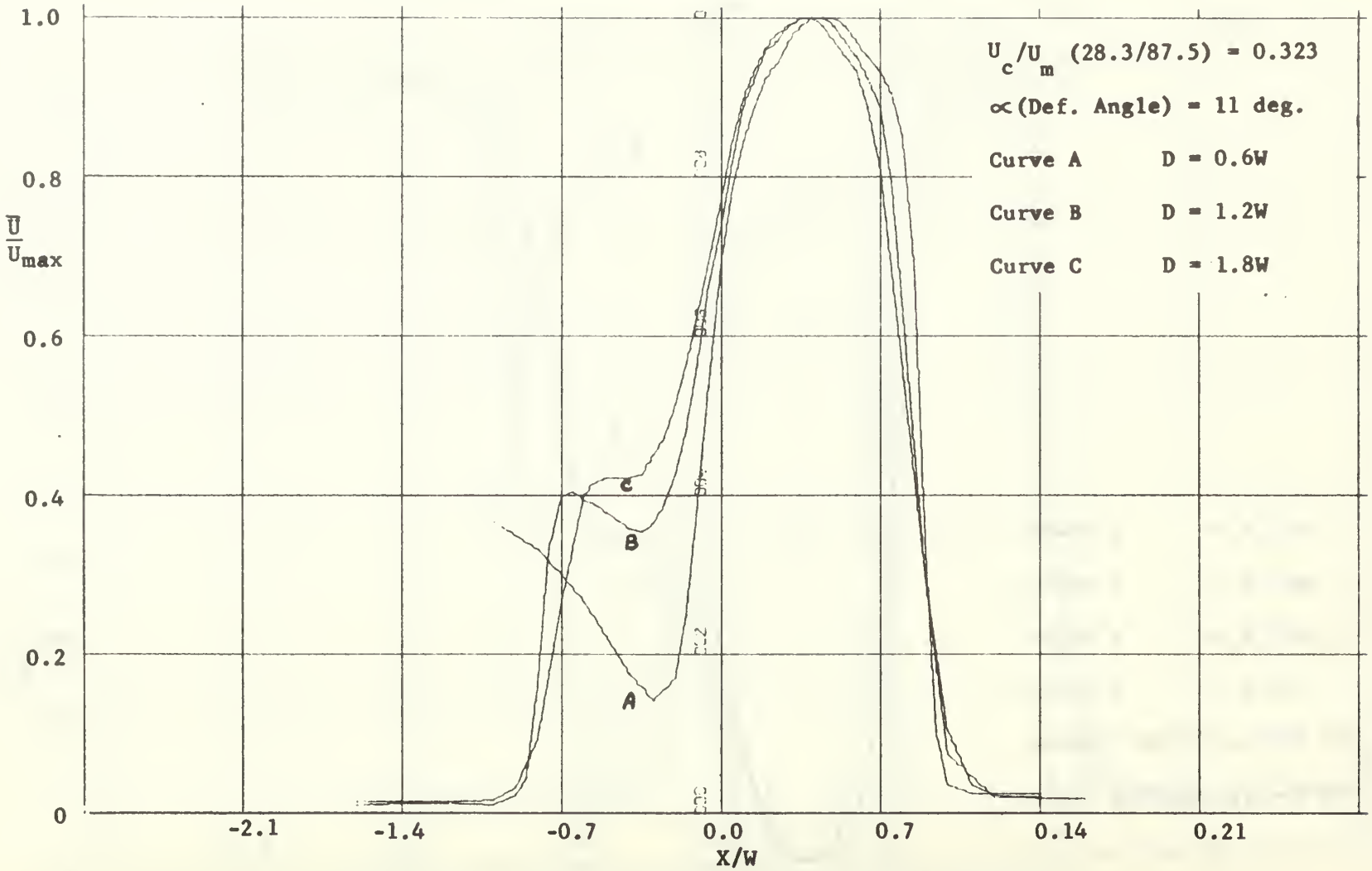

FIGURE 36. MIXING-REGION NORMALIZED VELOCITY PROFILES

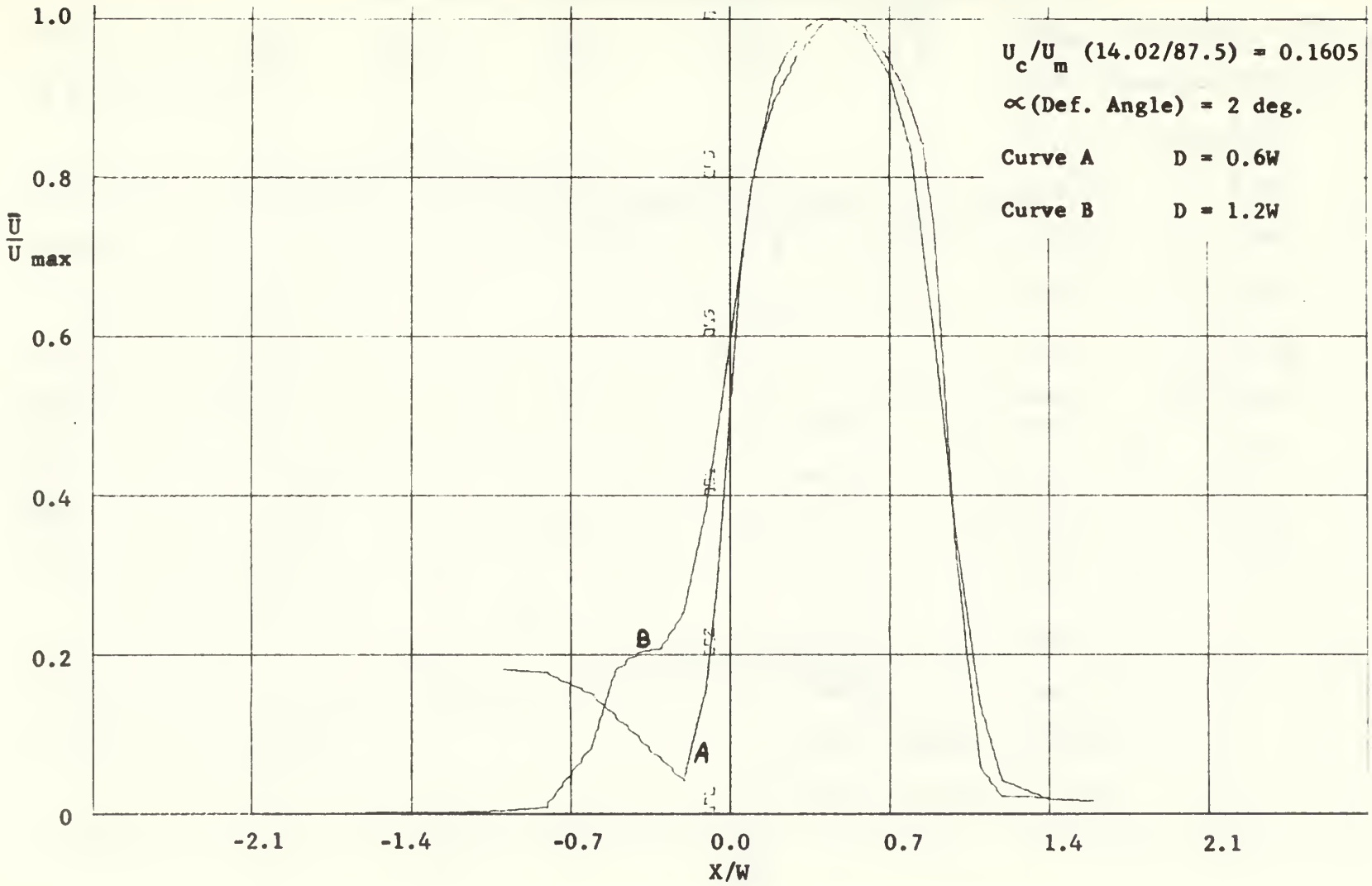

FIGURE 37. MIXING-REGION NORMALIZED VELOCITY PROFILES

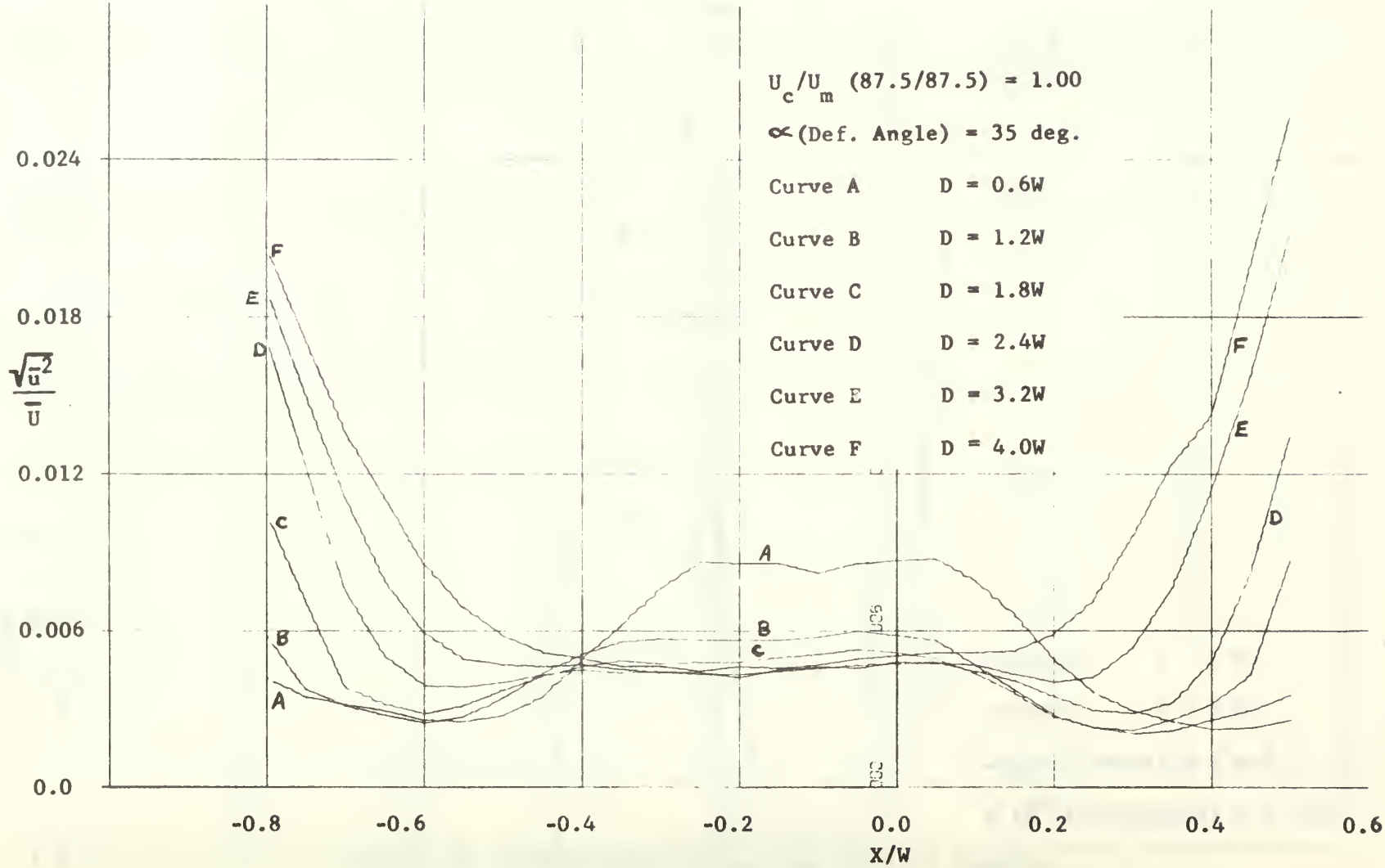

FIGURE 38. MIXING-REGION TURBULENCE INTENSITY PROFILES

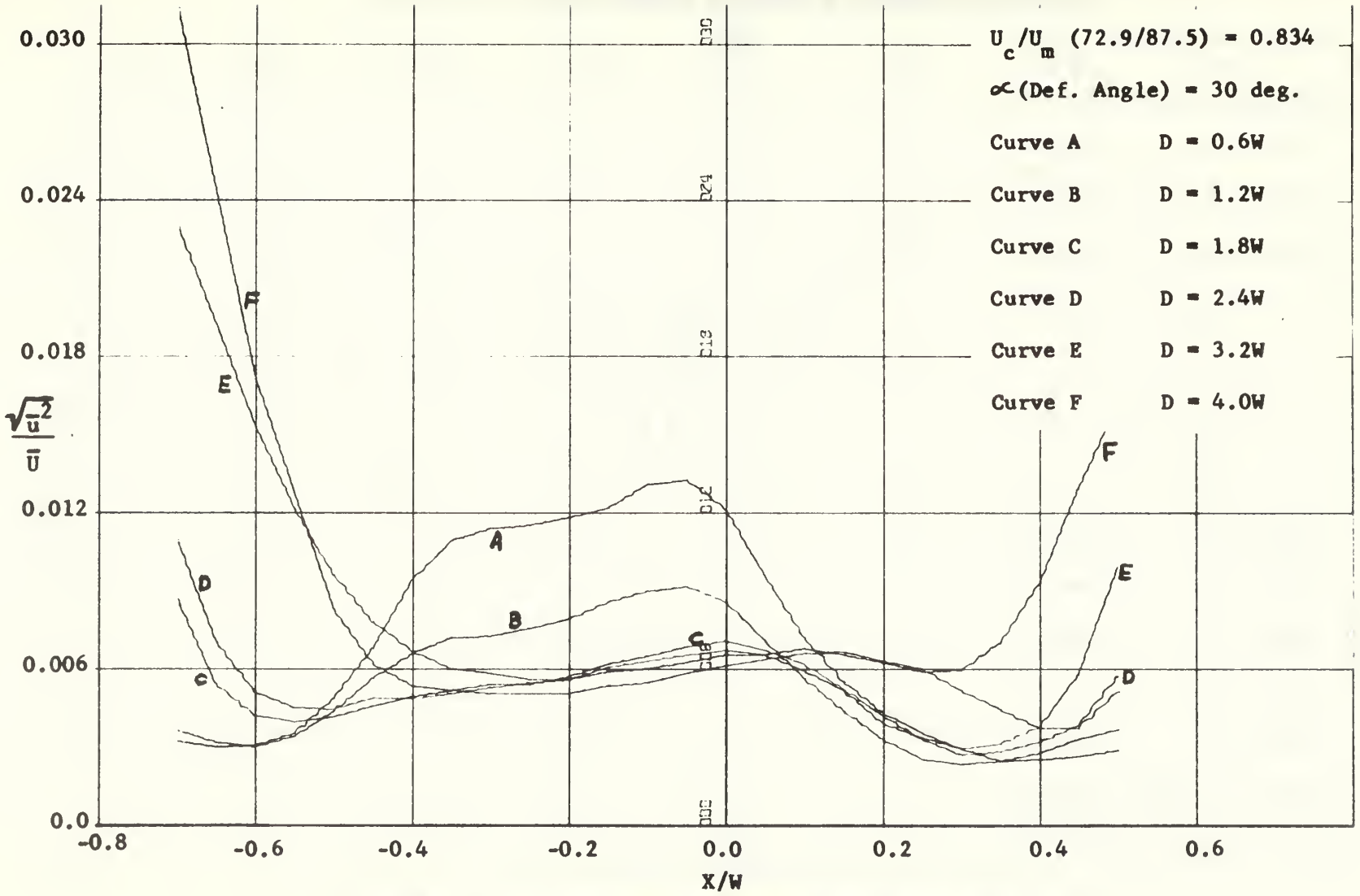

FIGURE 39. MIXING-REGION TURBULENCE INTENSITY PROFILES

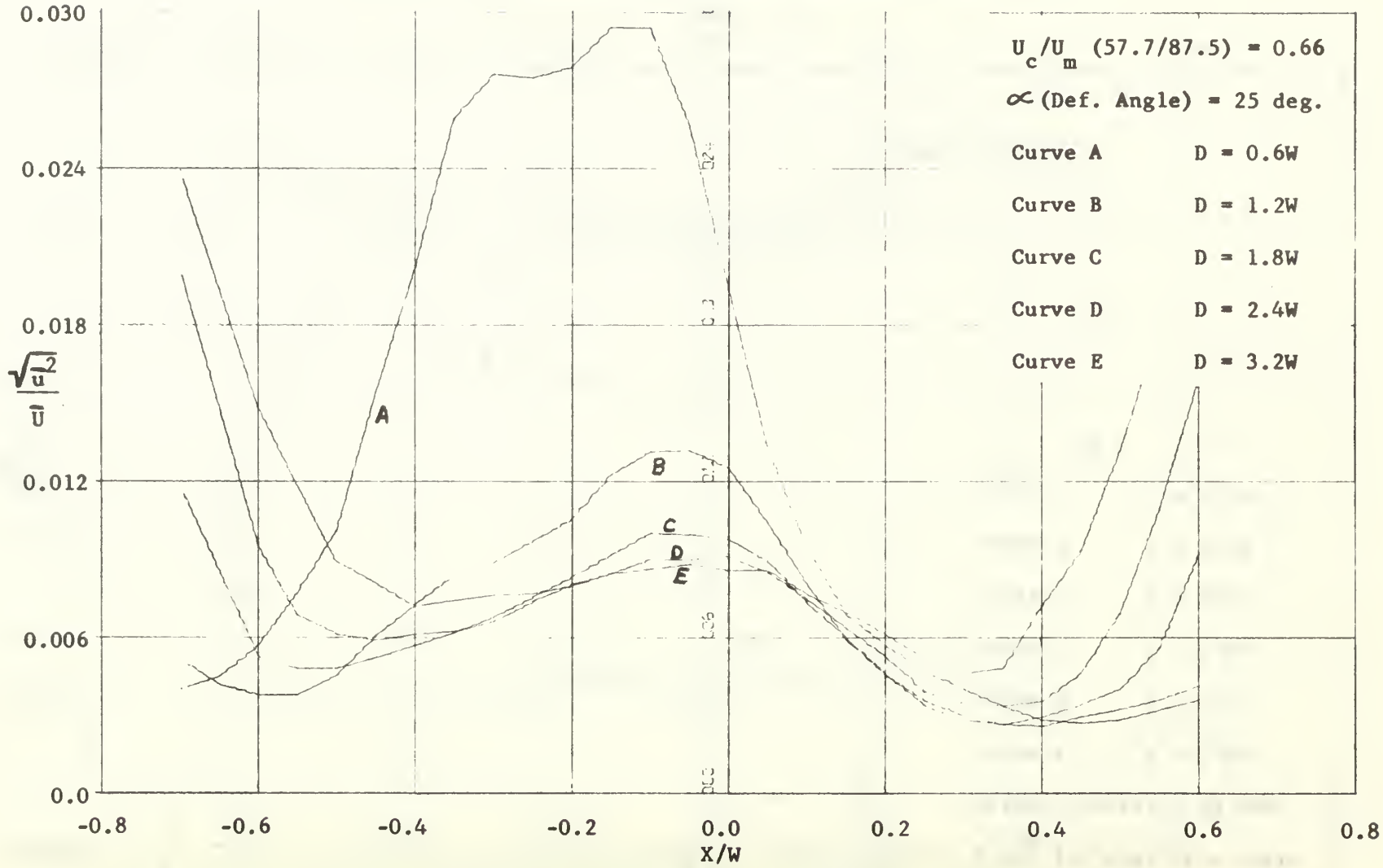

FIGURE 40. MIXING-REGION TURBULENCE INTENSITY PROFILES

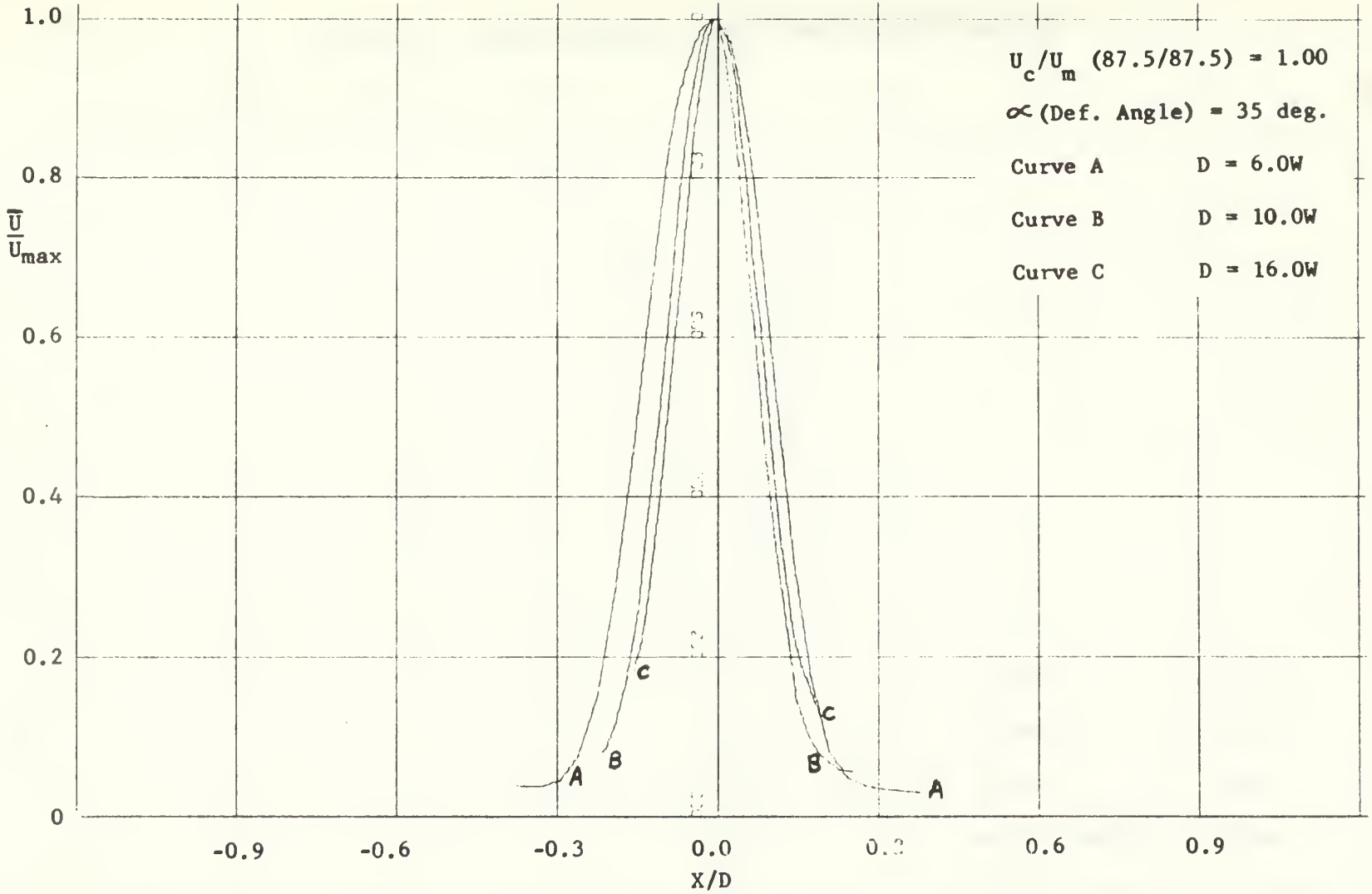

FIGURE 41. FULLY-DEVELOPED NORMALIZED VELOCITY PROFILES

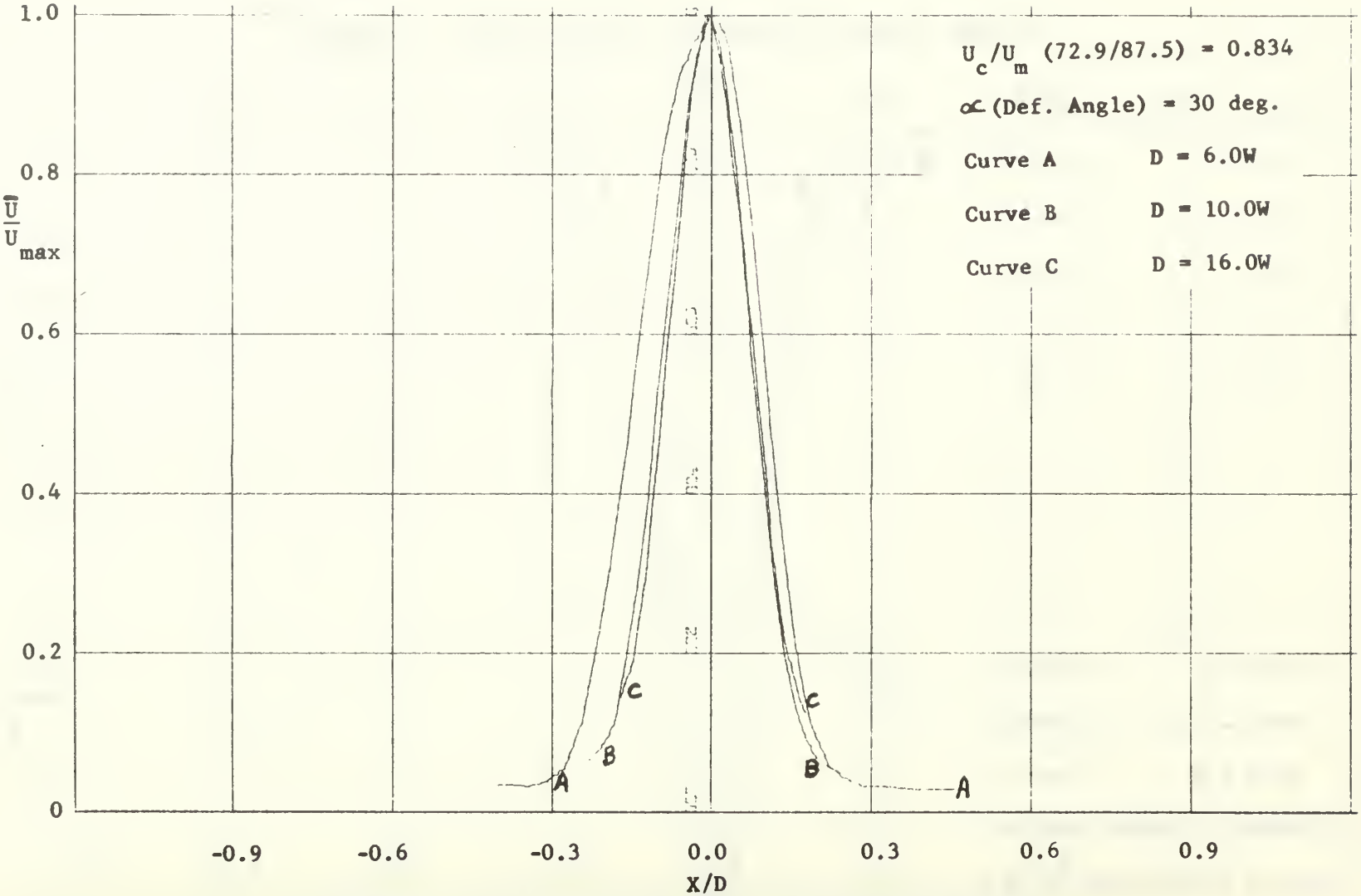

FIGURE 42. FULLY-DEVELOPED NORMALIZED VELOCITY PROFILES

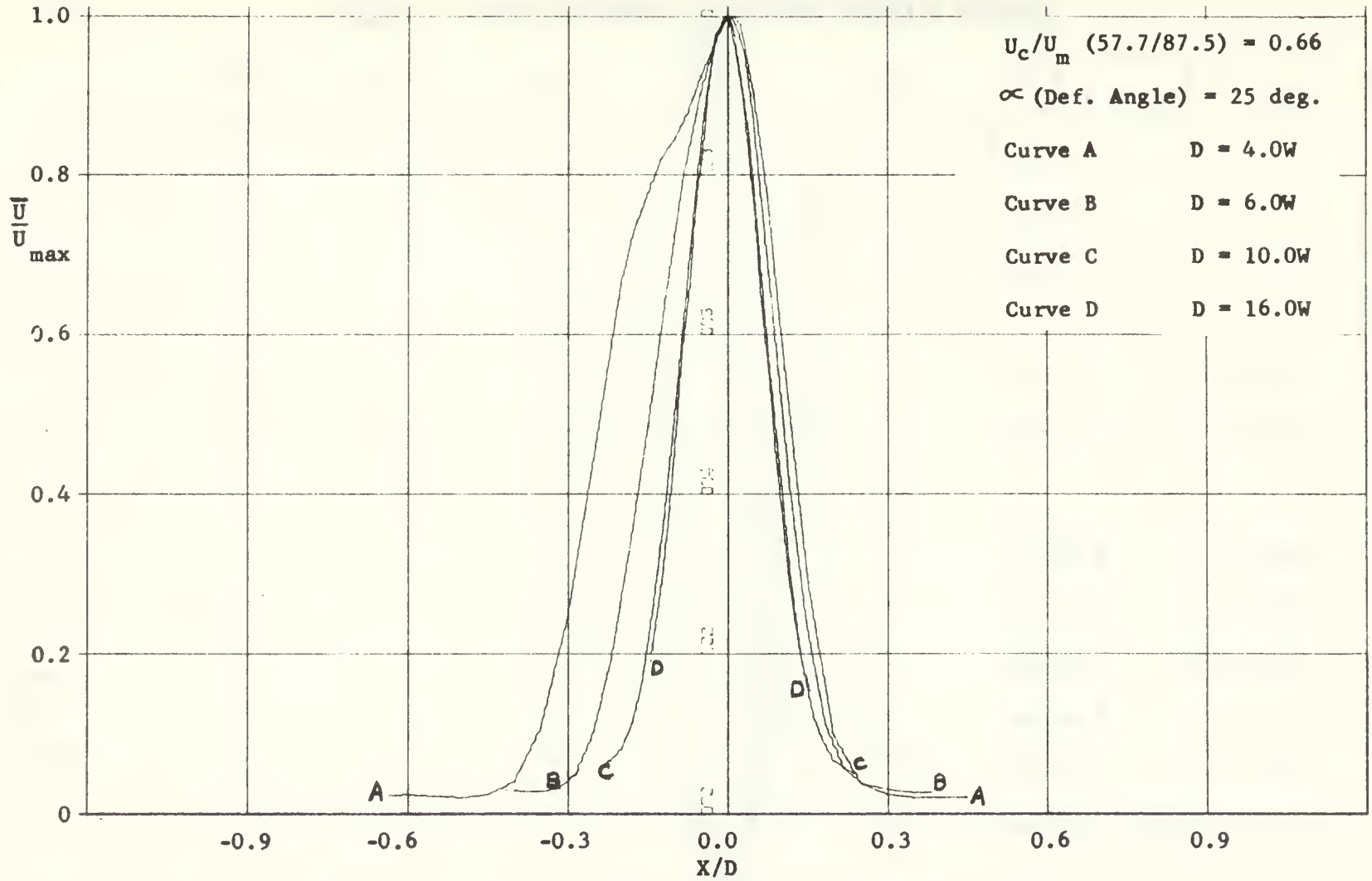

FIGURE 43. FULLY-DEVELOPED NORMALIZED VELOCITY PROFILES

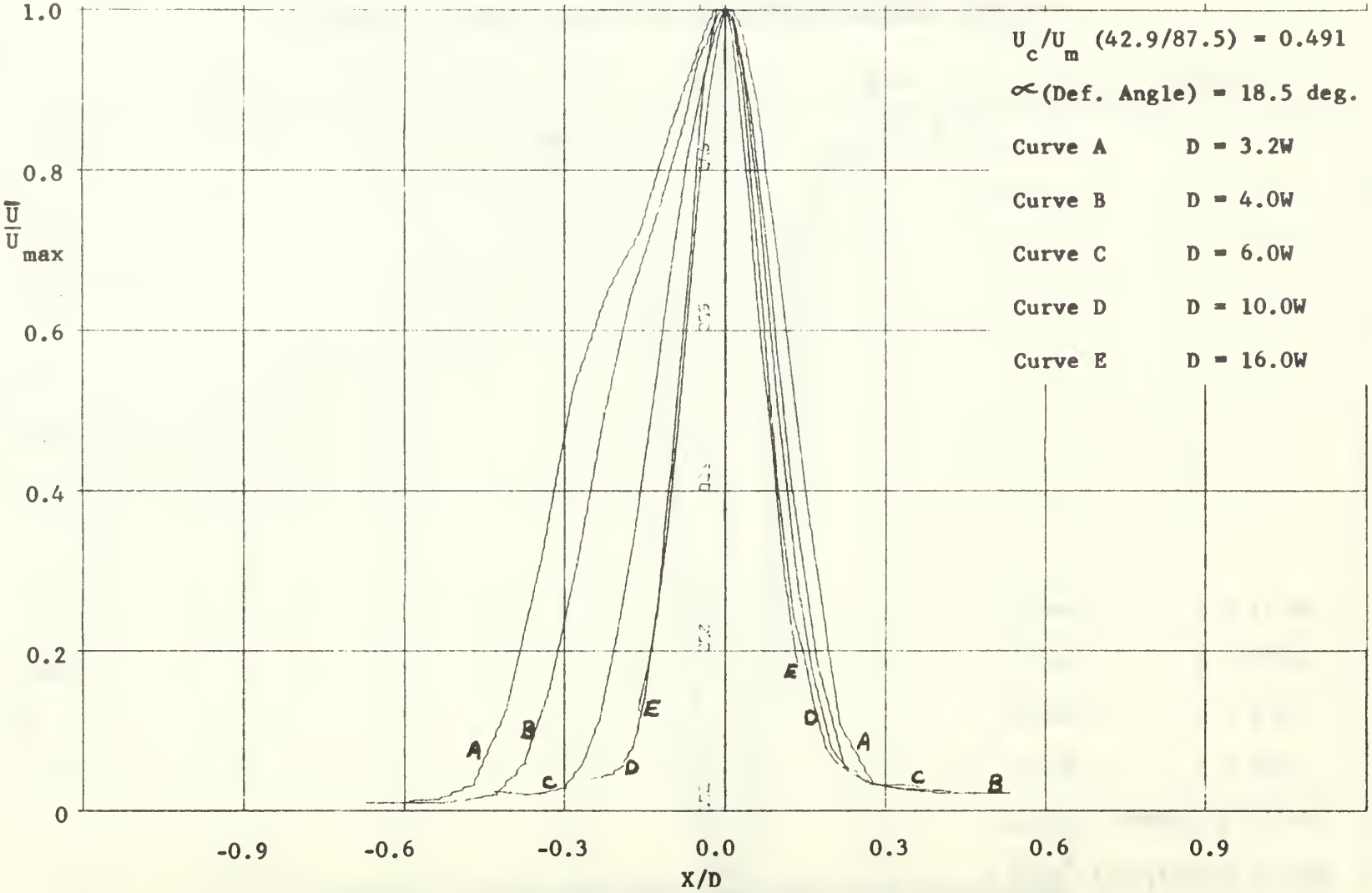

FIGURE 44. FULLY-DEVELOPED NORMALIZED VELOCITY PROFILES

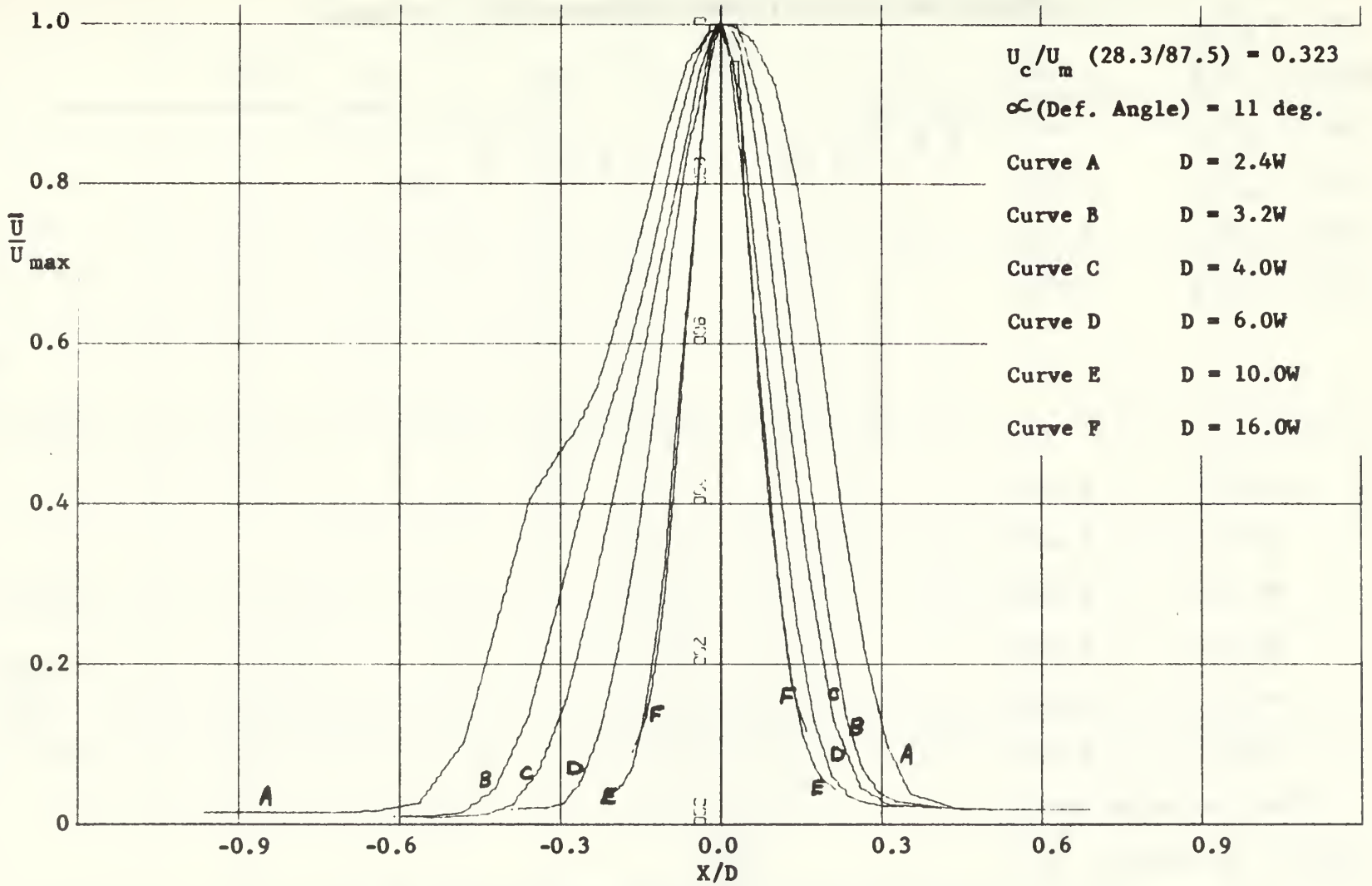

FIGURE 45. FULLY-DEVELOPED NORMALIZED VELOCITY PROFILES

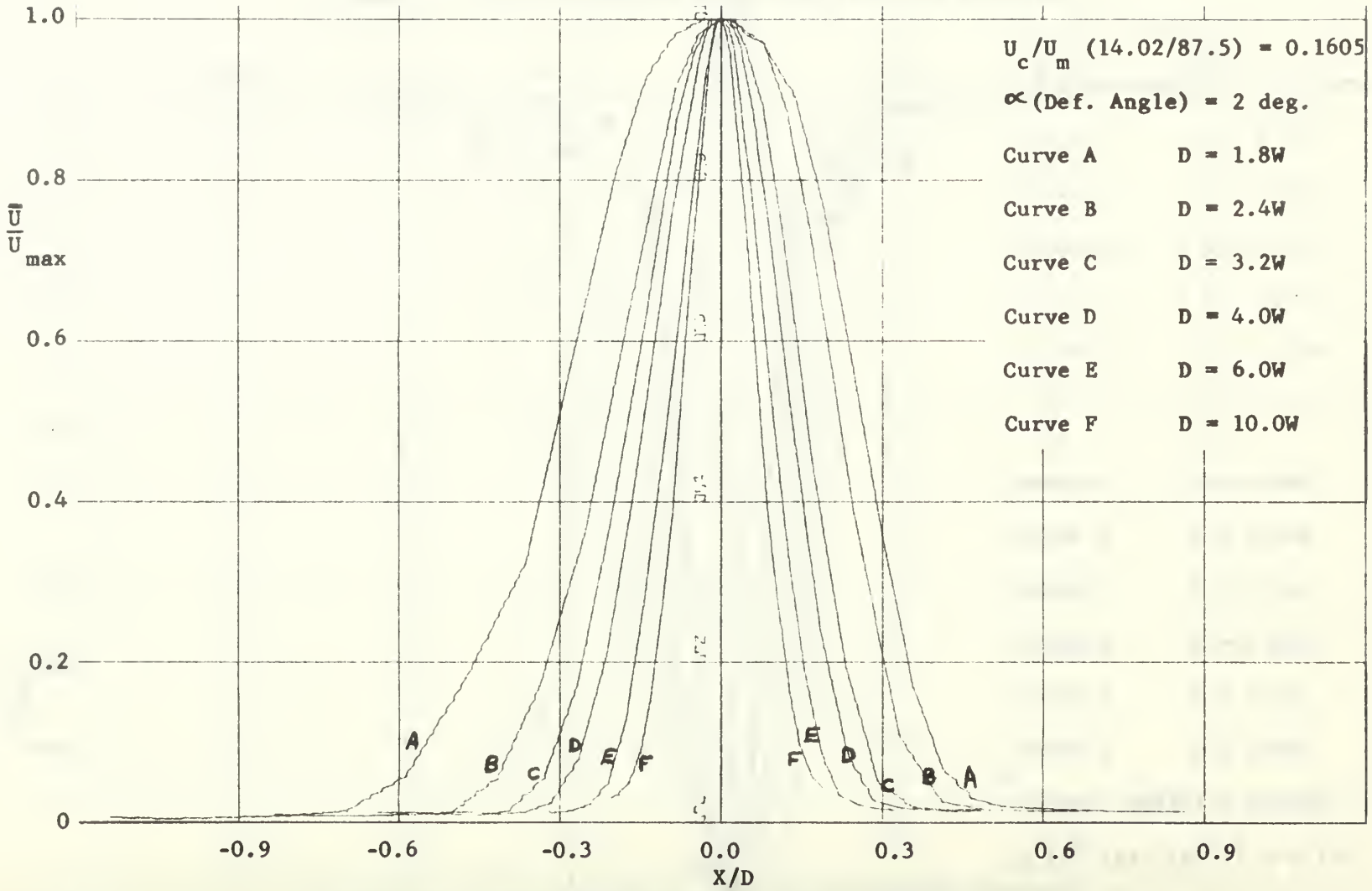

FIGURE 46. FULLY-DEVELOPED NORMALIZED VELOCITY PROFILES

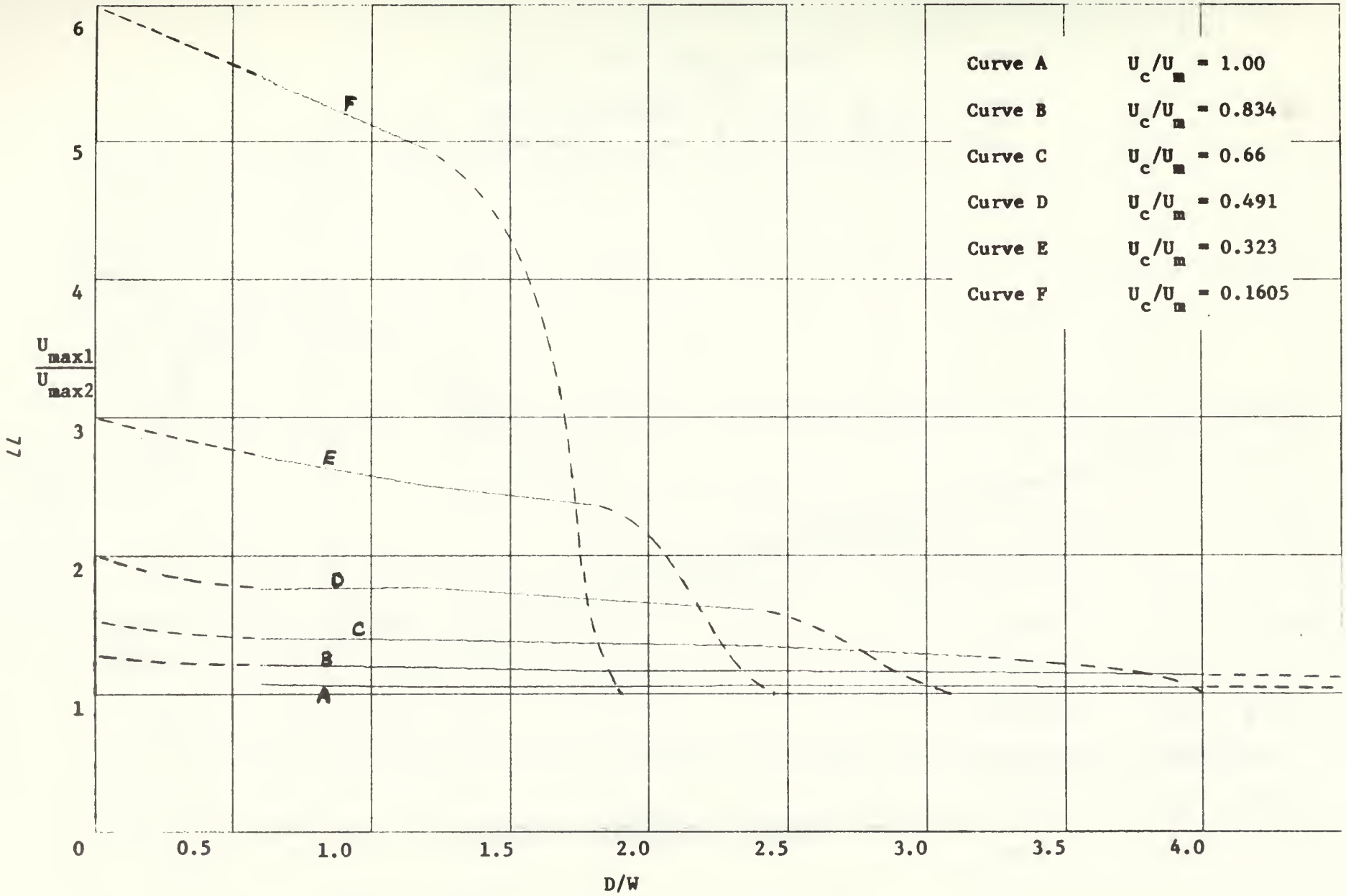

FIGURE 47. MIXING-REGION VELOCITY PROPORTIONS

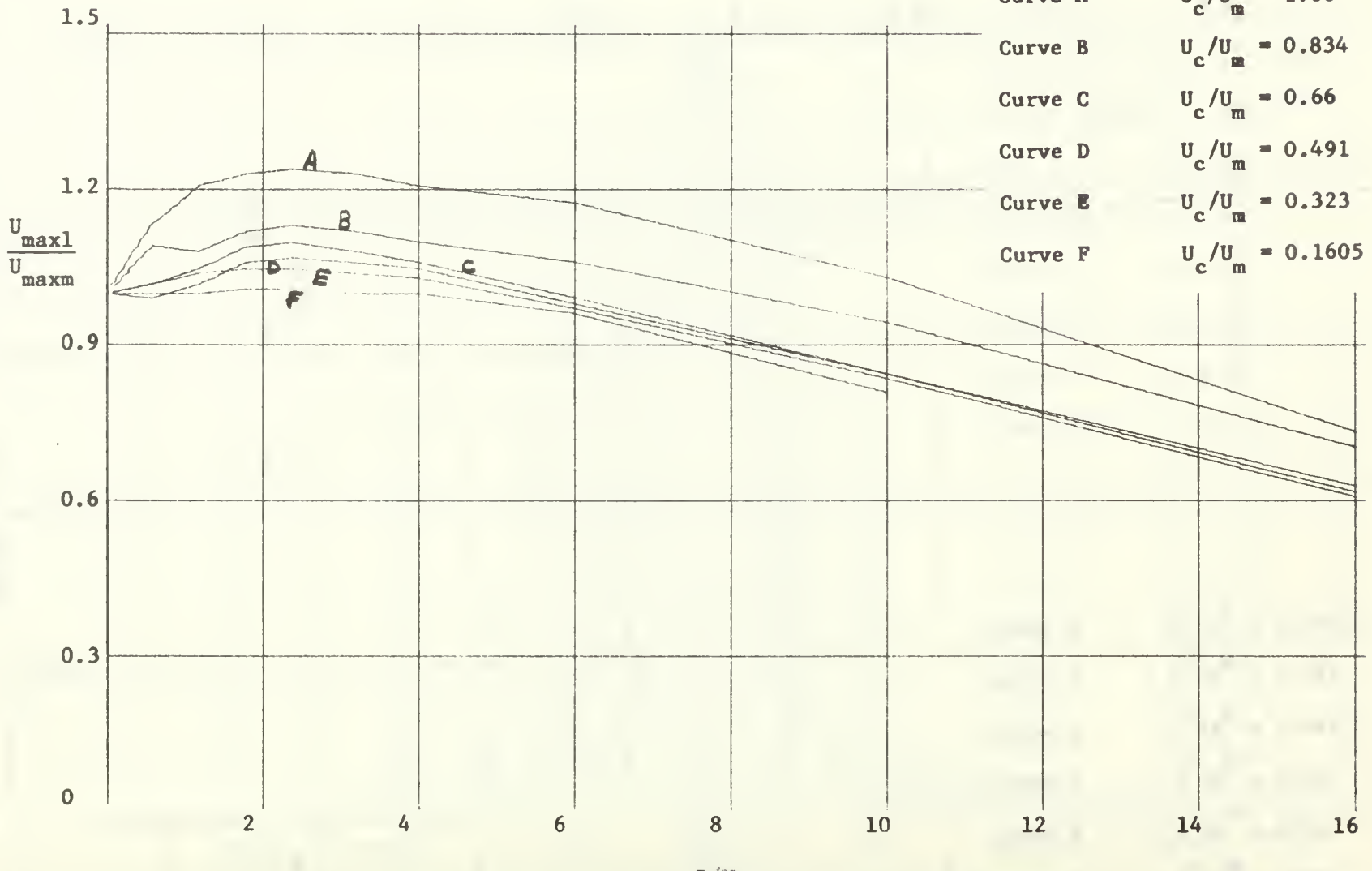

FIGURE 48. VENA CONTRACTA RATIOS

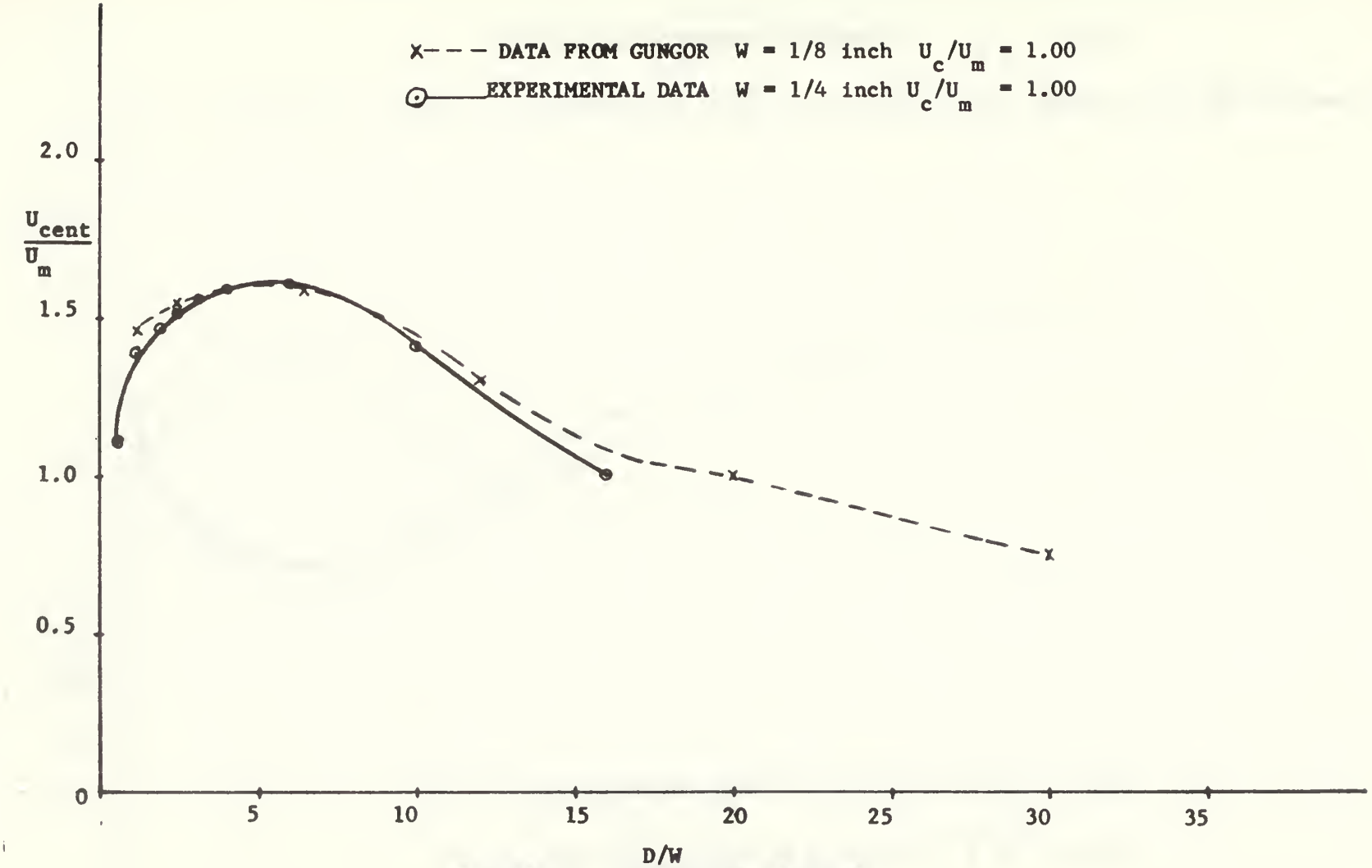

FIGURE 49. CENTERLINE VELOCITY

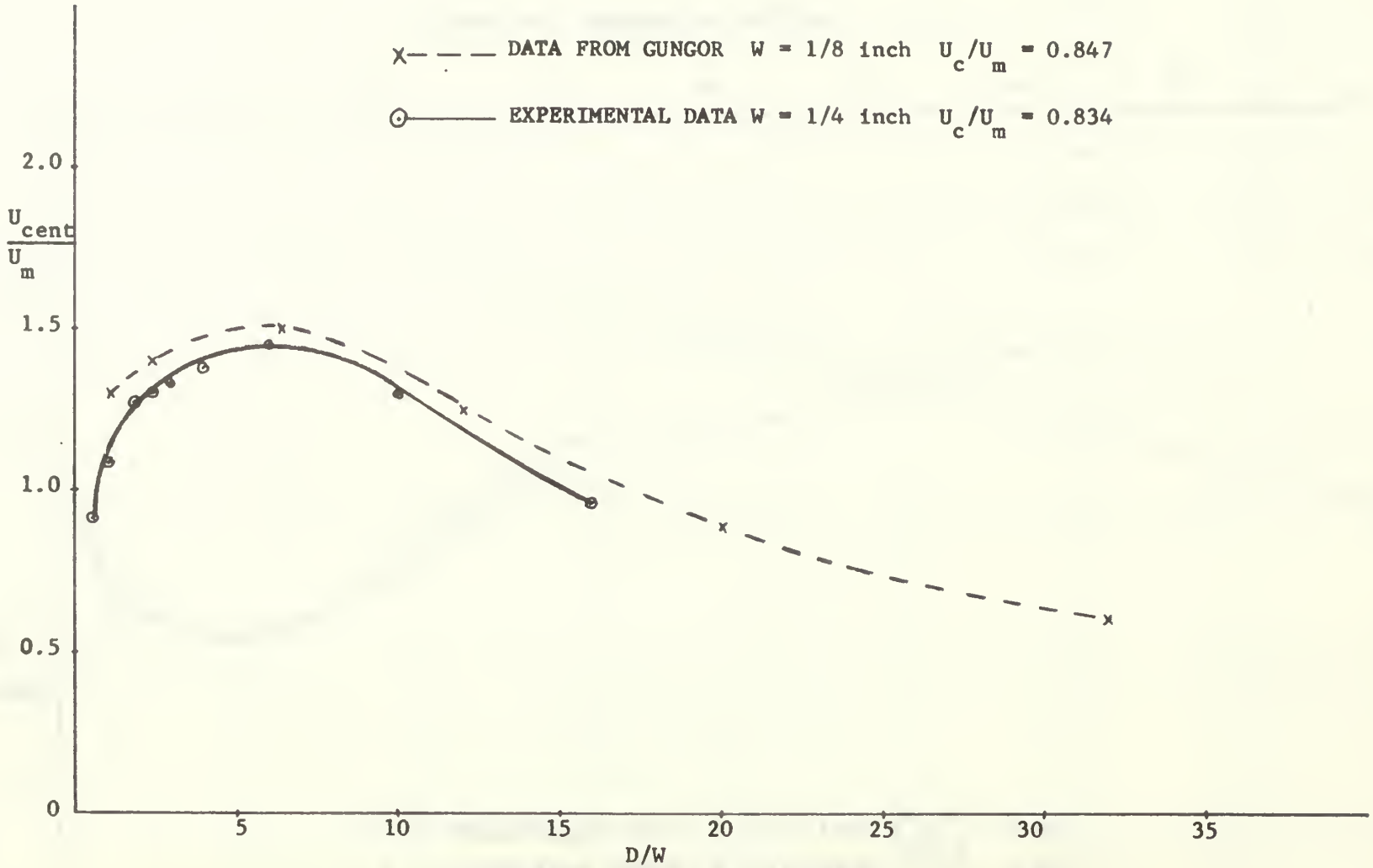

FIGURE 50. CENTERLINE VELOCITY

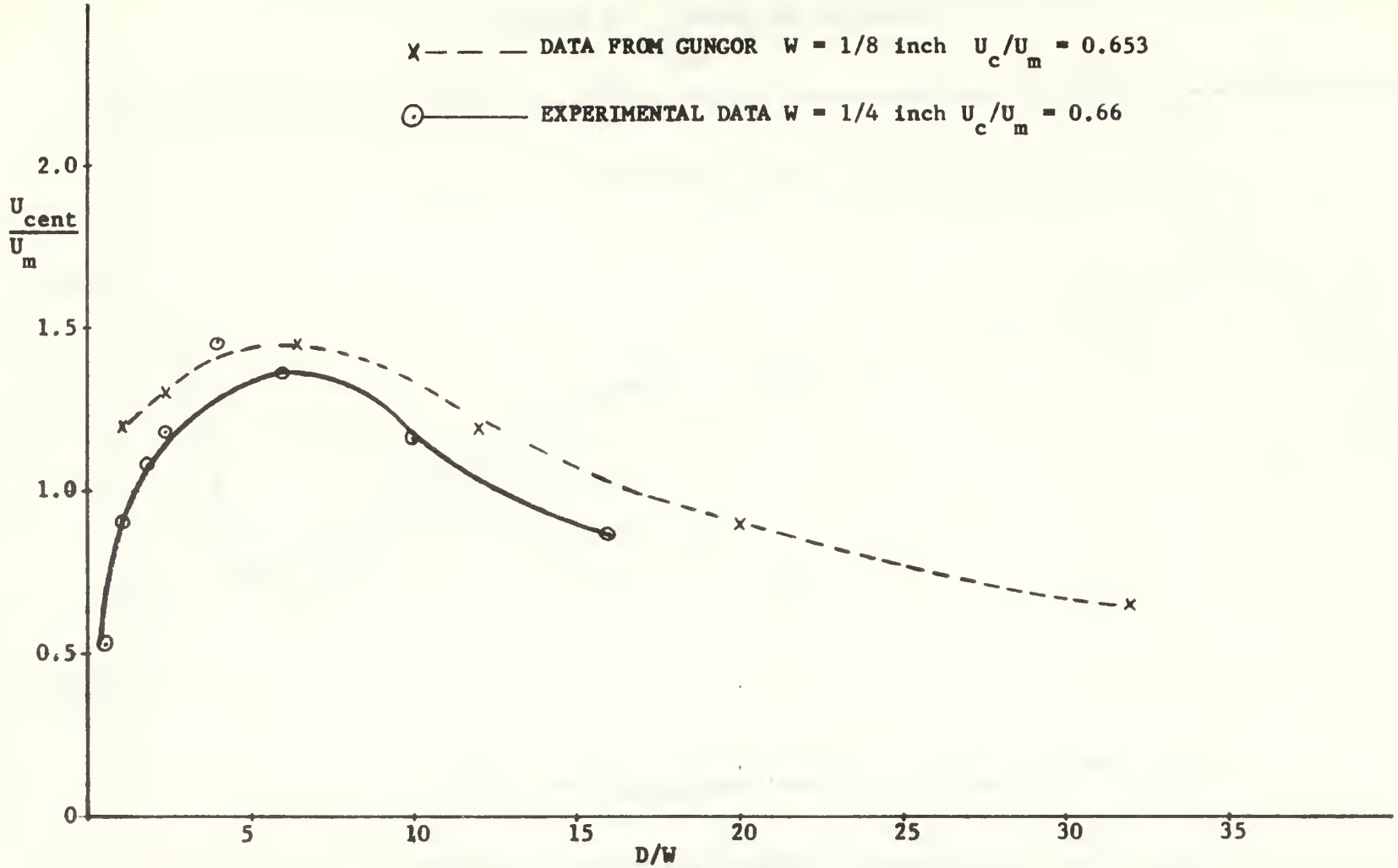

FIGURE 51. CENTERLINE VELOCITY

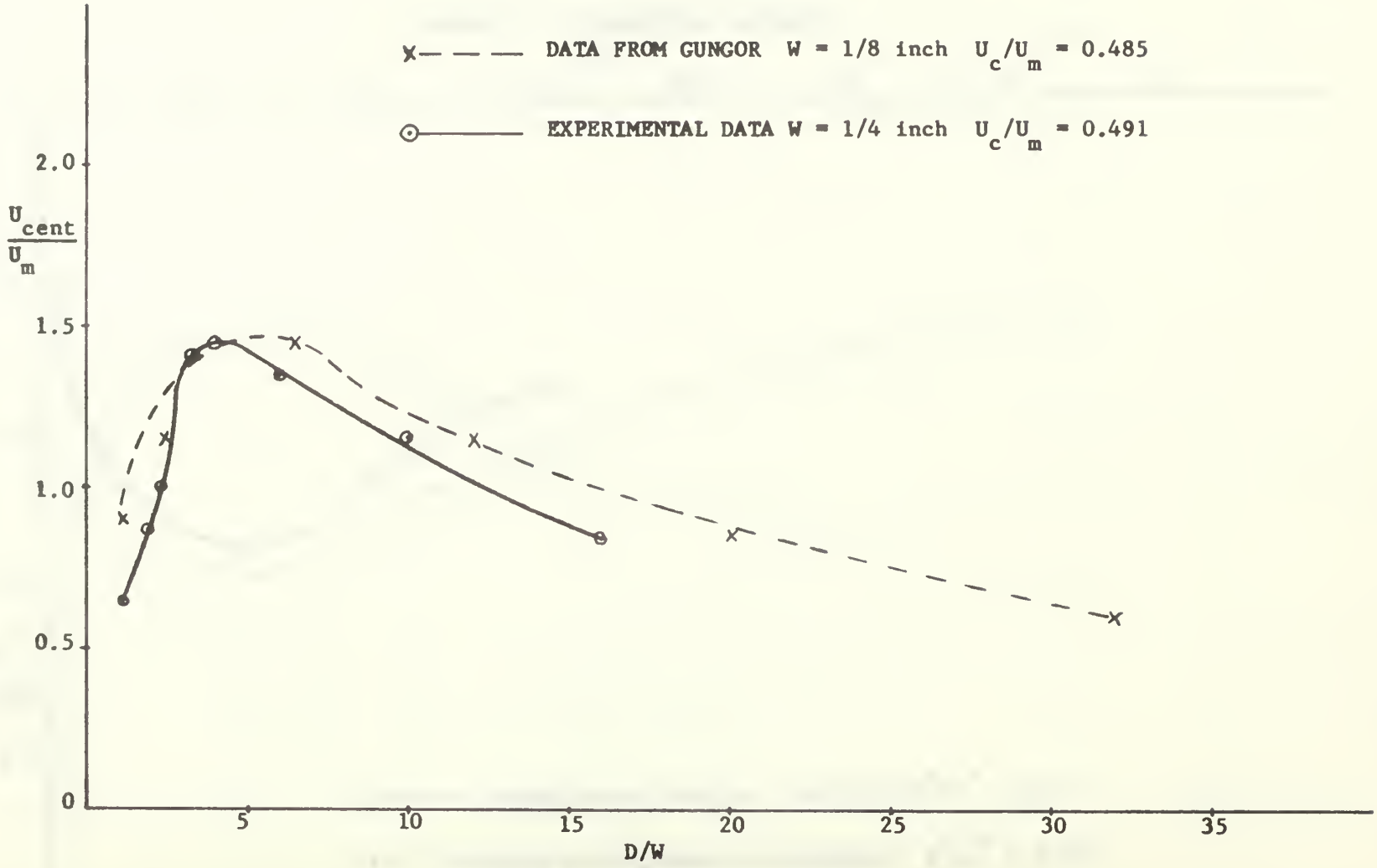

FIGURE 52. CENTERLINE VELOCITY

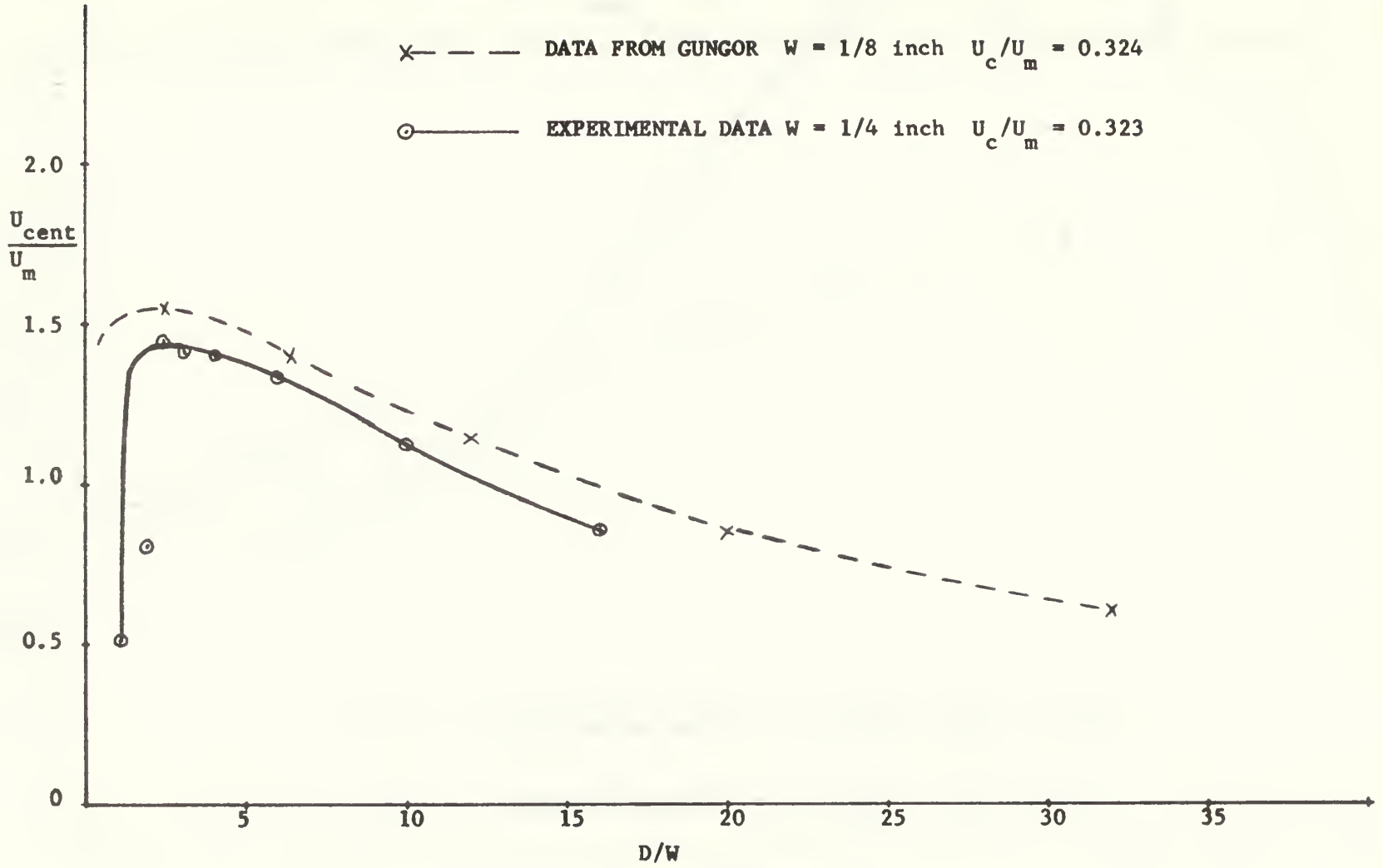

FIGURE 53. CENTERLINE VELOCITY

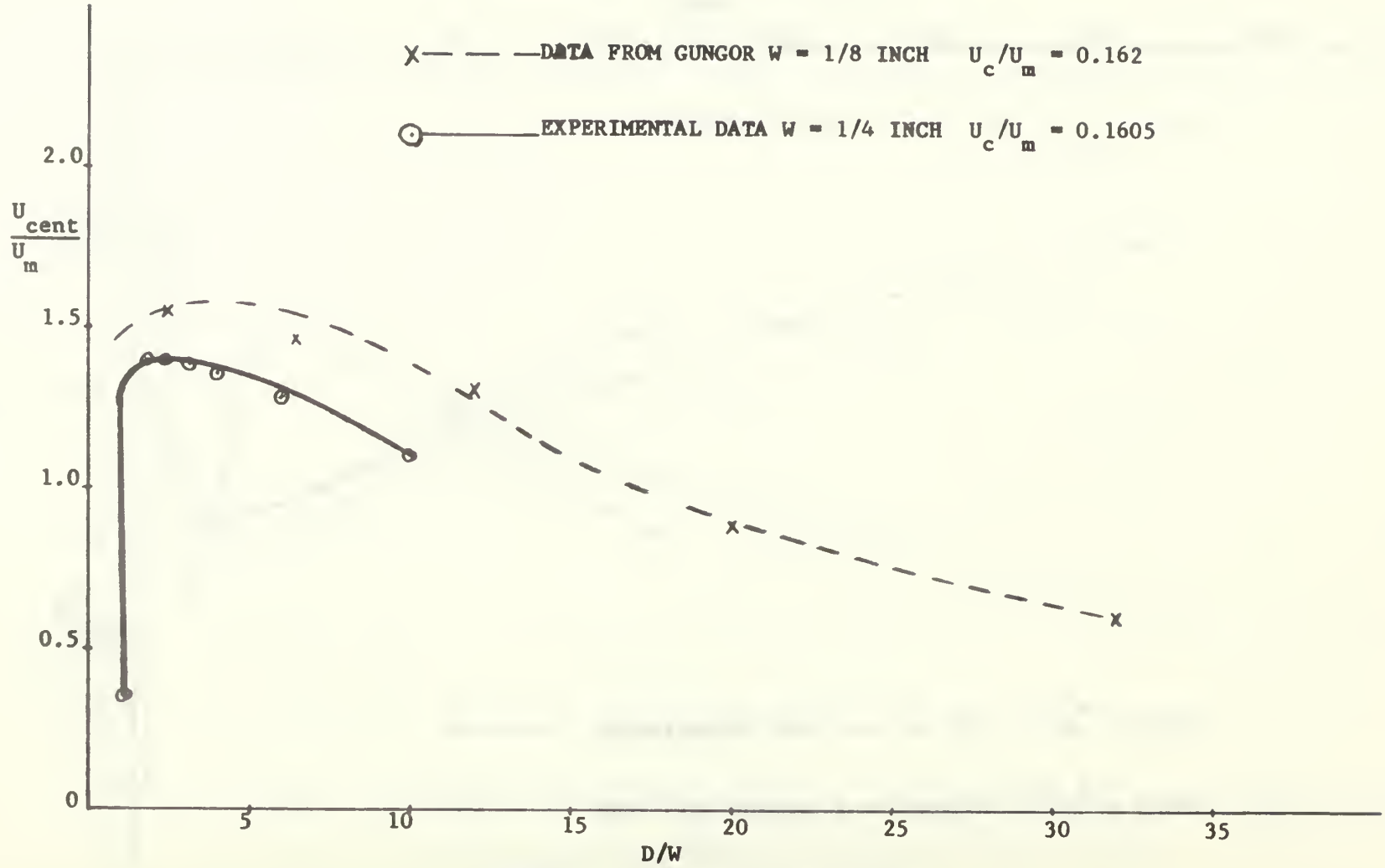

FIGURE 54. CENTERLINE VELOCITY

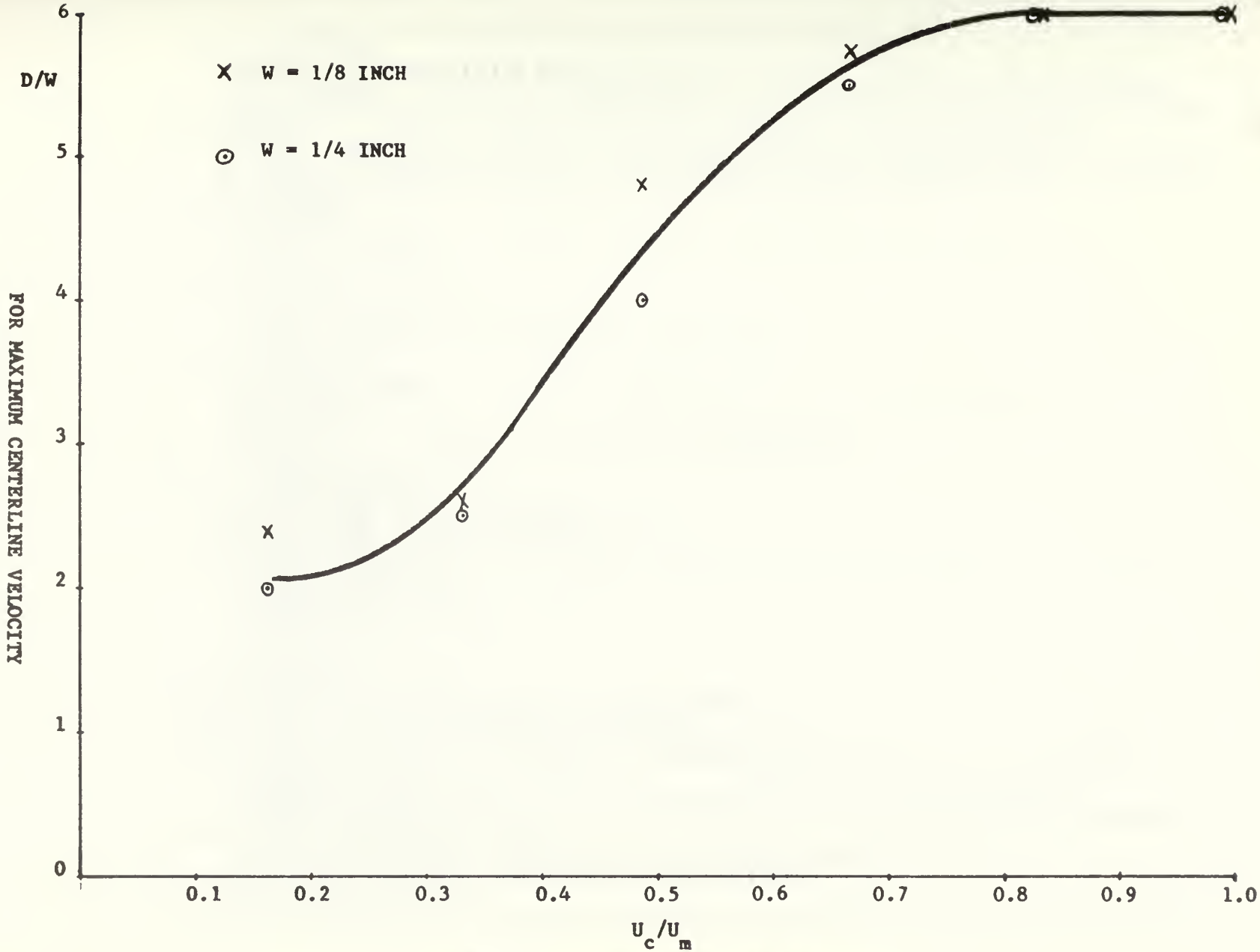

FIGURE 55. MAXIMUM CENTERLINE VELOCITY

```
C  ***********************************************************************
C     COMPUTER PROGRAM A
C   LOGARITHMIC CALIBRATION CURVE APPROXIMATION
C     THIS PROGRAM FITS POLYNOMIALS OF VARYING DEGREE(2-10)
C     TO THE CALIBRATION DATA
C  ***********************************************************************
      DIMENSION X(100),Y(100),V(100),W(100),A(20),RX(20),RH(20),
     *F(100),G(100)
      INTEGER R(20)
C   P(PRESURE IN INCHES OF WATER )=1/12*1/33.9*14.7*144=5.2 LBF/FT**2
C   1INCHES OF WATER (PRESURE ) =5.2 LBF/FT**2
C   V(VELOCITY) = SQRT(2*P/AIR DENSITY)
C   AIR DENSITY WAS TAKEN 0.0744 LBM/FT**3
C   E=2/0.0744*32.2=868
C   V=SQRT(P*E).
      REAL LABEL /'    '/
      REAL*8 ITITLE(12)
      P(Z)=Z*5.2
      VV(Z)=SQRT(Z*E)
      READ(5,12) N,E
   12 FORMAT(I5,F10.5)
C     READ IN THE VOLTAGE READINGS
      READ(5,13) (Y(I),I=1,N)
   13 FORMAT(7F10.0)
      DO 200 I=2,N
  200 Y(I)=Y(I)-1.600
C     PRESSURES IN INCHES OF WATER ARE INCREMENTED
      B=0.01
      X(1)=0.0
      DO 100 I=1,10
      X(I+1)=X(I)+B
  100 CONTINUE
      D=0.1
      DO 300 I=11,14
      X(I+1)=X(I)+D
  300 CONTINUE
      T=0.5
      DO 500 I=15,53
      X(I+1)=X(I)+T
  500 CONTINUE
      WRITE(6,1)
    1 FORMAT(1H1,T10,' I',T25,' P(IN.WATER)',T50,' R(VOLT)',T75,
     *' VELOCITY(FT/SEC)',////)
      DO 600 I=1,N
      C=X(I)
      CC=P(C)
      X(I)=VV(CC)
      WRITE(6,2) I,C,Y(I),X(I)
```

```
    2 FORMAT(1HC,T5,I5,T25,F10.5,T50,F10.5,T75,F10.5)
  6CC CONTINUE
      READ(5,14) (ITITLE(K),K=1,12)
      CALL DRAW(54,X,Y,0,0,LABEL,ITITLE,40.0,0.40,0,0,0,0,9,6,1,LAST)
C ***************************************************************
C NOW WITH CALCULATED VELOCITIES AND ANEMOMETER VOLTAGE READINGS
C  SUBROUTINE CHBFT IS USED TO FIND POLYNOMIAL COEFFICIENTS.
C ***************************************************************
      WRITE(6,16)
   16 FORMAT(1H1,T20,' LOGARITHMIC FORM OF DATA',////)
      WRITE(6,17)
   17 FORMAT(1HC,T25,' LN(VOLT)',T50,' LN(VELOCITY)',////)
      DO 19 I=2,N
      J=I-1
      X(J)=ALOG(X(I))
      Y(J)=ALOG(Y(I))
      WRITE (6,20) J,Y(J),X(J)
   20 FORMAT(1HC,T5,I5,T25,F15.7,T50,F15.7)
   19 CONTINUE
      WRITE(6,30)
   30 FORMAT(1H1,T25,' ACTUAL POINTS PLOTTED (F(I) AND G(I))')
      DO 900 I=1,27
      J=2*I-1
      F(I)=X(J)
      G(I)=Y(J)
      WRITE(6,31) F(I),G(I)
   31 FORMAT(1HC,10X,F15.7,10X,F15.7)
  9CC CONTINUE
      READ(5,14) (ITITLE(K),K=1,12)
   14 FORMAT(6A8)
      CALL DRAW(53,X,Y,0,0,LABEL,ITITLE,0.80,0.30,0,0,0,0,9,6,1,LAST)
      WRITE(6,3) LAST
    3 FORMAT(1H1,' LAST=',I2)
      N=N-1
      M=1
      DO 950 L=1,9
      M=M+1
      M1=M+1
      CALL CHBFT(Y,X,N,A,M,RX,RH,R)
      WRITE(6,5)
    5 FORMAT(1H1,10X,' POLYNOMIAL COEFFICIENTS')
      WRITE(6,6) (A(I),I=1,M1)
    6 FORMAT(1HC,10X,E14.7)
      DY=(Y(N)-Y(1))/99
      YZERO=Y(1)-DY
      DO 70 I=1,100
      W(I)=YZERO+DY*I
      V(I)=A(M+1)
```

```
      DO 60 J=1,M
      JM=M1-J
   60 V(I)=W(I)*V(I)+A(JM)
   70 CONTINUE
      READ(5,14) (ITITLE(K),K=1,12)
      CALL DRAW(27,F,G,1,2,LABEL,ITITLE,0.80,0.30,0,0,0,0,9,6,1,LAST)
      WRITE(6,3) LAST
      CALL DRAW(100,V,W,3,0,LABEL,ITITLE,0.80,0.30,0,0,0,0,9,6,1,LAST)
      WRITE(6,3) LAST
  950 CONTINUE
      STOP
      END
C     SUBROUTINE CHBFT
C
C     PURPOSE:
C         SUBROUTINE CHBFT  EVALUATES THE COEFFICIENTS OF AN MTH ORDER
C         POLYNOMIAL P(X)=A(1)+A(2)*X+A(3)*X**2+...+A(M+1)X**M  SUCH
C         THAT THE MAXIMUM ERROR ABS(P(X(I))-Y(I)) IS A MINIMUM OVER
C         THE N (N.GT.M+1) SAMPLE POINTS X(I),Y(I), I=1,2,...,N.  THE
C         X(I) MUST FORM A STRICTLY MONOTONIC SEQUENCE; I.E.,
C         X(1).LT.X(2).LT.X(3).LT....X(N). THIS SUBROUTINE IS A
C         CONVERSION FROM ALGOL TO FORTRAN OF ALGORITHM 318, CHEBYSCHEV
C         CURVE-FIT FROM"COMMUNICATIONS OF THE ACM"VOL.10,NUMBER 12,
C         DECEMBER,1967. THE AUTHOR OF THE ALGOL VERSION WAS
C         J. BOOTHROYD FROM THE UNIVERSITY OF TASMANIA.
C
C     USAGE:
C         CALL CHBFT (X,Y,N,A,M,RX,RH,R)
C
C         DESCRIPTION OF PARAMETERS:
C         X     -ARRAY OF ABSCISSAE DIMENSIONED REAL*4 X(N)
C         Y     -ARRAY OF ORDINATES DIMENSIONED REAL*4 Y(N)
C         N     -NUMBER OF SAMPLE POINTS  (INTEGER)
C         A     -ARRAY OF THE OUTPUTTED POLYNOMIAL COEFFICIENTS
C                DIMENSIONED AT LEAST A(M+2) (REAL*4)
C         M     -ORDER OF DESIRED APPROXIMATING POLYNOMIAL
C         RX    -WORK ARRAY DIMENSIONED AT LEAST REAL*4 RX(M+2)
C         RH    -WORK ARRAY DIMENSIONED AT LEAST REAL*4 RH(M+2)
C         R     -INTEGER WORK ARRAY DIMENSIONED AT LEAST R(M+2)
C
C     REMARKS:
C         THE POLYNOMIAL P(X) IS A BEST-FIT POLYNOMIAL IN THE CHEBYSCHEV
C         SENSE AS DESCRIBED BY STIEFEL(NUMERICAL METHODS OF
C         TCHEBYCHEFF APPROXIMATION), IN LANGER(ED.),"ON NUMERICAL
C         APPROXIMATION",U.OF WISCONSIN PRESS, 1959, PP. 217-232.
C         STIEFEL (P.221) SHOWS THAT THE PROCEDURE MUST TERMINATE AFTER
C         A FINITE NUMBER OF STEPS. AT EXIT THE ABSOLUTE VALUE OF
C         A(M+1) YIELDS THE FINAL REFERENCE DEVIATION. NEGATIVE A(M+1)
```

```
C          INDICATES THAT THE PROCEDURE HAS BEEN TERMINATED FOLLOWING
C          THE DETECTION OF CYCLING.
C
C      NOTE:  DIVIDED DIFFERENCES AND NEWTON'S INTERPOLATING FORMULA IS
C          USED FOR COMPUTING THE POLYNOMIAL COEFFICIENTS.
C
C



      SUBROUTINE CHBFT(X,Y,N,A,M,RX,RH,R)
      REAL*4 NEXTHI
      INTEGER RI,RJ,R(1)
      DIMENSION X(1),Y(1),A(1),RX(1),RH(1)
      MPLUS1=M+1
      MPLUS2=M+2
      PREVH=0.0
C     DETERMINE INDEX VECTOR FOR INITIAL REFERENCE SET
      R(1)=1
      R(MPLUS2)=N
      D=(N-1)/MPLUS1
      H=D
      DO 1 I=2,MPLUS1
      R(I)=H+1.0
    1 H=H+D
    2 H=-1.0
C     SELECT M+2 REFERENCE PAIRS AND SET ALTERNATIVE DEVIATION VECTOR
      DO 3 I=1,MPLUS2
      RI=R(I)
      RX(I)=X(RI)
      A(I)=Y(RI)
      H=-H
    3 RH(I)=H
C     COMPUTE M+1 LEADING DIVIDED DIFFERENCES
      DO 4 J=1,MPLUS1
      I1=MPLUS2
      AI1=A(I1)
      RHI1=RH(I1)
      I=MPLUS1
    5 DENOM=RX(I1)-RX(I-J+1)
      AI=A(I)
      RHI=RH(I)
      A(I1)=(AI1-AI)/DENOM
      RH(I1)=(RHI1-RHI)/DENOM
      I1=I
      AI1=AI
      RHI1=RHI
```

```
      I=I-1
      IF(I-J) 4,5,5
    4 CONTINUE
C     EQUATE (M+1) THE DIFFERENCE TO ZERO TO DETERMINE H
      H=-A(MPLUS2)/RH(MPLUS2)
C     WITH H KNOWN, COMBINE THE FUNCTION AND DEVIATION DIFFERENCES
      DO 6 I=1,MPLUS2
    6 A(I)=A(I)+RH(I)*H
C     COMPUTE POLYNOMIAL COEFFICIENTS
      J=M
    7 XJ=RX(J)
      I=J
      AI=A(I)
      JPLUS1=J+1
      DO 8 I1=JPLUS1,MPLUS1
      AI1=A(I1)
      A(I)=AI-XJ*AI1
      AI=AI1
    8 I=I1
      J=J-1
      IF(J-1) 9,7,7
    9 CONTINUE
C     IF THE REFERENCE DEVIATION IS NOT INCREASING MONOTONICALLY
C     THEN EXIT
      HMAX=ABS(H)
      IF(HMAX.GT.PREVH) GO TO 29
      A(MPLUS2)=-HMAX
      RETURN
C     FIND THE INDEX,IMAX,AND VALUE,HIMAX, OF THE LARGEST ABSOLUTE
C     ERROR FOR ALL SAMPLE POINTS
   29 A(MPLUS2)=HMAX
      PREVH=HMAX
      IMAX=R(1)
      HIMAX=H
      J=1
      RJ=R(J)
      DO110 I=1,N
      IF(I.EQ.RJ) GO TO 11
      XI=X(I)
      HI=A(MPLUS1)
      K=M
   12 HI=HI*XI+A(K)
      K=K-1
      IF(K-1)112,12,12
  112 HI=Y(I)
      ABSHI=ABS(HI)
      IF(ABSHI.LE.HMAX) GO TO 11
      HMAX=ABSHI
```

```
      HIMAX=HI
      IMAX=I
      GO TO110
   11 IF(J.GE.MPLUS2) GO TO110
      J=J+1
      RJ=R(J)
  110 CONTINUE
C     IF THE MAXIMUM ERROR OCCURS AT A NONREFERENCE POINT, EXCHANGE THIS
C     POINT WITH THE NEAREST REFERENCE POINT HAVING AN ERROR OF THE
C     SAME SIGN AND REPEAT
      IF(IMAX.EQ.R(1)) RETURN
      DO 14 I=2,MPLUS2
      IF(IMAX.LT.R(I)) GO TO 15
   14 CONTINUE
      I=MPLUS2
   15 NEXTHI=H
      IF((I-I/2*2).NE.0) NEXTHI=-H
      IF(HIMAX*NEXTHI.GE.0) GO TO 115
      IF(IMAX.GE.R(1))      GO TO 116
      J1=MPLUS2
      J=M
  117 R(J1)=R(J)
      J1=J
      J=J-1
      IF(J-1)118,117,117
  118 R(1)=IMAX
      GO TO 2
  116 IF(IMAX.LE.R(MPLUS2)) GO TO 120
      J=1
      DO 121 J1=1,MPLUS2
      R(J)=R(J1)
  121 J=J1
      R(MPLUS2)=IMAX
      GO TO 2
  115 R(I)=IMAX
      GO TO 2
  120 R(I-1)=IMAX
      GO TO 2
      END
```

```
C*************************************************************************
C     PROGRAM B
C     MAIN DATA REDUCTION PROGRAM
C     VELOCITY AND TURBULENCE INTENSITY PROFILES ARE CALCULATED AND
C     PLOTTED ON THE SAME GRAPH FOR EACH STATION AND FLOW RATIO.
C*************************************************************************
      DIMENSION A(10),B(10),R(100),P1(100),P2(100),P3(100),R4(100),
     *X(100),Y(100),V(100),W(100),T(100),TURIN(100),Z(100)
      REAL LABEL/'    '/
      REAL*8 TITLE(12)
C*************************************************************************
C     A(I) ARE THE POLYNOMIAL COEFFICIENTS
C     B(I) ARE THE DERIVATIVE COEFFICIENTS
C*************************************************************************
      READ(5,1) (A(I),I=1,3)
    1 FORMAT(3E15.7)
C*************************************************************************
C   N   TO COMPUTE THE DERIVATIVE COEFFICIENTS
C*************************************************************************
      DO 10 I=1,2
   10 B(I)=A(I+1)*I
      WRITE(6,2)
    2 FORMAT(1H1,T23,' POLYNOMIAL COEFFICIENTS',////)
      WRITE(6,3) (A(I),I=1,3)
    3 FORMAT(1HO,T25,E14.7)
      WRITE(6,4)
    4 FORMAT(1HO,//////,T25,' DERIVATIVE COEFFICIENTS',////)
      WRITE(6,3) (B(I),I=1,2)
      DO 300 KROP=1,5
      NUM=9
      DO 200 KPOK=1,NUM
      IF(KROP.EQ.5) NUM=8
      READ(5,5) II,JJ,KK,LL,MM,NN,MPT,D,RZERO,S
    5 FORMAT(7I5,3F10.5)
C*************************************************************************
C   NOW TO INTRODUCE THE VOLTAGE READINGS
C*************************************************************************
      READ(5,6) (R(I),I=1,NN)
    6 FORMAT(7F10.5)
      READ(5,6) (T(I),I=1,NN)
C*************************************************************************
C  NOW THE STEP-JUMPS ON THE TRAVERSING PATH ARE CALCULATED
C*************************************************************************
      X(1)=S
      DO 20 I=2,II
      X(I)=X(I-1)+0.050
   20 CONTINUE
      IA=II+1
```

```
      DO 30 I=IA,JJ
      X(I)=X(I-1)+0.0250
   30 CONTINUE
      JA=JJ+1
      DO 40 I=JA,KK
      X(I)=X(I-1)+0.0125
   40 CONTINUE
      KA=KK+1
      DO 50 I=KA,LL
      X(I)=X(I-1)+0.0250
   50 CONTINUE
      LA=LL+1
      DO 60 I=LA,MM
      X(I)=X(I-1)+0.050
   60 CONTINUE
      DO 70 I=1,NN
      R1(I)=R(I)-RZERO
   70 CONTINUE
C*****************************************************************
C  NOW TO CALCULATE THE LOGS OF THE VOLTAGE READINGS
C*****************************************************************
      DO 80 I=1,NN
      R2(I)=ALOG(R1(I))
   80 CONTINUE
C*****************************************************************
C  NOW TO CALCULATE LOG(VELOCITY) USING THE POLYNOMIAL APPROXIMATION
C*****************************************************************
      DO 90 I=1,NN
      R3(I)=A(1)+A(2)*R2(I)+A(3)*(R2(I)**2)
   90 CONTINUE
C*****************************************************************
C  NOW TO TAKE THE ANTILOG TO FIND THE VELOCITIES
C*****************************************************************
      DO 100 I=1,NN
      Y(I)=EXP(R3(I))
  100 CONTINUE
      WRITE(6,7)
    7 FORMAT(1H1,T25,' RAW FORM OF VELOCITY DATA',////)
      WRITE(6,8)
    8 FORMAT(1HO,T10,' X',T25,' VOLTAGE',T50,' VOLT-RZERO',
     *T75,' VELOCITY',T100,' TURBULENCE',////)
      WRITE(6,9) (I,X(I),R(I),R1(I),Y(I),T(I),I=1,NN)
    9 FORMAT(1HO,I5,T10,F10.5,T25,F10.5,T50,F10.5,T75,F10.5,T100,F10.5)
C*****************************************************************
C  NOW TO PUT THE VELOCITY DATA IN THE PROPER FORM FOR GRAPHING.
C*****************************************************************
      UMAX=Y(MPT)
      DO 110 I=1,NN
```

```
      Z(I)=X(I)/0.25
      V(I)=Y(I)/UMAX
  110 CONTINUE
      WRITE(6,11)
   11 FORMAT(1H1,T35,' VELOCITY PROFILE DATA',////)
      WRITE(6,12)
   12 FORMAT(1HO,T25,' X/W',T50,' U/UMAX',////)
      WRITE(6,13) (I,Z(I),V(I),I=1,NN)
   13 FORMAT(1HO,I5,T25,F10.5,T50,F10.5)
      READ(5,14) (ITITLE(IKA),IKA=1,12)
   14 FORMAT(6A8)
      CALL DRAW(NN,Z,V,1,0,LABEL,ITITLE,0.7,0.20,0,0,0,0,9,6,1,LAST)
C*****************************************************************
C   NOW TO CALCULATE THE TURBULENCE INTENSITIES
C   FIRST THE LOGS OF THE DERIVATIVES
C*****************************************************************
      DO 120 I=1,NN
      R4(I)=B(1)+B(2)*R2(I)
      W(I)=EXP(R4(I))
  120 CONTINUE
C*****************************************************************
C   TURBULENCE INTENSITY
C*****************************************************************
      DO 130 I=1,NN
      TURIN(I)=W(I)*(T(I)/Y(I))
  130 CONTINUE
      WRITE(6,16)
   16 FORMAT(1H1,T35,' TURBULENCE PROFILE DATA',////)
      WRITE(6,17)
   17 FORMAT(1HO,T25,' X/W',T50,' TURBULENCE INTENSITY',////)
      WRITE(6,18) (I,Z(I),TURIN(I),I=1,NN)
   18 FORMAT(1HO,I5,T25,F10.5,T50,F10.5)
      CALL DRAW(NN,Z,TURIN,3,0,LABEL,ITITLE,0.7,0.2,0,0,0,0,9,6,1,LAST)
  200 CONTINUE
  300 CONTINUE
      STOP
      END
```

REFERENCES

1. Dosanjh, D. S. and Sheeran, W. J., "Experiments with Two-Dimensional, Transversely Impinging Jets," AIAA Journal, v. 1, p. 329-333, February 1963.

2. Douglas, J. F. and Neeve, R. S., Investigation Into the Behavior of a Jet Interaction Proportional Amplifier, paper presented at Second Cranfield Fluidics Conference, Cambridge, England, 5 January 1967.

3. Moynihan, F. A., Jet Interaction Noise, paper presented at Harry Diamond Laboratories Symposium, May 1964.

4. Moynihan, F. A. and Reilly, R. J., Deflection and Relative Flow of Three Interacting Jets, paper presented at Harry Diamond Laboratories Symposium, May 1964.

5. Gungor, N., A Theoretical and Experimental Study of the Impingement of Two Subsonic Jets, M. S. Thesis, Naval Postgraduate School, Monterey, California, June 1969.

6. Operating and Service Manual 1050 Series, Constant-Temperature Anemometers and Related Acessories, Thermo-Systems, Inc.

7. National Advisory Committee for Aeronautics, Technical Note 2843, Auxillary Equipment and Techniques for Adapting the Constant Temperature Hot-Wire Anemometer to Specific Problems in Air Flow Measurements, by J. C. Laurence, and L. G. Landes, November 1962.

8. Pai, S., Fluid Dynamics of Jets, p. 96-136, Van Nostrand, 1954.

INITIAL DISTRIBUTION LIST

		No. Copies
1.	Defense Documentation Center Cameron Station Alexandria, Virginia 22314	20
2.	Library, Code 0212 Naval Postgraduate School Monterey, California 93940	2
3.	Department of Mechanical Engineering Naval Postgraduate School Monterey, California 93940	2
4.	Naval Ship Systems Command (Code 2052) Via: Code 031 Department of the Navy Washington, D. C. 20360	1
5.	LTJG S. B. Weeks, USN 16158 Via Media San Lorenzo, California 94580	2
6.	Professor T. Sarpkaya Department of Mechanical Engineering Naval Postgraduate School Monterey, California 93940	3

DOCUMENT CONTROL DATA - R & D

(Security classification of title, body of abstract and indexing annotation must be entered when the overall report is classified)

ORIGINATING ACTIVITY (Corporate author)	2a. REPORT SECURITY CLASSIFICATION
Naval Postgraduate School Monterey, California 93940	Unclassified
	2b. GROUP

REPORT TITLE

A Theoretical and Experimental Investigation of Turbulent Jet Interaction

DESCRIPTIVE NOTES *(Type of report and inclusive dates)*

Master's Thesis, October 1969

AUTHOR(S) *(First name, middle initial, last name)*

WEEKS, Steven Brian

REPORT DATE	7a. TOTAL NO. OF PAGES	7b. NO. OF REFS
October, 1969	95	8

a. CONTRACT OR GRANT NO.	9a. ORIGINATOR'S REPORT NUMBER(S)
b. PROJECT NO. U. S. Army Research Office Durham, North Carolina	
c. MIPR No. ARO D-4-69	9b. OTHER REPORT NO(S) *(Any other numbers that may be assigned this report)*
d.	

10. DISTRIBUTION STATEMENT

This document has been approved for public release and sale, its distribution is unlimited.

11. SUPPLEMENTARY NOTES	12. SPONSORING MILITARY ACTIVITY
	Naval Postgraduate School Monterey, California 93940

13. ABSTRACT

The interaction of two impinging plane turbulent jets has been investigated for the purpose of understanding the performance of proportional fluid amplifiers and momentum-exchange devices. Velocity and turbulence profiles were measured across and at various distances along the combined jet axis through the use of a constant temperature hot-wire anemometer. Experimentally determined jet deflection angles were found to agree quite well with those predicted in a previous work by the free-streamline theory. The results, which are presented in terms of normalized parameters, show that the jet interaction may be divided into three regions: mixing; transition; and fully developed. A vena-contracta effect was found to exist in the mixing region. A discussion of each of the three regions is presented in detail along with generalizations for similar geometries.

14 KEY WORDS	LINK A		LINK B		LINK C	
	ROLE	WT	ROLE	WT	ROLE	WT
Jet interaction						
Turbulent jets						
Proportional amplifiers						
Beam deflection						
Fluidics						